Universal Correlations in the Quantum Spectra of Chaotic Systems and Exactly Solvable Many-Body Problems

by

Eduardo Rezende Mucciolo

Submitted to the Department of Physics
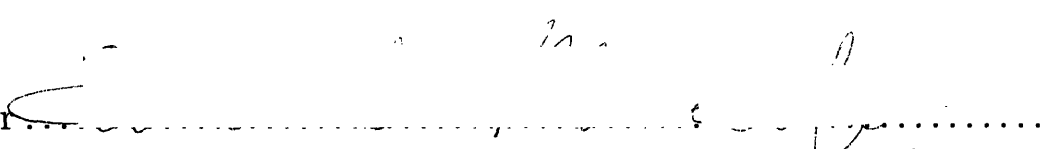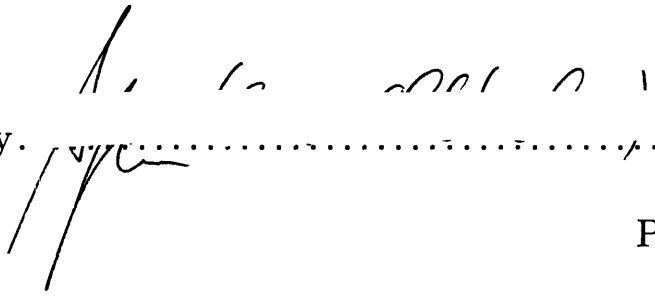in partial fulfillment of the requirements for the degree of

Doctor of Philosophy

at the

MASSACHUSETTS INSTITUTE OF TECHNOLOGY

August 1994

Author...
Department of Physics
August 10, 1994

Certified by...
Boris L. Altshuler
Professor of Physics
Thesis Supervisor

Accepted by..
George F. Koster
Chairman, Departmental Committee on Graduate Students

Universal Correlations in the Quantum Spectra of Chaotic Systems and Exactly Solvable Many-Body Problems

by

Eduardo Rezende Mucciolo

Submitted to the Department of Physics
on August 10, 1994, in partial fulfillment of the
requirements for the degree of
Doctor of Philosophy

Abstract

The problem of a single particle moving chaotically in the presence of either a random potential or irregular boundaries serves as the basis for the investigation of three different problems in condensed matter theory. The first one is related to the statistics of level widths and conductance peaks in a quantum dot with extended contacts. Level widths are determined by the amplitude of the wavefunction averaged over the contact area. The distribution function of level widths for two-point contacts is evaluated exactly, which allows us to determine the distribution of conductance peaks in the resonance regime. The second problem we consider is the mapping of a parametric spectral correlations of chaotic systems into the exact dynamical structure function of the $1/r^2$ model of interacting particles in one dimension. We interpret the density fluctuations of this model in terms of the exact excitations for three representative values of the coupling constant. The third problem is the manifestation of quantum chaos in the energy spectra of crystals. We analyze the *ab initio* band structure of silicon and the tight-binding spectrum of the alloy $Al_xGa_{1-x}As$, and show that some of their statistical properties obey the universal predictions of quantum chaos derived from the theory of random matrices and the supersymmetric nonlinear σ model.

Thesis Supervisor: Boris L. Altshuler
Title: Professor of Physics

Acknowledgments

Contents

Chapter 1

Introduction

The problem of a single particle moving in the presence of a background potential, despite its apparent simplicity, continues to be one of the main topics of investigation in the field of condensed matter theory. What could be initially thought as an exercise in elementary quantum mechanics, turns out to be the source of a wide variety of phenomena. The techniques specially developed to investigate this type of problem have also become useful tools in the study of many-body systems.

A well-known example where the single-particle picture leads not just to a good understanding, but also to an accurate description of the underlying physics is the theory of mesoscopic systems [1]. This field deals with the properties of submicron-size metallic systems in which phase coherence is maintained throughout the sample, but disorder makes the electron motion diffusive. Apart from the renormalization of some constants, such as the electron mass, the electron-electron interaction does not play an important role when the temperature is kept low enough and the disorder is weak [2].

Recently, new technologies have changed the definition of mesoscopic systems to also include structures where disorder is negligible and the electron motion is essentially ballistic [3]. It is the irregularity of the boundaries that makes the motion of a single electron inside such systems nonintegrable, resembling therefore the disordered case. In some experiments [4, 5, 6, 7, 8] one has actually been able to finely shape the island into different stadium geometries and observe the effects of chaotic and regular behaviors.

From the theoretical viewpoint, either the case of disordered grains or ballistic cavities can be described through the same statistical approach. The basic assumption is that the complexity of the electron motion in these systems causes the matrix elements of the Hamiltonian to be random and uncorrelated. This is one of main ideas behind the study of some of the statistical properties of a quantum dot presented in Chapter 2. A quantum dot is a microstructure where the number of electrons is controlled by tunnel junctions [9, 10]. The striking feature of these systems is the appearance of resonances in the conductance as the gate voltage (the chemical potential) is varied. The height of these resonances or peaks is connected to the width of the energy levels inside the dot. For a system that is weakly coupled to the external world and at low temperatures, the level width statistics reflects the

character of the fluctuations of the electron wavefunction amplitude in the contact regions. The question we address in Chapter 2 is how the size of the contacts affects the distribution of level widths and, consequently, the distribution of conductance peaks. Analytical calculations and numerical simulations indicate that the size of the leads influences strongly the shape of the distributions, particularly in the regions of small widths and short peaks.

One of the most powerful mathematical tools used in the investigation of statistical properties of random systems is the supersymmetry method invented by Efetov [11]. Similarly to random matrix theory, the supersymmetry technique has also being applied to completely distinct physical systems. One of the most interesting cases is found in the mapping introduced by Simons, Lee, and Altshuler [12]. These authors have shown that the parametric correlator of spectral densities of a chaotic system [13, 14, 15, 16], under a suitable change of variables, coincides with the exact dynamical structure factor of the one-dimensional Sutherland model [17, 18]. This result has created new grounds for the understanding of excitations in strongly interacting many-body systems of the $1/r^2$ class. The investigation of the content of the dynamical structure factor for three representative values of the coupling constant is the subject of Chapter 3. Our main result is that bare density fluctuations involve only a finite number of quasiparticles and quasiholes.

In Chapter 4 we come back to the single-particle problem. Motivated by the work of Sinai [19], Laughlin [20], and Taniguchi and Altshuler [21], we search for the universal signatures of quantum chaos in periodic systems. In the classical limit, the motion of electrons in a crystalline environment is very likely to show chaotic behavior. Even very simple unit cells should yield some degree of chaoticity. However, semiclassical theory indicates that the low-lying energy levels of a quantum system are associated with short periodic orbits which are system dependent [22]. To probe the universal features of a crystal, we analyze the statistical properties of high-energy bands of Silicon calculated by a *ab initio* algorithm, taking care to avoid crossing symmetry lines in momentum space. We find good agreement with the predictions of random matrix theory and the parametric correlation function theory of Simons, Szafer, and Altshuler [13, 14, 15, 16]. We also obtain similar results analyzing the band structure of a tight-binding $Al_xGa_{1-x}As$ supercell.

The reader can find an introduction to the basic elements of the supersymmetry technique in Appendix A. The most involved calculation of Chapter 2, that of the joint probability distribution of level widths, is explained in some detail in Appendix B.

Chapter 2

Statistical Properties of Level Widths and Conductance Peaks in a Quantum Dot

2.1 Introduction

Usually any measurement of conductance in a metallic system assumes at least two attached leads. The existence of these leads connecting the system to reservoirs broadens the electronic energy levels. For a macroscopic sample, the width of an energy level is typically much larger than the distance between neighboring levels. As a result, one observes a smooth dependence of the conductance on the Fermi energy.

Recently, the advances in nanometer technology have made possible the fabrication of very small semiconductor devices, known generically as quantum dots [3, 9, 10], where one has a fixed number of conduction electrons confined into an island. In these systems, one can narrow the level width by reducing either the transversal size of the leads or their transmittance. In the first case it is customary to speak about channels: If we consider an ideal lead as a wave guide with a given cross section, we can associate a channel to each state due to transverse quantization. In three dimensions, the number of channels is approximately the area, in units of electron wavelength, of the contact between lead and dot and each channel is characterized by its transmittance.

The conductance of a system can be calculated through the well-known Landauer-Büttiker formula [23, 24]. Following this approach, the distribution of conductances of a quantum dot has been evaluated for two distinct cases: for weakly coupled point-like leads [25] of a closed system, and for leads with any number of channels attached to a ballistic cavity [26, 27].

Here we will consider the situation at low transmittance, when leads behave as tunnel contacts. In this case, each electron eigenstate corresponds to a peak in the Fermi energy (gate voltage) dependence of the conductance [9, 10]. This allows one to make a real spectroscopy of electrons in quantum dots. The height of each peak is determined by the probabilities of tunneling through the leads, as well as by the amplitude of the wavefunction near the contacts. The later means that these heights

are randomly distributed. The distribution function of the peaks has been determined for the case of point-like contacts in Refs. [25, 28, 29]. Here we will deduce the distribution considering leads of arbitrary size.

We begin by studying the statistics of level widths, which is connected to the fluctuations of conductance peaks through the Landauer-Büttiker formula. The supersymmetry technique and the nonlinear σ model [11, 30] provide the framework for the exact calculation of the distribution of level widths for leads with two-point contact. The distribution differs drastically from the single-point case, but we find that inclusion of correlation between the wavefunction fluctuations at the two points in the lead does not significantly alter the overall form of the distribution of level widths. This analytical result is confirmed through numerical simulations of a quantum dot. The exact distribution of conductance peaks is also evaluated for two-point leads and we find that it deviate from the single-point distribution mainly for small peak heights, where it shows a linear dependence.

For leads with many point contacts, we do not know of any method that enables a general evaluation of the distribution function. Thus, we assume that the wavefunction at each point fluctuates independently and proceed to calculate the total distribution. By comparing numerical with analytical results, we show that this approximation yields a good qualitative understanding of the large-lead limit, since correlations do not effect the behavior of the distribution very strongly.

An important use of quantum dots is found in the study of chaos [4, 5, 6, 7, 8, 31]. Because one can obtain extremely clean samples and shape them into different forms, it is now possible to fabricate the so-called quantum billiards, where one has a unique chance to study quantum and semiclassical physics [31, 32]. Although the supersymmetry method assumes averaging over disorder, one can conjecture on very firm grounds (the ergodic hypothesis) that it applies quite generally to quantum chaos problems. Therefore, we expect that our results should be able to describe any system where the underlying dynamics is chaotic, regardless as to whether it is diffusive or ballistic

The organization of this chapter goes as follows. In Sec. 2.2 we describe the model used and the basic concepts related to conductance peaks and level widths. The way the numerical simulations were done is explained in Sec. 2.3. Some of the results found in Ref. [25], which initially motivated the present work, are reviewed in Sec. 2.4. The case of two-point leads is treated exactly in Sec. 2.5 and the case of many-point leads, under the approximation of independent point fluctuations, is left to Sec. 2.6. Finally, in Sec. 2.7 we draw our conclusions and point out some experimental consequences of our work.

2.2   Formulation of the problem

The electronic system we consider is formed by noninteracting spinless fermions confined to a small region through some strong confining potential. The system is probed by two leads, which described by discrete sets of points that are weakly coupled to

the system. More precisely, we have the Hamiltonian [25, 33]

$$H = -\frac{\nabla^2}{2m} + U(r) + \frac{i}{2\pi\mathcal{N}}\left[\alpha_R \sum_{r_R \in A_R} \delta(r - r_R) + \alpha_L \sum_{r_L \in A_L} \delta(r - r_L)\right] , \qquad (2.1)$$

where $U(r)$ is the potential (containing the effect of disorder and confining walls) and $\mathcal{N} = 1/(V\Delta)$ is the mean density of states, with V denoting the total volume and Δ the average level spacing. The term inside the brackets represents the contact leads, denoted by $A_{R,L}$, and $\alpha_{R,L}$ are the dimensionless coupling parameters. The indices R and L stand for right and left leads, respectively.

In a situation characteristic of scattering experiments, when $\alpha_{R,L} \gg 1$ and the leads are open, the number of channels is equal to the number of wavelengths which fit into the lead cross section. As we shall demonstrate, for the weakly coupled leads of a *closed* quantum dot, the distinction between point-like (single-channel) and multichannel leads is more subtle and deserves a careful analysis.

When tunneling through the leads in totally suppressed ($\alpha_{R,L} = 0$) the energy levels have zero intrinsic width. The levels will gain a small but finite width if the coupling to the leads is made very weak, i.e., if $0 < \alpha_{R,L} \ll 1$. As one can show by first order perturbation theory, the broadening will be caused by local fluctuations of the electron wavefunction in the regions of contact with the leads. Calling the total level width Γ_ν, we have

$$\Gamma_\nu = \gamma_{\nu,R} + \gamma_{\nu,L} , \qquad (2.2)$$

with the partial level widths given by

$$\gamma_{\nu,k} = \alpha_k \left(\frac{V\Delta}{\pi}\right) \sum_{r_k \in A_k} |\psi_\nu(r_k)|^2 \qquad (k = R, L) , \qquad (2.3)$$

where ψ_ν is a single-particle eigenfunction of the Hamiltonian (2.1) for $\alpha_{R,L} = 0$.

The knowledge of the statistical properties of $\gamma_{\nu,k}$ is crucial to describe some important and measurable effects in quantum dots. From the distribution of level widths we can extract the distribution of conductance peaks in the resonance regime. It is rather simple to understand why: Let us assume that the conductance at a given energy E can be evaluated through the Landauer-Büttiker formula [23, 24],

$$G(E) = \frac{2e^2}{h} \frac{\alpha_R \alpha_L}{(\pi\mathcal{N})^2} \sum_{r_R \in A_R} \sum_{r_L \in A_L} \left|\sum_\nu \frac{\psi_\nu^*(r_R)\psi_\nu(r_L)}{E - \varepsilon_\nu + i\Gamma_\nu/2}\right|^2 , \qquad (2.4)$$

where ε_ν is the eigenvalue associated with the eigenfunction ψ_ν. In the resonance regime ($\Gamma_\nu, T \ll \Delta$), only the eigenstate whose energy is the closest to E significantly contributes to the conductance. $G(E)$ is very small when E is between adjacent energy levels, and grows rapidly when $E \to \varepsilon_\nu$. Therefore, at a peak of the conductance, we have

$$G_\nu = \frac{2e^2}{h} \frac{4\alpha_R \alpha_L}{(\pi\mathcal{N}\Gamma_\nu)^2} \sum_{r_R \in A_R} \sum_{r_L \in A_L} |\psi_\nu(r_R)|^2 |\psi_\nu(r_L)|^2 . \qquad (2.5)$$

10

Using the last equation, plus Eqs. (2.2) and (2.3), we obtain the Breit-Wigner formula

$$G_\nu = \frac{2e^2}{h} \frac{4\gamma_{\nu,R}\gamma_{\nu,L}}{(\gamma_{\nu,R} + \gamma_{\nu,L})^2} \; ,$$

(2.6)

which is correct at zero temperature, or when $T \ll \alpha_{R,L}\Delta$. In order to describe a wider range of temperatures, we have to use instead the well-known relation

$$G_\nu = \frac{2e^2}{h} \int \frac{d\epsilon}{4T} \frac{\gamma_{\nu,R}\gamma_{\nu,L}}{\epsilon^2 + (\gamma_{\nu,R} + \gamma_{\nu,L})^2/4} \cosh^{-2}\left(\frac{\epsilon}{2T}\right) \; .$$

(2.7)

Call N be the number of points in each lead. When the leads are placed very far apart, the connection between the distribution of level widths, $P_N(\gamma_{\nu,k})$, and the distribution of conductance peaks, $R_N(g_m)$, is given by the convolution

$$R_N(g_m) = \int_0^\infty d\gamma_{\nu,R} P_N(\gamma_{\nu,R}) \int_0^\infty d\gamma_{\nu,L} P_N(\gamma_{\nu,L}) \; \delta\left(g_m - G_\nu h/2e^2\right) \; .$$

(2.8)

From Eq. (2.7) we can extract another limit, which occurs when the temperature exceeds the intrinsic energy level width, $T \gg \alpha_{R,L}\Delta$, but is still low enough so that there are well-resolved resonance peaks ($T \ll \Delta$). In fact, this intermediate regime is typical of some experiments [4] and is described by the Hauser-Feshbach formula

$$G_\nu = \frac{2e^2}{h} \left(\frac{\pi}{2T}\right) \frac{\gamma_{\nu,R}\gamma_{\nu,L}}{\gamma_{\nu,R} + \gamma_{\nu,L}} \; .$$

(2.9)

In practice, one can generate many peaks in the conductance by varying the energy E (i.e., by sweeping the gate voltage in the quantum dot), or, else, by varying some external parameter, say, a magnetic field. Similarly, in numerical calculations one can apply a Aharonov-Bohm flux ϕ to the system, and then generate a family of curves $\varepsilon_\nu(\phi)$ that yields a random sequence of conductance peaks $G_\nu(\phi)$. As long as the system is ergodic, all these procedures are equivalent to the construction of an ensemble of different realizations of disorder (in the case of a diffusive regime) or boundaries (if the regime is ballistic).

2.3   Numerical simulation

Before we move to the analytical calculations, let us describe the numerical simulation of a disordered quantum dot carried out to illustrate the main points of our work (the results of these simulations will be shown and discussed togethet with the analytical ones). Our motivation was to obtain the histogram $P_N(\gamma)$ for $N \geq 2$ as a function of the separation between the points within the lead. We used a two-dimensional Anderson model of noninteracting spinless electrons with nearest-neighbor hopping

and diagonal disorder, i.e., the Hamiltonian

$$H_A = -\sum_{\langle i,j \rangle} (c_i^\dagger c_j + c_j^\dagger c_i) + \sum_{i=1}^{N} w_i \, c_i^\dagger c_i \; , \qquad (2.10)$$

with w_i uniformly distributed in the interval $[-W/2\,,W/2]$. We restricted our calculations to only one realization of $\{w_i\}$; hence, no average over disorder was performed. On the other hand, we imposed quasiperiodic boundary conditions to the electrons by making the geometry toroidal and introducing Aharonov-Bohm phases in the hops,

$$c_i^\dagger c_j \longrightarrow c_i^\dagger c_j e^{-i\phi_{ij}} \; , \qquad (2.11)$$

where ϕ_{ij} assumes one of two values, ϕ_x or ϕ_y, depending on whether the hop occurs along the x or y axis, respectively. By varying ϕ_x and ϕ_y within the interval $(0,\pi)$ we obtained a large set of states, thus creating the statistical ensemble needed to construct the histograms.

For a given set of phases ϕ_x and ϕ_y the Hamiltonian was diagonalized through standard procedures and all eigenstates obtained. The leads were then chosen as sets of sites placed throughout the grid, such that we could probe the density fluctuations at different regions of the dot. Notice that the leads were passive objects, which did not affect the eigenstates.

Briefly, we mention the existence of a technical complication, intrinsic to simulations of quasiperiodic systems, which is the crossover with respect to time-reversal breaking. The threshold for breaking time-reversal symmetry with Aharonov-Bohm fluxes is proportional to the conductance of the system [34]. If the disorder is too strong or the system too small, a complete time-reversal symmetry breaking may never be achieved due to the periodic nature of fluxes. As a result, in order to fall into the class of the unitary ensemble and be able to compare the simulations with the calculations to follow, we needed to work with a large grid (32×23) and keep the disorder very low. The system was then maintained marginally diffusive ($W \approx 1$).

2.4 Point-like leads

We will consider first the simple case of point-like leads, namely, when the typical size of the contact is smaller than the transversal area λ^{d-1}, where λ is the electron wavelength. In the lattice version of the problem, this certainly happens when the lead consists of a single site. For a chaotic system with broken time-reversal symmetry, the amplitude $v = V|\psi_\nu(r)|^2$ fluctuates according to an exponential distribution. This result follows from the assumption that the components of the eigenfunction are not correlated among themselves and are uniformly distributed [22]. Therefore, by connecting v to the level width γ_k [see Eq. (2.3)] we can write

$$P_1(\gamma_k) = \left(\frac{\pi}{\alpha_k \Delta}\right) \exp\left(-\frac{\pi \gamma_k}{\alpha_k \Delta}\right) \; . \qquad (2.12)$$

12

(To simplify the notation, we will hereafter drop the eigenstate label.) In Fig. 2-1 we have plotted $P_1(\gamma_k)$ obtained from our numerical simulation against Eq. (2.12) for two different regions of the spectrum. The states around the bottom of the band used in the evaluation of the level width distribution were checked to be extended over the entire grid.

If the distance between the right and left leads is much larger than the electron wavelength λ (so that the wavefunction fluctuations at $r_R \in A_R$ and $r_L \in A_L$ are independent), we can use Eq. (2.6) or Eq. (2.9), together with Eqs. (2.8) and (2.12), to evaluate analytically the distribution of conductance peaks for single-point leads, $R_1(g_m)$. This calculation has been recently done in the literature [25, 28]. In Ref. [28], Jalabert, Stone, and Alhassid found an expression for the conductance distribution at intermediate temperatures not only for single-channel leads, but for multichannel ones as well. Their derivation, based on random matrix theory, enabled them to consider the case of time-reversal symmetry, although they were constrained to treat only the case of independent channels. In addition, for simplicity, they treated only the situation of symmetric leads. A similar work is found in Ref. [29], where Stone and Bruus studied the effect of chaotic and regular dynamics in the distribution of conductance peaks.

On the other hand, the authors in Ref. [25] performed their analysis exclusively for the case of broken time-reversal symmetry and point-like leads, but took into account a possible asymmetry between the leads. Since we shall extend their work, we will display and comment on some of their results. For $T \ll \alpha_{R,L}\Delta$ they obtained the following distribution

$$R_1(g_m) = \frac{\theta(1 - g_m)}{2\sqrt{1 - g_m}} \frac{[1 + (2 - g_m)(a^2 - 1)]}{[1 + g_m(a^2 - 1)]^2} \, , \tag{2.13}$$

where the asymmetry parameter a is given by

$$a = \frac{1}{2}\left(\sqrt{\frac{\alpha_R}{\alpha_L}} + \sqrt{\frac{\alpha_L}{\alpha_R}}\right) \, . \tag{2.14}$$

Notice that, according to Eq. (2.14), for $a = 1$ (symmetric leads), the most probable value of g_m is 1. However, for $a > 1$ the distribution begins shifting to lower values of g_m. For $a \gg 1$, the most probable value of g_m tends to zero. This is exactly what one would expect to happen in a resonance tunneling experiment at zero temperature: The conductance is maximum when the barriers are identical.

For the intermediate regime, when $\alpha_{R,L}\Delta \ll T \ll \Delta$, it is convenient to rescale the distribution to obtain [25]

$$\mathcal{R}_1(x) \equiv \frac{\sqrt{\alpha_R \alpha_L}\Delta}{4T}R_1(g_m) = xe^{-ax}[K_0(x) + aK_1(x)] \, , \tag{2.15}$$

where

$$x \equiv \frac{4Tg_m}{\sqrt{\alpha_R \alpha_L}\Delta} \, , \tag{2.16}$$

13

and $K_n(x)$ is the modified Bessel function of order n. Notice that the rescaling of g_m to x and of R_1 to $\mathcal{R}_1$ turned the distribution into a temperature-independent function, whose form depends only on the asymmetry between the leads. We also point out that for both temperature regimes, one has an finite offset in the distribution, i.e., $R_1(g_m \to 0) \neq 0$.

2.5 Two-point leads

In this and the following sections the main goal will be to study the effect of extended leads in the distribution of level widths and conductance peaks. We start by analyzing the situation of two-point leads, where the level width is given by

$$\gamma_k = \frac{\alpha_k \Delta}{\pi}(v_1 + v_2) \ .$$
(2.17)

The amplitudes are defined as $v_j = V|\psi_\nu(r_j)|^2$, $j = 1, 2$. When the points 1 and 2 are far apart ($r = |r_1 - r_2| \gg \lambda$), the amplitudes fluctuate independently and the distribution of level widths is equal to the convolution of the distributions for the isolated amplitudes [see Eq. (2.12)]. Consequently,

$$P_2(\gamma_k) = \left(\frac{\pi}{\alpha_k \Delta}\right)^2 \gamma_k \, \exp\left(-\frac{\pi \gamma_k}{\alpha_k \Delta}\right) \ .$$
(2.18)

Notice that the most probable value of γ_k is not zero, as for the one-point case, but $\alpha_k \Delta / \pi$. This fact by itself signals a strong qualitative change in the distribution. What happens, then, when we move the points closer together, so that $r \approx \lambda$? This question can only be fully answered if we know the joint probability distribution

$$Q_2(v_1, v_2; r) = \left\langle \delta\left(v_1 - V|\psi_\nu(r_1)|^2\right) \delta\left(v_2 - V|\psi_\nu(r_2)|^2\right)\right\rangle \ .$$
(2.19)

However, a simple analysis can be made before one starts seeking the exact form of $Q_2(v_1, v_2; r)$: Since there is no special reason for $Q_2(0, 0; r)$ to be singular if $r \neq 0$, we should have $P_2(\gamma_k \to 0) \propto \gamma_k$. On the other hand, $Q_2(0, 0; 0)$ is apparently singular in order to Eq. (2.12) hold.

The exact calculation of $Q_2(v_1, v_2; r)$ can be performed by the supersymmetry method (see Appendices A and B). The result depends on the symmetry of the Hamiltonian; here we will consider only the case of broken time-reversal invariance (unitary ensemble), which yields [35]

$$Q_2(v_1, v_2; r) = \frac{1}{1 - f^2} \exp\left(-\frac{v_1 + v_2}{1 - f^2}\right) I_0\left(\frac{2f}{1 - f^2}\sqrt{v_1 v_2}\right) \ ,$$
(2.20)

where $f = f(r)$ is the Friedel-like function

$$f(r) \;\; = \;\; \frac{1}{\mathcal{N}} \int \frac{d^d p}{(2\pi)^d} \, e^{-ip \cdot r} \, \delta(p^2/2m - E)$$

14

$$= \begin{cases} J_0(2\pi r/\lambda) & (d = 2) \\[2mm] (\lambda/2\pi r)\sin(2\pi r/\lambda) & (d = 3) \ , \end{cases} \tag{2.21}$$

and $I_0(x)$ and $J_0(x)$ are Bessel functions of order zero. We mention that, by virtue of Eq. (2.21), $Q_2(v_1, v_2; r)$ contains only one length scale, which is λ. This is always correct if $r \ll l$, where l is the mean free path. For $r > l$, $f(r)$ gains an factor of the type $e^{-r/l}$.

The exact expression for the two-point distribution of level widths can be readily calculated:

$$\begin{aligned} P_2(\gamma_k) &= \int_0^\infty dv_1 \int_0^\infty dv_2 \ Q_2(v_1, v_2; r) \ \delta\Big(\gamma_k - (\alpha_k \Delta/\pi)(v_1 + v_2)\Big) \\ &= \left[\frac{\pi}{\alpha_k \Delta f}\right] \exp\left(-\frac{\pi \gamma_k}{\alpha_k \Delta[1 - f^2]}\right) \sinh\left(\frac{\pi \gamma_k f}{\alpha_k \Delta[1 - f^2]}\right) \ . \end{aligned} \tag{2.22}$$

The limit $r \gg \lambda$ (points placed far apart) can be easily extracted from Eq. (2.22) and it agrees with Eq. (2.18). For the opposite limit, $r = 0$, when the points coincide, one gets

$$P_2(\gamma_k) = \left(\frac{\pi}{2\alpha_k \Delta}\right) \exp\left(-\frac{\pi \gamma_k}{2\alpha_k \Delta}\right) \ , \tag{2.23}$$

which is the distribution for a point-like lead with a coupling constant twice as large, as we would expect.

The large fluctuation tail of the distribution tends to an exponential function, just as Eq. (2.12). The correlation between points, however, renormalizes the coupling constant α_k to $\alpha_k[1 + f]$. Notice also the linear behavior at $\gamma_k \to 0$, *for any $r \neq 0$*, consistent with what we anticipated. The slope of the distribution at small widths becomes steeper as the distance between points decreases, but the qualitative aspect is rather independent of f and one can usually approximate $P_2(\gamma_k)$ by Eq. (2.18).

We stress that the main effect of correlation within the lead is that the characteristic number of channels of a lead is not quite accurately given by the cross section divided by the electron wavelength. We can say that there is a crossover between single and double-channel behavior driven by the distance between the points, i.e., by the parameter f.

In Fig. 2-2 we show some distributions of level widths for two-site leads with different site separations obtained from our numerical simulation. One observes that the correlation between sites is small, even for $r = 1$ (in lattice units) and at the low energy portion of the spectrum (where λ is larger than at the middle of the spectrum). This effect, peculiar to the tight-binding model adopted here, can also be visualized in Fig. 2-3, where we have plotted the density autocorrelator as a function of site separation.

Given Eq. (2.22) we can proceed to evaluate $R_2(g_m)$. In analogy to the point-like case, an analytical treatment is viable only for the two temperature regimes $T \ll \alpha_{R,L}\Delta$ and $\alpha_{R,L}\Delta \ll T \ll \Delta$; for T comparable to $\alpha_{R,L}\Delta$, one has to compute the distribution numerically and the dependence on the temperature cannot be rescaled

15

out of the distribution. For simplicity, we will concentrate on the analytical results. We first present the expression we obtained for the resonance conductance distribution in the $T \ll \alpha_{R,L}\Delta$ regime:

$$R_2(g_m) = \frac{\theta(1 - g_m)}{4f^2\sqrt{1 - g_m}} \left\{ \frac{[1 + f^2][1 + (2 - g_m)(a^2 - 1)]}{[1 + g_m(a^2 - 1)]^2} \right.$$
$$- \frac{[1 - f^2][1 + (2 - g_m)(a_+^2 - 1)]}{2[1 + g_m(a_+^2 - 1)]^2}$$
$$\left. - \frac{[1 - f^2][1 + (2 - g_m)(a_-^2 - 1)]}{2[1 + g_m(a_-^2 - 1)]^2} \right\} , \qquad (2.24)$$

where

$$a_\pm = (a \pm f\sqrt{a^2 - 1})/\sqrt{1 - f^2} , \qquad (2.25)$$

and f is defined in Eq. (2.21). In Fig. 2-4 we show $R_2(g_m)$ for different values of f and the asymmetry parameter a. Notice that the most probable value of g_m is maximum when the leads are symmetric, as we have argued in the previous section.

Clearly, by setting $r = 0$ in Eq. (2.24) we recover Eq. (2.13). In the opposite limit, $r \gg \lambda$, we can expand all terms to $O(f^2)$ and obtain

$$R_2(g_m) = \frac{3g_m\theta(1 - g_m)}{4\sqrt{1 - g_m}\,[1 + g_m(a^2 - 1)]^4}$$
$$\times \left\{ [1 + 8a^2(a^2 - 1)] + 2g_m(a^2 - 1)(1 - 4a^2) \right.$$
$$\left. + g_m^2(a^2 - 1)^2 \right\} . \qquad (2.26)$$

The distribution of conductance peaks in the regime $\alpha_{R,L}\Delta \ll T \ll \Delta$ can again be expressed as a universal, temperature independent function if one uses the rescaling shown in Eqs. (2.15) and (2.16). After some straightforward manipulation we obtain

$$\mathcal{R}_2(x) = \frac{x^2}{4f^2} \sum_{p=0}^{3} (-1)^p e^{-a_p x_p} [K_0(x_p) + a_p K_1(x_p)] , \qquad (2.27)$$

where $x_0 = x/[1 + f]$, $x_2 = x/[1 - f]$, $x_{1,3} = x/\sqrt{1 - f^2}$, $a_0 = a_2 = a$, $a_1 = a_+$, and $a_3 = a_-$. In Fig. 2-5 we have plotted $\mathcal{R}_2(x)$ for different values of f and a. When we set $r = 0$ in Eq. (2.27), we recover Eq. (2.15) with coupling constants twice as large. On the other hand, in the limit $r \gg \lambda$, one has, after an expansion to $O(f^2)$,

$$\mathcal{R}_2(x) = \frac{x^2 e^{-ax}}{2} \left[x(a^2 + 1)K_0(x) + (2ax + 2a^2 - 1)K_1(x) \right] . \qquad (2.28)$$

In both temperature regimes, the most notable difference between $R_2(g_m)$ and $R_1(g_m)$ is in the small g_m behavior: $R_2(g_m \to 0)$ is linear in g_m *for any* $r \neq 0$, in contrast to $R_1(g_m)$, which tends to a constant in the same limit. Correlations between points within the leads do not affect the linear dependence.

2.6 N-point leads

Some of the conclusions we have drawn for the two-point lead are straightforward to extend to the N-point case. For instance, let us call $Q_N(v_1, v_2, ..., v_N)$ the joint probability distribution of the amplitudes $v_j = V|\psi(r_j)|^2$ at N points. Then, since $Q_N(0, 0, ..., 0)$ is nonsingular for any arrangement where points do not coincide (i.e., when no two points are completely correlated), we *always* have $P_N(\gamma_k \to 0) \propto \gamma_k^{N-1}$.

Unfortunately, the supersymmetry technique becomes impractical to use in any derivation where $N > 2$. We do not know of any other method suitable for this task either. Therefore, in this section we will simply assume that the point fluctuations within the leads are completely independent, which is certainly correct for small enough values of γ_k or g_m. We will then derive expressions for $P_N(\gamma_k)$ and $R_N(g_m)$ and look at the numerical simulations to gain some insight about the general case, when correlations can be present.

If the amplitudes v_j fluctuate independently, we are allowed to convolute N distributions given by Eq. (2.12) to obtain the distribution of level widths for a N-point lead. In this way, we find that

$$P_N(\gamma_k) = \frac{1}{\Gamma(N)} \left(\frac{\pi}{\alpha_k \Delta}\right)^N \gamma_k^{N-1} \exp\left(-\frac{\pi \gamma_k}{\alpha_k \Delta}\right) , \qquad (2.29)$$

where $\gamma_k = (\alpha_k \Delta / \pi) \sum_{j=1}^N v_j$, and, following our definition, $\langle \gamma_k \rangle = N \alpha_k \Delta / \pi$. In the limit $N \gg 1$ one can check that the distribution becomes Gaussian around $\gamma_k \approx \alpha_k \Delta N / \pi$, with a width proportional to $1/\sqrt{N}$,

$$P_N(\gamma_k) \approx \frac{1}{\sqrt{2\pi N}} \left(\frac{\pi}{\alpha_k \Delta}\right) \exp\left(-\frac{(\gamma_k - \alpha_k \Delta N / \pi)^2}{2\alpha_k^2 \Delta^2 N / \pi^2}\right) . \qquad (2.30)$$

The results of our simulations for $N = 4$, 9, and 16 are shown in Fig. 2-6 for two different lead geometries and for extended eigenstates around the bottom of the energy band. The deviation from Eq. (2.30) becomes substantial for large N when the lead sites are close together. This indicates that the modest site-to-site correlation (see Fig. 2-3) can add up to make the effective number of channels smaller than the number of sites, particularly for small widths. As we move the sites farther apart, correlations become negligible and the distributions start to agree with Eq. (2.30).

From Eq. (2.29), together with Eqs. (2.6), (2.9), and (2.8), we can proceed to evaluate $R_N(g_m)$. In the very low temperature regime, $T \ll \alpha_{R,L} \Delta$, we obtain

$$
\begin{aligned}
R_N(g_m) &= \left(\frac{g_m}{4}\right)^{N-1} \frac{\Gamma(N)\theta(1 - g_m)}{2\Gamma(N)\sqrt{1 - g_m}\,[1 + g_m(a^2 - 1)]^{2N}} \\
&\times \sum_{k=0}^N \frac{(2N)! a^{2(N-k)}[(a^2 - 1)(1 - g_m)]^k}{(2N - 2k)!(2N + 2k)!} ,
\end{aligned} \qquad (2.31)
$$

which contains all the essential features of R_1 and R_2. In the other regime, where

17

$\alpha_{R,L}\Delta \ll T \ll \Delta$, we obtain, after the appropriate rescaling,

$$\mathcal{R}_N(x) = \left(\frac{x}{2}\right)^{2N-1} \frac{(2N)!e^{-ax}}{\Gamma(N)^2} \left\{ \frac{K_0(x)}{(N!)^2} \right.$$
$$\left. + \sum_{l=1}^{N} \frac{[(\alpha_R/\alpha_L)^{l/2} + (\alpha_L/\alpha_R)^{l/2}]K_l(x)}{(N-l)!(N+l)!} \right\} . \qquad (2.32)$$

One can easily check that Eq. (2.31) becomes equivalent to Eqs. (2.13) and (2.26) for $N = 1$ and $N = 2$, respectively. Similarly, Eq. (2.32) is reduced to Eq. (2.15) for $N = 1$, and to Eq. (2.28) for $N = 2$. We remark that both Eqs. (2.31) and (2.32) yield the same limit $R_N(g_m \to 0) \propto g_m^{N-1}$, i.e., the distributions behave like a power law for small peak heights.

The large N limit makes the distribution of conductance peaks narrower. For instance, when $N \gg 1$, Eq. (2.32) tends to a Gaussian law, centered around $x \sim O(N)$,

$$\mathcal{R}_N(x) \approx \frac{a}{\sqrt{4\pi N}} \exp\left(-\frac{(x - 2N/a)^2}{4N/a^2}\right) . \qquad (2.33)$$

Because $\langle g_m \rangle \sim O(N)$, but $\delta g_m \sim O(\sqrt{N})$, fluctuations in the height of resonance peaks are suppressed for very large leads. This should be contrasted to the universal fluctuations of the conductance as a whole, which obey $\delta g_m/\langle g_m \rangle \sim O(1)$. Furthermore, $\langle g_m \rangle \propto (1/\alpha_R + 1/\alpha_L)^{-1}$, which is the classical result (Ohm's law).

2.7   Conclusions

We have considered the statistics of the widths of electronic states inside a quantum dot coupled to a bulk reservoir through contact leads. It is well-known that in the case of point-like contacts the distribution of widths obeys a universal exponential law, which corresponds to Gaussian fluctuations of the wavefunction. We have shown that the statistics of the widths is strongly influenced by the size of the contact area between the leads and the dot. For two-point contacts we presented the exact expression for the distribution function of widths and found that it closely resembles the result one obtains by assuming no correlation between the points. The correlation effects appear only for large fluctuations, whose contribution to any observable quantity is exponentially small. Following this observation, we suggested that the N-point lead can be considered as a set of N points fluctuating independently. We evaluated the distribution of widths analytically and compared the results with direct measurements from numerical simulations. A good qualitative agreement was found.

The central region of the distribution tends to be Gaussian as N increases. Therefore, the fluctuations in the level width are suppressed for large leads and we can describe the dot in terms of the average parameters. In the region of very large widths, the distribution does not follow a Gaussian law, but rather decays exponentially. For small widths, the distribution behaves as a power law.

For the continuous system with extended leads we can expect a similar behavior.

The distribution of widths is Gaussian around the average, which is proportional to the effective number of channels $N_0 = A/\lambda^{d-1}$, where A is the cross section of the lead contact. The tail of the distribution for very large widths is exponential. In the region of small widths the distribution behaves as

$$P(\gamma_k) \propto \gamma_k^N \; . \tag{2.34}$$

The effective number of channels N is equal to the number of independent "points" in the lead, which increases for small γ_k as $N \propto N_0/\gamma_k$.

The relevance of these results to experiments appears in the determination of the distribution of conductance peaks in the resonance regime. The main consequence of the finite extension of the leads is found in the power law behavior of the distribution at small peak heights. As the lead becomes very large, the distribution tends to a Gaussian law. The possibility of asymmetry between the leads is taken into account in our work. Finally, we point out that Eqs. (2.24) and (2.27) can be used to describe the statistics of four-probe dots where the constrictions are made very narrow (point-like leads).
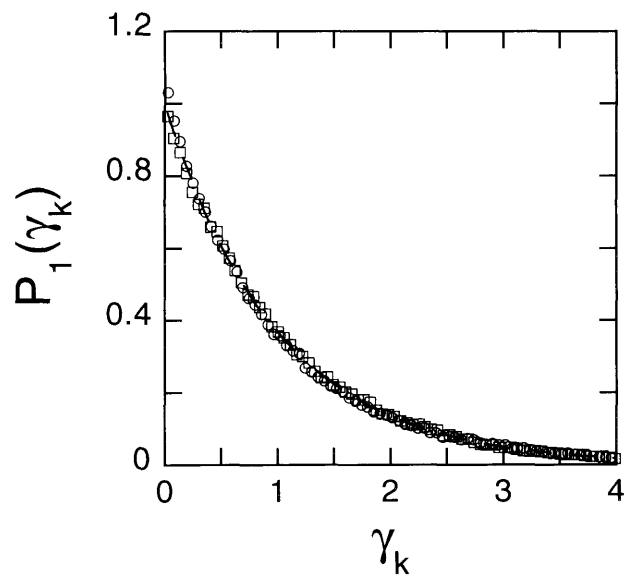
Figure 2-1: Histogram of level widths for single-site leads at two regions of the energy band: middle (circles) and bottom (squares). The dashed line is the universal prediction (exponential law). The level width is rescaled so that $\langle \gamma_k \rangle = 1$. The error bars are smaller than the dot size.
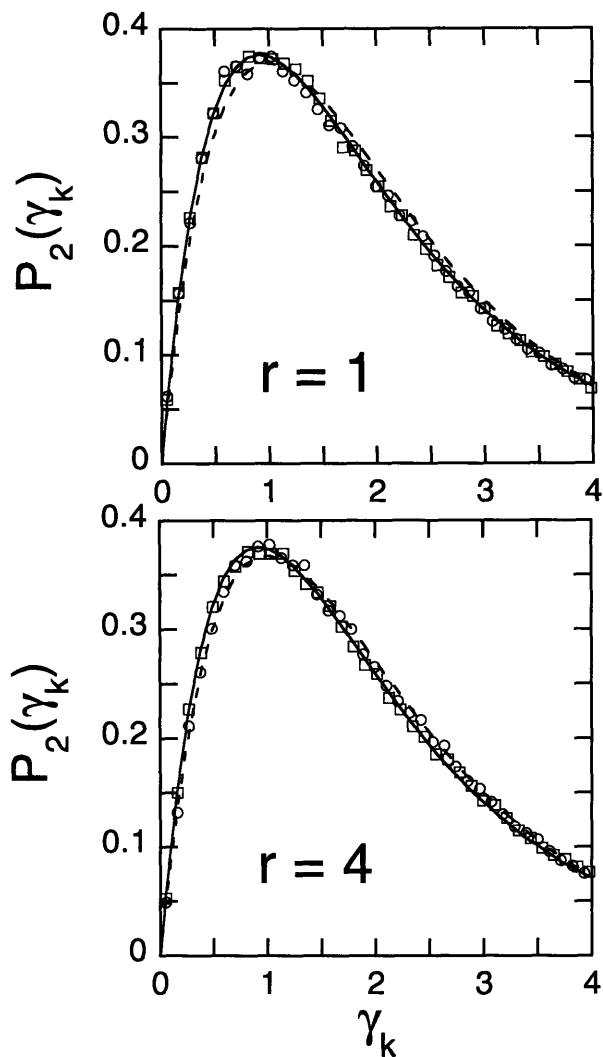
Figure 2-2: Histograms of level widths for two-site leads at two regions of the energy band: middle (squares) and bottom (circles). The level width is rescaled so that $\langle \gamma_k \rangle = 2$. r is the distance in lattice units between sites within the lead. The solid and dashed curves are the predictions for $f = 0.35$ and $f = 0$, respectively. Error bars are smaller than the dot size.
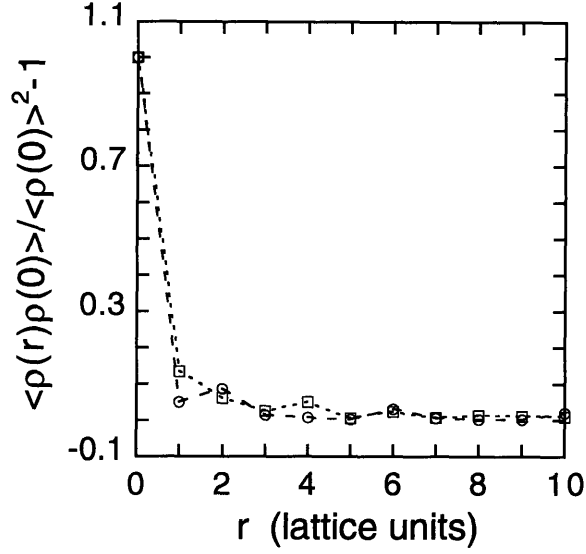
Figure 2-3: Density-density correlator as a function of site separation for two regions of the energy band: middle (circles) and bottom (squares). The density is defined as $\rho(r) = |\psi_\nu(r)|^2$ and the average is performed over ν (eigenstate) and grid location. The error bars are typically of the same order as the dot sizes.

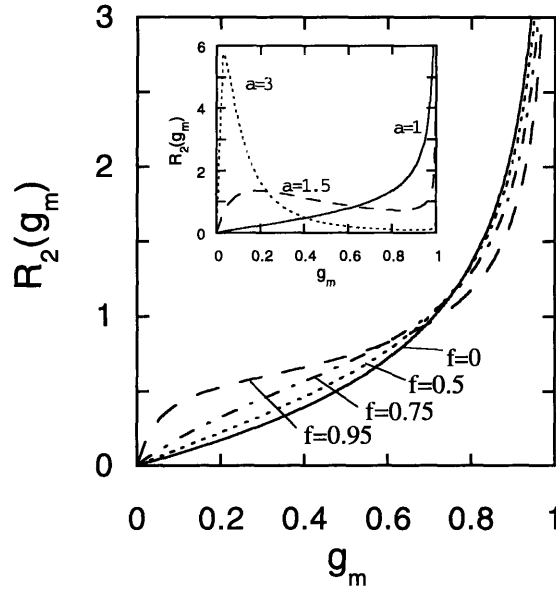Figure 2-4: Distribution of resonance conductance peaks in a dot with two-point leads at very low temperatures ($T \ll \alpha_{1,2}\Delta$). The main plot shows the curves for the symmetric case ($a = 1$) and different separation of lead sites. Notice the liner behavior as $g_m \to 0$ for any $f \neq 1$. The insert shows the dependence with the asymmetry parameter for a fixed distance between sites ($f = 0.5$).
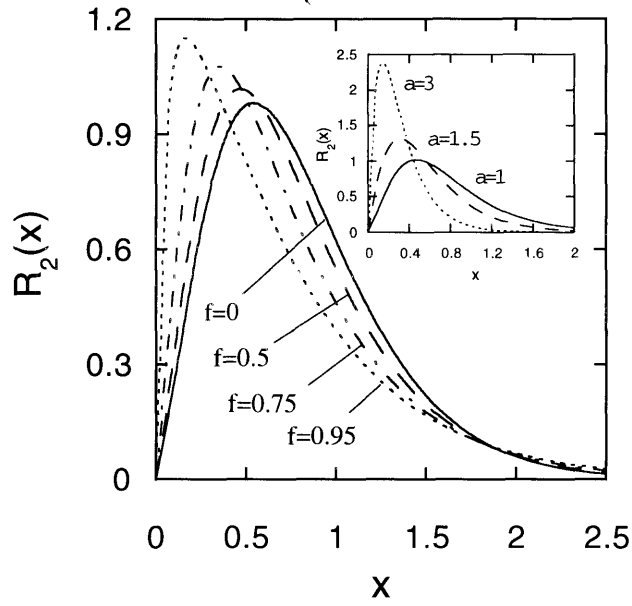
Figure 2-5: Distribution of resonance conductance peaks in a dot with two-point leads at intermediate temperatures $(\alpha_{1,2}\Delta \ll T \ll \Delta)$. The conductance is expressed in the rescaled form $x = 4Tg_m/\sqrt{\alpha_1\alpha_2}\Delta$. The main plot shows the curves at $a = 1$ (symmetric case) and variable distance between the lead sites. The insert shows the dependence on the asymmetry parameter for a fixed $f = 0.5$.
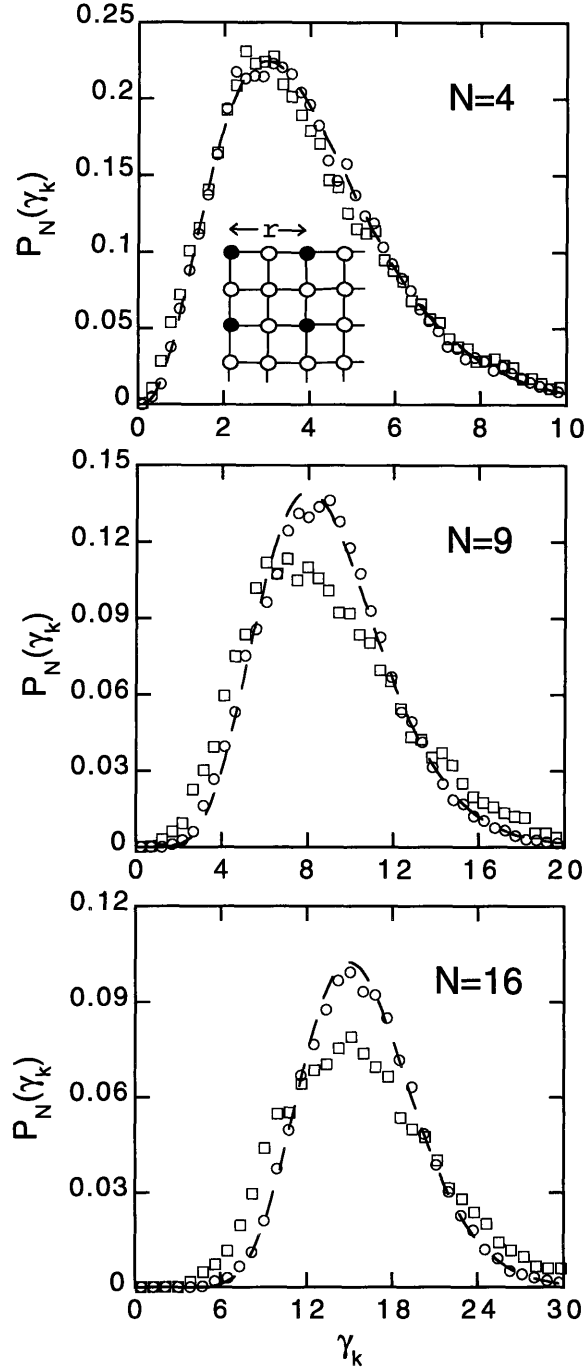
Figure 2-6: Histogram of level widths for N-site leads and for eigenstates at the bottom of the energy band. The level width is rescaled so that $\langle \gamma_k \rangle = N$. The dashed line is the prediction for independent site fluctuations of the wavefunction. The squares correspond to leads where sites were placed together ($r = 1$) and the circles correspond to leads with $r = 3$. As an example, in the insert we show how a $N = 4$ lead with $r = 2$ was implemented. For clarity, error bars are not shown, but the typical size can be inferred by the scattering of the points.

Chapter 3

Exact Dynamical Correlations of the $1/r^2$ Model

3.1 Introduction

The $1/r^2$ system of interacting particles, introduced by Calogero [36] and Sutherland [17, 18], and indeed even earlier by Dyson [37], within a relaxational framework in the course of his discussion of the Brownian motion of Random Matrices, has continued to be of great importance in theoretical physics. In the recent past, it has also generated great interest in the context of a discrete version, i.e., a spin 1/2 model introduced independently by Haldane [38] and Shastry [39], and in terms of its algebraic content [40, 41, 42, 43, 44, 45, 46]; some generalizations have also appeared in the literature [47, 48, 49]. Its interest derives from the combination of beautiful mathematical structure and rich physical phenomena of quantum fluctuations in a low dimensional system (quasi-long-range order, non-Fermi-Liquid behavior, etc.), as well as surprising tractability.

In a recent development in an apparently completely different physical system, namely that of electrons in a random medium, Simons *et al.* [12, 50] have succeeded in computing a certain correlation function depending on two variables, say space and time, and conjectured that this represents the density-density correlation function of the above $1/r^2$ model at three appropriate values of the coupling constant $\beta = 1$, 2, and 4, corresponding to orthogonal, unitary, and symplectic ensembles, respectively. The results are obtained due to a suggested equivalence of the problem to the evolution of energy eigenvalues of a disordered metallic grain subject to an arbitrary perturbation [14, 15, 16] to that of the $1/r^2$ many-body problem. The mapping, performed on the level of the two-point, time-dependent, density-density correlation functions, leads to an explicit exact result for the density-density correlation of the $1/r^2$ model for the above values of the coupling constant. The result, astonishingly enough, is valid at *all length and energy scales*, not just in asymptotic regions. This conjecture has been explicitly confirmed in a recent work by Narayan and Shastry [51], where they established the correspondence between the evolution of the distribution of eigenvalues of a random matrix subject to a random Gaussian

perturbation, and a Fokker-Planck equation which is equivalent to the $1/r^2$ model. At the same time, Simons *et al.* [52] have established a direct connection between the $1/r^2$ model and correlations in the spectra of random matrices through a continuous matrix model.

The excitation spectrum of the $1/r^2$ model is available in great detail from the asymptotic Bethe ansatz (ABA) invented by Sutherland [17, 18, 53]. The picture that arises is that of an underlying gas consisting of quasiparticles obeying Fermi statistics, and interacting weakly with each other through a Hartree-Fock interaction leading to a back flow. This picture indeed gives *all* the excited states of the model. The remaining problem then, is that of an appropriate decomposition of the "bare" particles into "quasiparticles". The explicit knowledge of the correlation functions provides us with an opportunity to describe the intermediate states in $S(q, \omega)$ phenomenologically as combinations of the "quasiparticles", whose energies are available from the ABA. This is analogous to quark spectroscopy in the theory of elementary particles, the ABA quasiparticles and quasiholes are our quarks in the present scheme. We also provide a nontrivial check on the conjecture by comparing the explicitly known functions of the momentum q of the $1/r^2$ model with those obtained by integrating the explicit correlation functions.

The plan of this chapter is as follows. In Sec. 3.2, we define the $1/r^2$ model, and summarize the known information about its moments. The dynamical correlations found in Refs. [12, 50] are summarized and their Fourier transforms given. The small q hydrodynamic limit of these correlators is calculated, and the saturation of the spectrum by a sound like linear mode (i.e. $\omega = sq$) is demonstrated. Sec. 3.3 contains a summary of the results of the asymptotic Bethe ansatz for the $1/r^2$ model, where we write down the dispersion of the effective quasiparticles and quasiholes. In Section 3.4, we rework the expressions for the structure function for the three ensembles into forms wherein the energy conserving δ functions are shown to have a natural interpretation in terms of multi quasiparticle-quasihole pairs. In Sec. 3.5, we discuss the discrete $1/r^2$ model, and display its first three relevant moments explicitly. The similarity to the continuum $1/r^2$ model in terms of the exhaustion of the structure function by "spinons" at low q is pointed out, and this is highlighted to be a unique feature characterizing this family of models. In Sec. 3.6, we summarize our results.

3.2   Universal correlation functions applied to the $1/r^2$ model

The Calogero-Sutherland system with periodic boundary conditions has a Hamiltonian describing spinless fermions confined to a ring and interacting through a $1/r^2$ pairwise potential [17, 18]:

$$H = -\sum_{i=1}^{N} \frac{\partial^2}{\partial r_i^2} + \beta(\beta/2 - 1) \sum_{i>j} \frac{(\pi/L)^2}{\sin^2[\pi(r_i - r_j)/L]} . \tag{3.1}$$

For simplicity we have chosen the mass to be $1/2$. The ring has length L and the

number of particles is N. The statistics of the particles can be chosen arbitrarily since the particles cannot get past each other owing to the singular nature of the interaction at the origin; we declare them to be fermions for convenience (they are indeed so at $\beta = 2$), and one might imagine the system to be that of fermions with either repulsive ($\beta > 2$) or attractive ($\beta < 2$) interactions. Unless explicitly specified, we will assume that the system is in the thermodynamic limit ($L \to \infty$ and $N \to \infty$) and has a finite $O(1)$ density ($d = N/L$).

It was first argued in Ref. [12] that the time-dependent correlation functions of this one-dimensional Hamiltonian are equivalent to certain universal correlation functions [14, 15, 16] of the energy spectra of weakly disordered metallic grains when $\beta = 1, 2$, or 4. For spectra subject to some arbitrary perturbation, X, exact analytical expressions were derived for the two-point density correlation function,

$$k(E, X) = \langle \rho(\bar{E} - E, \bar{X} + X)\rho(\bar{E}, \bar{X}) \rangle - \langle \rho(\bar{E}, \bar{X}) \rangle^2 , \qquad (3.2)$$

where $\rho(\bar{E}, \bar{X}) = \sum_{i=1}^{N} \delta\left(\bar{E} - E_i(\bar{X})\right)$ is the density of states of the system and $\langle \cdots \rangle$ denotes a statistical average which can be performed over a range of energy or over X. It was shown that after the following rescaling in which the parameters become dimensionless, $\epsilon_i = E_i/\Delta$ and $x = X\sqrt{\langle[\partial\epsilon_i(X)/\partial X]^2\rangle}$, Eq. (3.2) becomes universal, depending only on the symmetry of the Dyson ensemble. In fact, the universality is not specific to disordered metals but applies equally to all non-integrable or quantum chaotic systems [14, 15, 16].

Remarkably, by performing the change of variables

$$x^2 \equiv -2it, \quad \epsilon \equiv r, \qquad (3.3)$$

where t is the time coordinate and r is the spatial coordinate, Eq. (3.2) becomes equivalent to the two-point particle density correlator of the ground state of the Sutherland model. The coordinate r will be given in units of the mean interparticle distance $1/d$ (although $d \equiv \langle \rho \rangle = 1$, we will continue to display the "d" dependence in order to retain generality). The resulting correlation function, after the change of variables, is

$$k(r, t) = \langle \rho(\bar{r} - r, \bar{t} + t)\rho(\bar{r}, \bar{t}) \rangle - d^2 , \qquad (3.4)$$

with $\rho(r, t) = \sum_{i=1}^{N} \delta\left(r - r_i(t)\right)$. The expectation value $\langle \cdots \rangle$ is to be taken on the ground state of H.

Once we have an expression for $k(r, t)$, we can calculate the dynamical structure factor $S(q, \omega)$ [54]. The explicit connection between $k(r, t)$ and $S(q, \omega)$ is made by taking the space and time Fourier transforms of $k(r, t)$,

$$S(q, \omega) = \frac{1}{2\pi d} \int dr \int dt \, k(r, t) \, e^{-i(qr - \omega t)} .$$

$S(q, \omega)$ has a representation in terms of the excited states of the system:

$$S(q, \omega) \equiv \frac{1}{N} \sum_{\nu \neq 0} |\langle \nu | \rho_q | 0 \rangle|^2 \delta(\omega - E_\nu + E_0) , \qquad (3.5)$$

where $H|\nu\rangle = E_\nu |\nu\rangle$, and

$$\rho_q = \int dr \ \rho(r) \ e^{-iqr} = \sum_{i=1}^{N} e^{-iqr_i} . \qquad (3.6)$$

In the following, we will present exact analytical expressions and discuss some of the properties of $S(q, \omega)$ for the three special values of β.

3.2.1   The moments of $S(q, \omega)$

We begin by stating some important sum rules [54] concerning the function $S(q, \omega)$. Defining the moments of this function as

$$I_n(q) \equiv \int_0^\infty d\omega \ \omega^n \ S(q, \omega) , \qquad (3.7)$$

it follows from the velocity independence of the interaction that

$$I_1(q) = q^2 . \qquad (3.8)$$

This is the statement of particle conservation and is the familiar f-sum rule. Another sum rule follows from the compressibility relation[54]:

$$\lim_{q \to 0} I_{-1}(q) = \frac{1}{s^2} , \qquad (3.9)$$

where $s^2 = 2(\partial P/\partial d)$ is the square of the sound velocity and P is the pressure. However, since $P = -(\partial E/\partial L)$ and for the Sutherland model the ground state energy is known to be $E_0 = (\pi^2 \beta^2/12)(N^3/L^2)$ [17, 18], it follows that Eq. (3.9) can also be written as

$$\lim_{q \to 0} I_{-1}(q) = \frac{1}{\pi^2 d^2 \beta^2} . \qquad (3.10)$$

Finally, we note that the connection between the $1/r^2$ model in the static limit and the distribution of eigenvalues of a random matrix was established by Sutherland in his early papers [17, 18]. Consequently, the zeroth moment, $I_0(q)$ [also called the static form factor and usually denoted by $S(q)$] had been determined before for all three values of β from random matrix theory (RMT) [55]. Therefore, from the results of Ref. [17, 18] we anticipate the following expressions:

$$I_0^u(q) = \frac{1}{2k_F}[|q| + (2k_F - |q|)\theta(|q| - 2k_F)] \qquad (\beta = 2) , \qquad (3.11)$$

$$I_0^o(q) = \begin{cases} \frac{|q|}{k_F}\left[1 - \frac{1}{2}\ln\left(1 + \frac{|q|}{k_F}\right)\right], & |q| < 2k_F \\ 2 - \frac{|q|}{2k_F}\ln\left|\frac{|q|+k_F}{|q|-k_F}\right|, & |q| > 2k_F \end{cases} \quad (\beta = 1), \tag{3.12}$$

and

$$I_0^s(q) = \begin{cases} \frac{|q|}{4k_F}\left[1 - \frac{1}{2}\ln\left|1 - \frac{|q|}{2k_F}\right|\right], & |q| < 4k_F \\ 1, & |q| > 4k_F \end{cases} \quad (\beta = 4). \tag{3.13}$$

For small q we find the limiting behavior

$$I_0(q) \xrightarrow{q \to 0} \frac{q}{\beta k_F}. \tag{3.14}$$

At this point we should also mention that Forrester [56] has presented a formula for the static $S(r)$ [the inverse Fourier transform of $I_0(q)$] for all even values of β in terms of generalized hypergeometric functions. More recently [57] he has shown that one can rewrite his formula in an integral form which allows an asymptotic analysis consisted with Eq. (3.14).

In terms of the three moments given above, we can calculate two characteristic frequencies whose q dependencies give us an idea of the dispersion relations of the excited modes. This approach has been used before by Hohenberg and Brinkman [58] in a different context (that of the isotropic Heisenberg spin chains). Here we name the first frequency the "Feynman spectrum" [59],

$$\omega_{\mathcal{F}}(q) \equiv \frac{I_1(q)}{I_0(q)} = \frac{q^2}{S(q)}, \tag{3.15}$$

which has the small q behavior

$$\omega_{\mathcal{F}}(q) \xrightarrow{q \to 0} \beta q k_F, \tag{3.16}$$

and the second one we call the "hydrodynamical spectrum",

$$\omega_{\mathcal{H}}(q) \equiv \sqrt{\frac{I_1(q)}{I_{-1}(q)}} \xrightarrow{q \to 0} \beta q k_F. \tag{3.17}$$

In Fig. 3-1 we have plotted these dispersion relations for the three values of β for which we know the moments exactly. For the repulsive and noninteracting cases there is a logarithmic dip at $q = 2k_F$, while for the attractive case the dispersion grows monotonically. The appearance of a dip can be interpreted as a tendency towards "crystallization" (i.e. the particles tend to arrange themselves in a lattice with spacing $1/d$) as the strength of the repulsive interaction increases.

3.2.2 Static correlation functions: real space

We note that the static density-density correlations are simply related to the Fourier transforms of the moments $I_0(q)$. Writing the density correlation function in the form

$$k(r,0) = d\ \delta(r) + d^2\ C(r)\ ,\tag{3.18}$$

the dimensionless correlation function $C(r)$ satisfies the relations $\lim_{r\to 0} C(r) \to -1$ and $\lim_{r\to\infty} C(r) \to 0$. It may be written as

$$C(r) = \frac{1}{d}\int_{-\infty}^{\infty}\frac{dq}{2\pi}\cos(qr)[I_0(q)-1]\ .\tag{3.19}$$

The correlation function, in scaled variables, has the representation

$$C(\hat{r}/d) = \int_{-\infty}^{\infty}\frac{d\hat{q}}{2}\cos(\pi\hat{q}\hat{r})[I_0(\hat{q}k_F)-1]\ .\tag{3.20}$$

Explicit expressions are available for the various ensembles from Mehta [60] by noting that $C(r = \hat{r}/d)$ is nothing but the two-level cluster function $-Y_2(\hat{r})$, where $\hat{r}$ is the separation in units of the average interparticle spacing $1/d$.

3.2.3 Dynamical correlations

We now recapitulate the results from Ref. [12, 50] for the dynamical correlation function and present explicit expressions for $S(q,\omega)$. We note that $S(q,\omega)$ is real and positive; moreover, it vanishes for $\omega < 0$ and it depends only on the absolute value of q.

Unitary Ensemble

We will first examine the simplest case when $\beta = 2$ and the system is non-interacting, which corresponds to the unitary ensemble. It can be readily shown that

$$k^u(r,t) = \frac{d^2}{2}\int_1^{\infty}d\lambda_1\int_{-1}^1 d\lambda\,\exp[-ik_F^2 t(\lambda_1^2-\lambda^2)]\cos[k_F r(\lambda_1-\lambda)]\ ,\tag{3.21}$$

where $\lambda = k/k_F$, $\lambda_1 = k_1/k_F$, and $k_F = \pi d$ (k_F is the Fermi momentum). Taking the Fourier transform in both space and time we get

$$\begin{aligned}
S^u(q,\omega) &= \frac{1}{2k_F^2}\int_1^{\infty}d\lambda_1\int_{-1}^1 d\lambda\,\delta(\lambda_1^2-\lambda^2-\omega/k_F^2)\,\delta(\lambda_1-\lambda-|q|/k_F)\\
&= \frac{1}{4k_F|q|}\,\theta(\omega+q^2-2k_F|q|)\,\theta(\omega-q^2+2k_F|q|)\\
&\quad\times\theta(2k_F|q|+q^2-\omega)\ .
\end{aligned}\tag{3.22}$$

In the Fig. 3-2 we have plotted the region of support corresponding to Eq. (3.22), which is nothing but the particle-hole continuum (in this case all excitations are in

the form of pairs). The tridimensional plot of $S^u(q, \omega)$ is shown in Fig. 3-3.

From Eq. (3.22) we can of course compute all the moments of $S^u(q, \omega)$ exactly. The three moments I_1^u, I_0^u, and I_{-1}^u are plotted in Fig. 3-4 and we remark that they are in agreement with the sum rules of Eqs. (3.8,3.10) and the identity Eq. (3.11).

Orthogonal Ensemble

Secondly, we will consider the orthogonal (attractive) case, when $\beta = 1$. This value of the coupling constant leads to a more complicated expression for the two-point correlation function; after Ref. [12], we have

$$
\begin{aligned}
k^o(r, t) &= d^2 \int_{-1}^{1} d\lambda \int_{1}^{\infty} d\lambda_1 \int_{1}^{\infty} d\lambda_2 \, \frac{(1 - \lambda^2)(\lambda_1 \lambda_2 - \lambda)^2}{(\lambda_1^2 + \lambda_2^2 + \lambda^2 - 2\lambda\lambda_1\lambda_2 - 1)^2} \\
&\quad \times \exp[-ik_F^2 t (2\lambda_1^2 \lambda_2^2 - \lambda_1^2 - \lambda_2^2 - \lambda^2 + 1)/2] \\
&\quad \times \cos[k_F r(\lambda_1 \lambda_2 - \lambda)] \,.
\end{aligned}
\tag{3.23}
$$

Taking the Fourier transform of $k^o(r, t)$ in space and time yields

$$
\begin{aligned}
S^o(q, \omega) &= \frac{2q^2}{k_F^4} \int_{1}^{\infty} d\lambda_1 \int_{1}^{\infty} d\lambda_2 \, \frac{[1 - (\lambda_1 \lambda_2 - |q|/k_F)^2]}{(\lambda_1^2 + \lambda_2^2 + q^2/k_F^2 - \lambda_1^2 \lambda_2^2 - 1)^2} \\
&\quad \times \delta(\lambda_1^2 + \lambda_2^2 + q^2/k_F^2 - 1 - \lambda_1^2 \lambda_2^2 - 2\lambda_1 \lambda_2 |q|/k_F + 2\omega/k_F^2) \\
&\quad \times \theta(\lambda_1 \lambda_2 - |q|/k_F + 1) \, \theta(1 - \lambda_1 \lambda_2 + |q|/k_F) \,.
\end{aligned}
\tag{3.24}
$$

The region of support of $S^o(q, \omega)$ is plotted in Fig. 3-5. and it shows a continuum similar to the excitation of a single particle-hole pair in the non-interacting case. However, as we will later discuss in detail, the excited states have a more complex structure. The tridimensional plot of $S^o(q, \omega)$ obtained by numerically integrating Eq. (3.24) and using a Gaussian regularization of the delta function is shown in Fig. 3-6. The ridge along $\omega = q(q + k_F)$ indicates an algebraic (inverse square root) divergence.

The evaluation of I_0^o starting from Eq. (3.24) has been done analytically by Efetov [11] and it can be readily generalized for any I_n^o, $n > 0$. However, we have only been able to evaluate numerically the moments with $n < 0$. The moments I_1^o, I_0^o, and I_{-1}^o are plotted in Fig. 3-7 and they obey exactly the sum rules of Eqs. (3.8) and (3.10), and the identity Eq. (3.12).

Symplectic Ensemble

Finally, we look at the repulsive case, when $\beta = 4$. In the context of RMT this corresponds to the symplectic ensemble. We start with the correlation function originally obtained in Ref. [50],

$$
\begin{aligned}
k^s(r, t) &= \frac{d^2}{2} \int_{1}^{\infty} d\lambda \int_{-1}^{1} d\lambda_1 \int_{-1}^{1} d\lambda_2 \, \frac{(\lambda^2 - 1)(\lambda - \lambda_1 \lambda_2)^2}{(\lambda_1^2 + \lambda_2^2 + \lambda^2 - 2\lambda\lambda_1\lambda_2 - 1)^2} \\
&\quad \times \exp[-4ik_F^2 t (\lambda_1^2 + \lambda_2^2 + \lambda^2 - 2\lambda_1^2 \lambda_2^2 - 1)] \\
&\quad \times \cos[2k_F r(\lambda - \lambda_1 \lambda_2)] \,.
\end{aligned}
\tag{3.25}
$$

We take the Fourier transform of $k^s(r, t)$ to get

$$
\begin{aligned}
S^s(q, \omega) &= \frac{q^2}{64 k_F^4} \int_{-1}^{1} d\lambda_1 \int_{-1}^{1} d\lambda_2 \frac{[(\lambda_1 \lambda_2 + |q|/2k_F)^2 - 1]}{(\lambda_1^2 + \lambda_2^2 + q^2/4k_F^2 - \lambda_1^2 \lambda_2^2 - 1)^2} \\
&\times \delta(\lambda_1^2 + \lambda_2^2 + q^2/4k_F^2 - 1 - \lambda_1^2 \lambda_2^2 + \lambda_1 \lambda_2 |q|/k_F - \omega/4k_F^2) \\
&\times \theta(\lambda_1 \lambda_2 + |q|/2k_F - 1) \, .
\end{aligned}
\tag{3.26}
$$

The region of support of $S^s(q, \omega)$ is shown in Fig. 3-8. The continuum reaches $\omega = 0$ not only at $q = 0$ and $2k_F$, but at $q = 4k_F$ as well. The figure is similar to the one obtained when we excite two particle-hole pairs in the non-interacting case; in fact, the real structure of the excited states is more complicated than this simple picture, as we will later demonstrate. In Fig. 3-9 we show the tridimensional plot of $S^s(q, \omega)$ with a Gaussian regularization and a numerical integration of Eq. (3.26). The ridges along $\omega = 2q(2k_F - q)$ and $\omega = q^2 - 4k_F^2$ indicate an algebraic (inverse square root) divergence.

As for the orthogonal ensemble, the analytical evaluation of I_n^s can be done for $n > 0$ by generalizing the method of Ref. [11] for $n = 0$. For $n < 0$ we have only been able to proceed with a numerical evaluation. In Fig. 3-10 we have plotted the moments I_1^s, I_0^s, and I_{-1}^s. It is simple to check that the moments obtained in this way also agree with Eqs. (3.8), (3.10), and (3.13).

3.2.4 Spectrum saturation in the hydrodynamic limit

An important property of the Sutherland model is the saturation at $q \to 0$. As we have pointed out before in Eqs. (3.16) and (3.17), both the Feynman and hydrodynamical spectra tend to the same value in this limit. In fact, this is also true for any characteristic frequency defined as the ratio of any two moments. We shall prove it for the orthogonal ensemble: In Eq. (3.24) we change variables to

$$
\lambda_{1,2} = 1 + x_{1,2},
$$

which yields

$$
\begin{aligned}
I_n^o(q) &= \frac{2q^2}{k_F^4} \left(\frac{k_F^2}{2} \right)^{n+1} \int_0^\infty dx_1 \int_0^\infty dx_2 \frac{[1 - (1 + x_+ + x_1 x_2 - q/k_F)^2]}{[q^2/k_F^2 - x_1 x_2 (4 + x_1 x_2 + 2x_+)]^2} \\
&\times \left[-\frac{q^2}{k_F^2} + \frac{2q(1 + x_+ + x_1 x_2)}{k_F} + x_1 x_2 (4 + x_1 x_2 + 2x_+) \right]^n \\
&\times \theta(2 + x_+ + x_1 x_2 - q/k_F) \, \theta(q/k_F - x_+ - x_1 x_2) \, ,
\end{aligned}
\tag{3.27}
$$

where $x_\pm = x_1 \pm x_2$. This last expression can be much simplified in the limit $q \to 0$; it becomes

$$
I_n^o(q) \xrightarrow{q \to 0} \frac{2(q k_F)^{n+2}}{k_F^4} \int_0^{q/k_F} dx_1 \int_0^{q/k_F - x_1} dx_2 \frac{(q/k_F - x_+)}{(q^2/k_F^2 - x_+^2 + x_-^2)^2} \, .
\tag{3.28}
$$

32

Changing the integration variables to $x_\pm$ and performing the double integral we obtain

$$I_n^o(q) \xrightarrow{q \to 0} \frac{1}{k_F^2}(qk_F)^{n+1} . \tag{3.29}$$

As a result,

$$\left[\frac{I_{n+m}^o(q)}{I_n^o(q)}\right]_{q \to 0}^{1/m} \to qk_F . \tag{3.30}$$

The proof for the symplectic and unitary ensembles is quite analogous; one obtains for the three values of β

$$I_n(q) \xrightarrow{q \to 0} \frac{1}{\beta^2 k_F^2}(\beta q k_F)^{n+1} \tag{3.31}$$

This yields, for any integers n and m,

$$\left[\frac{I_{n+m}(q)}{I_n(q)}\right]_{q \to 0}^{1/m} \to \beta q k_F . \tag{3.32}$$

The saturation property can also be visualized in Figs. 3-2, 3-5, and 3-8: the fact that the lower and upper branches of parabola have the same linear term as $q \to 0$ implies that all characteristic frequencies must have the same asymptotics.

3.3   Asymptotic Bethe ansatz

We now summarize the results of the asymptotic Bethe ansatz [53], which gives an explicit expression for the "particle-hole" like excitations underlying the system. The *complete* excitation spectrum for the $1/r^2$ model can be described in remarkably simple terms as follows: The total energy of a state of the system is expressible as

$$E = \sum_n p_n^2 , \tag{3.33}$$

with the "pseudomomenta" p_n satisfying the equation,

$$p_n = k_n + \frac{\pi(\beta - 2)}{2L} \sum_{n \neq m} \text{sgn}(k_n - k_m) . \tag{3.34}$$

The total momentum of the state is

$$P = \sum_n p_n = \sum_n k_n . \tag{3.35}$$

The bare momenta are given by $k_n = 2\pi J_n/L$, where the J_n's are fermionic quantum numbers $J_1 < J_2 < J_3 \ldots < J_N$. Note that at $\beta = 2$ the interaction is turned off and we recover the free-fermion results. The important point is that the totality of states for the N particle sector is obtained by allowing the integers J_n to take on all values

consistent with Fermi statistics, not only for $\beta = 2$, but for *all* $\beta \in [1, +\infty)$. The summation in Eq. (3.34) is trivial to carry out and we find

$$p_n = k_n + \frac{(\beta - 2)\pi}{L}\left(n - \frac{N+1}{2}\right) . \tag{3.36}$$

We can now select an arbitrary state of the system by specifying that states $\{k_1, k_2, \ldots\}$ are occupied, i.e. by introducing the fermionic occupation numbers $n(k_j) = 0, 1$, such that

$$E = \sum_n \varepsilon(k_n)n(k_n) + \sum_{n \neq m} v(k_n - k_m)n(k_n)n(k_m) + \left[\frac{\pi(\beta - 2)}{2}\right]^2 , \tag{3.37}$$

with $\varepsilon(k) = k^2$ and $v(k) = \pi(\beta - 2)|k|/2L$. For future reference, the ground state is represented by $n_0(k_n) = 1$ for $|k_n| < k_F$ and $n_0(k_n) = 0$ otherwise, where $k_F = \pi d$. We remark that the above expression of the energy takes the form of a renormalized Hartree-Fock theory; a Hartree-Fock energy expectation value of the interacting Hamiltonian in a determinantal state $\prod c_{k_j}^\dagger |0\rangle$ leads to precisely this type of expression. Note that the Fourier transform of the two-body interaction can be deduced from the expansion

$$\left(\frac{\pi}{L}\right)^2 \frac{\beta(\beta - 2)}{\sin^2(\pi r/L)} = -\beta(\beta - 2)\frac{\pi}{L}\sum_q |q|\exp(iqr) .$$

Therefore, Eq. (3.37) states that a Hartree-Fock expression with a renormalization of the coupling constant $\beta(\beta - 2) \longrightarrow 2(\beta - 2)$ leads to the *exact spectrum* of the model.

We now consider the excitation spectrum near the ground state, wherein we excite a particle-hole pair in the free Fermi system and ask what the energy of the interacting system is by including the Hartree-Fock back flow term. From this point onwards we measure all momenta in units of k_F and energies in units of the Fermi energy. Let us suppose that one of the particles described by Eq. (3.37) has initially a momentum k, with $|k| < 1$; we promote it to some state labeled by $k + q$, with $|k + q| > 1$. The energy cost in units of the Fermi energy is equal to

$$\begin{aligned}
\triangle(q, k) &= \varepsilon(k + q) - \varepsilon(k) + 2\sum_{|k'|<1}[v(k + q - k') - v(k - k')] \\
&= q^2 + 2kq + \frac{(\beta - 2)}{2}(2|k + q| - k^2 - 1) ,
\end{aligned} \tag{3.38}$$

and the momentum of this state is simply q. This implies that we can associate a generalized energy corresponding to a particle $\varepsilon_>(k)$ (i.e. $|k| > 1$) and a hole $\varepsilon_<(k)$ (i.e. $|k| < 1$):

$$\begin{aligned}
\varepsilon_>(k) &= k^2 + (\beta - 2)|k| \\
\varepsilon_<(k) &= \frac{\beta}{2}k^2 + \left(\frac{\beta}{2} - 1\right) ,
\end{aligned} \tag{3.39}$$

such that

$$\triangle(q, k) = \varepsilon_>(k + q) - \varepsilon_<(k) \ . \tag{3.40}$$

Note that $\varepsilon_>(k)$ and $\varepsilon_<(k)$ are continuous and have continuous derivatives across the Fermi surface. These expressions for the particle and hole energies look different from the results of Sutherland [53] but their equivalence may be readily checked. We have chosen to label our states by the "bare" momenta "k_n", while Ref. [53] works with the pseudomomenta "p_n"; of course these are in one to one correspondence and so the choice is a matter of convenience.

We will introduce in the usual way, particle operators $A^\dagger(k)$ and hole operators $B^\dagger(k)$ with the convention that the momenta corresponding to these are constrained by $|k| > k_F$ for particles and $|k| \leq k_F$ for holes, with excitation energies

$$\begin{aligned} E_A(k) &= \varepsilon_>(k) - \mu \\ E_B(k) &= \mu - \varepsilon_<(-k) \ , \end{aligned} \tag{3.41}$$

where $\mu \equiv \varepsilon_>(k_F)$ is the "chemical potential". The quasiparticle-quasihole excitation created by the operator $A^\dagger(k+q)B^\dagger(-k)$ then has energy $E_A(k+q)+E_B(-k)$, which of course is equal to $\triangle(k, q)$. Having introduced the underlying fermionic quasiparticles and quasiholes through Eqs. (3.39), we would like to see if the excitations generated by the bare density fluctuation operator ρ_q can be expressed in terms of the latter. One of our objectives then, is to express the excitations of the system probed by the bare density fluctuation operator ρ_q in terms of the quasiparticle and quasihole operators. Recall that in Landau's Fermi Liquid Theory [61] one expresses the bare particles $c(k)$ in a series involving quasiparticles and quasiholes of the form

$$c(k) = \sqrt{z_k}\, B^\dagger(-k) + \sum_{(p,l)} M[k, p, l]\, B^\dagger(p)B^\dagger(l)A^\dagger(-k-p-l) + \ldots, \tag{3.42}$$

where $|k| \leq k_F$, and a similar expansion for particles, where z_k is the quasiparticle residue. The density fluctuation operator $\rho_q = \sum_k c^\dagger(k+q)c(k)$ then has a development in terms of $1, 2, 3, \ldots$ pairs of (quasi) particle-hole excitations. In one dimension, we expect z_k to vanish for arbitrary non-zero interactions, and hence the particle-hole series is expected to be such that the single pair should not appear. The expansions are somewhat non-unique, in view of the fact that we can add an arbitrary number of "zero energy" and "zero-momentum" particle-hole excitations to any given scheme.

3.4 Quasiparticle content of the structure function

For the unitary case there is no interaction and consequently quasiparticles and quasiholes are the same as particles and holes: Eq. (3.38) at $\beta = 2$ exactly describes the spectrum of Fig. 3-2. On the other hand, for the orthogonal and symplectic cases the simple creation of quasi particle-hole pairs cannot account for the whole excitation spectrum. In order to see that in general ($\beta \neq 2$), we begin by considering the

spectrum $(q \times \omega)$ for a particle-hole excitation (Eq. (3.38)), which is the familiar pair spectrum renormalized by the interaction. For a fixed q, the maximum value of ω occurs when $k = 1$: $\omega_{\max} = q^2 + \beta|q|$. The minimum value of ω depends on q: for $|q| < 2$ it occurs when $k = 1 - |q|$; for $|q| > 2$ it occurs when $k = -1$. This results in $\omega_{\min} = \beta|q|(2 - |q|)/2$ for $q < 2$, and $\omega_{\min} = (|q| - 2)[|q| + (\beta - 2)]$, for $q > 2$. The curves bound a continuum that does not agree with the hashed regions of either Figs. 3-5 or 3-8.

We can also promote two quasiparticles from the Fermi sea, instead of just one. The result is that the upper limit for ω is then given by $|q|(|q| + \beta)$ and the lower limits are $\beta|q|(2 - |q|)/2$, $\beta(|q| - 2)(4 - |q|)/2$, and $(|q| - 4)[|q| + 2(\beta - 2)]/2$ (for the intervals $|q| < 2$, $2 < |q| < 4$, and $|q| > 4$, respectively). Again, we note that the continuum bound by these curves is not equal to the hashed region in Fig. 3-8.

Below we recast the expressions for the correlation functions in the various ensembles in terms of new variables, in order to reveal their exact quasiparticle content.

Orthogonal Ensemble: Change of Variables

We now turn to the expression Eq. (3.24) of the structure function. Firstly we change variables and introduce

$$
\begin{aligned}
u &= \lambda_1 \lambda_2 \\
z &= \lambda_1 + \lambda_2 .
\end{aligned}
\tag{3.43}
$$

With this change of variables, we find

$$
S^o(q, \omega) = 2q^2 \int_{\max\{1, q-1\}}^{(1+q)} du \int_{2\sqrt{u}}^{(1+u)} dz \frac{1}{\sqrt{z^2 - 4u}} [1 - (u - q)^2]\delta(E)/D , \tag{3.44}
$$

where

$$
\begin{aligned}
\sqrt{D} &= z^2 + q^2 - (1 + u)^2 \\
E &= \sqrt{D} + 2\omega - 2uq .
\end{aligned}
\tag{3.45}
$$

In the expressions above and hereafter in this section we will set $q > 0$ without loss of generality. We change the integration variable u by defining $k = u - q$, in terms of which the k integration is restricted to $\max\{1 - q, -1\} \leq k \leq 1$, and is immediately recognizable as the momentum of a hole restricted to the Fermi surface with $|k + q|$ restricted to be a particle. The z integration can be conveniently transformed by introducing a "rapidity" variable

$$
z = 2\sqrt{(k + q)} \cosh \theta , \tag{3.46}
$$

and recalling that for the orthogonal case $\varepsilon_>(k) = k^2 - |k|$ and $\varepsilon_<(k) = (k^2 - 1)/2$

[see Eq.(3.39)], so that

$$S^o(q,\omega) = \frac{q^2}{2} \int_{\substack{|k|\le 1 \\ k+q>1}} dk \, \frac{[-\varepsilon_<(k)]}{[\omega - q(k+q)]^2} \int_0^{\ln\sqrt{(k+q)}} d\theta$$

$$\times \delta\left(\varepsilon_>(k+q) - \varepsilon_<(k) - 2(k+q)\sinh^2\theta - \omega\right) . \qquad (3.47)$$

The θ integration can be done simply, and gives the final result

$$S^o(q,\omega) = \frac{q^2}{4} \int_{\substack{|k|\le 1 \\ k+q>1}} dk \, \frac{[-\varepsilon_<(k)]}{[\omega - q(k+q)]^2}$$

$$\times \frac{\theta\left(\omega - \Delta(k,q) + (k+q-1)^2/2\right) \; \theta\left(\Delta(k,q) - \omega\right)}{\sqrt{\Delta(k,q) - \omega} \; \sqrt{\Delta(k,q) + 2(k+q) - \omega}} .$$

$$(3.48)$$

Bethe Quasi Particle-Hole Content: Orthogonal Ensemble

We can rewrite the energy conserving delta function in Eq. (3.47) as $\delta(\varepsilon_>^{(o)}(k+q|\theta) - \varepsilon_<(k) - \omega)$, where $\varepsilon_>^{(o)}(k|\theta) = \varepsilon_>(k) - 2k\sinh^2\theta$. One possible picture suggested then has the excited state particle possessing a "hidden" gauge variable θ, which lies in a limited range, as a hole would, endowed with energy but possessing no "physical momentum". The particle say for $k > 1$ has an energy $\varepsilon_>^{(o)}(k)$ which lies between $\frac{k^2-1}{2}$ and $k^2 - k$. We can also view the excited particle state as a combination of a particle and particle-hole pair, as follows. We write a schematic development for $k \ge 1$

$$c^\dagger(k) \sim \sum_{\frac{1+k}{2}\le p\le k} A^\dagger(p)A^\dagger(k-p+1)B^\dagger(-1) , \qquad (3.49)$$

The excitation energy of this complex is readily seen from Eqs. (3.39) and (3.41) to be $E_A(p) + E_A(k-p+1) + E_B(-1)$, with $\frac{1+k}{2} \le p \le k$. The sum of these three terms reproduces the variation in $\varepsilon_>^{(o)}(k|\theta)$ implied by the rapidity variable. The density fluctuation ρ_q is then seen to be formally a two quasi particle-hole object: writing $c(k) \sim B^\dagger(-k)$, we have

$$c^\dagger(k)c(k-q) \sim \sum_{\frac{1+k}{2}\le p\le k} A^\dagger(p)A^\dagger(k-p+1)B^\dagger(-1)B^\dagger(q-k) , \qquad (3.50)$$

where it is understood here and elsewhere that when two momenta coincide (as they would in, say, $[B^\dagger(-1)]^2$), then these should be separated by the smallest non-zero wave number. The above scheme for the density fluctuation operator $c^\dagger(k)c(k-q)$ is indicated in Fig. 3-11. We may therefore regard the density fluctuation as being built up from a particular set of (non-interacting) pair states consisting of annihilating two particles at momenta $k - q$ and 1, and creating a pair with total momentum $k + 1$, distributed over all possible relative momenta with appropriate form factors.

37

Symplectic Ensemble: Change of Variables

We recall for the symplectic case, the Bethe energies $\varepsilon_>(p) = p^2 + 2|p|$ and $\varepsilon_<(p) = 2p^2 + 1$ [Eq. (3.39)]. We now rewrite Eq. (3.26) using the same variables as in the previous case [Eq. (3.43)]. We find the result breaks up naturally into two pieces S_a and S_b, with the second piece S_b only arising for $q > 2$:

$$S^s(q,\omega) = S_a(q,\omega) + \theta(q-2) \, S_b(q,\omega) \,, \tag{3.51}$$

with

$$S_a(q,\omega) = \frac{q^2}{16} \int_{\max(0,1-q/2)}^1 du \int_{2\sqrt{u}}^{(1+u)} \frac{dz}{\sqrt{z^2-4u}} \, \delta(E_a) \frac{N_a}{D_a} \,, \tag{3.52}$$

and

$$S_b(q,\omega) = \frac{q^2}{16} \int_{\max\{-1,1-q/2\}}^0 du \int_0^{(1+u)} \frac{dz}{\sqrt{z^2-4u}} \, \delta(E_b) \frac{N_b}{D_b} \,, \tag{3.53}$$

where E, N and D are appropriately defined (see below). We write $u = (1+k)/2$ in S_a and $u = (l-1)/2$ in S_b, in terms of which Eqs. (3.52) and (3.53) take a more natural form

$$S_a(q,\omega) = \frac{q^2}{32} \int dk \, n_0(k)[1-n_0(k+q)] \int_{\sqrt{2(1+k)}}^{(3+k)/2} \frac{dz}{\sqrt{z^2-2(1+k)}} \, \delta(E_a) \frac{N_a}{D_a} \,, \tag{3.54}$$

and

$$S_b(q,\omega) = \frac{q^2}{32} \int dl \, n_0(l)[1-n_0(l+q-2)] \int_0^{(1+l)/2} \frac{dz}{\sqrt{z^2+2(1-l)}} \, \delta(E_b) \frac{N_b}{D_b} \,. \tag{3.55}$$

In Eq. (3.54) we further introduce the rapidity variable θ through $z = 8(1+k)\sinh^2\theta$, so as to eliminate the square root in the integrand. The result can be written compactly as follows

$$\begin{aligned}
S_a(q,\omega) &= \frac{q^2}{2} \int_{\substack{|k|\le 1 \\ k+q>1}} dk \, \frac{[\varepsilon_>(k+q)-3]}{[\omega-2q(1+k)]^2} \int_0^{\ln\sqrt{2/(1+k)}} d\theta \\
&\quad \times \delta\left(\triangle(k,q) + 8(1+k)\sinh^2\theta - \omega\right) \,.
\end{aligned} \tag{3.56}$$

We can perform explicitly the rapidity integrals and find the final result

$$\begin{aligned}
S_a(q,\omega) &= \frac{q^2}{4} \int_{\substack{|k|\le 1 \\ k+q>1}} dk \frac{[\varepsilon_>(k+q)-3]}{[\omega-\triangle(k,q)-(k-1)^2+q^2]^2} \\
&\quad \times \frac{\theta\left(\omega-\triangle(k,q)\right) \theta\left(\triangle(k,q)+(k-1)^2-\omega\right)}{\sqrt{\omega-\triangle(k,q)}\sqrt{\omega-\triangle(k,q)+8(1+k)}} \,.
\end{aligned} \tag{3.57}$$

We next turn to the other piece for $q > 2$. With $\alpha \equiv (q-2)$ and introducing the

rapidity variable ϕ through $z = 8(1 - l)\sinh^2(\phi)$, Eq. (3.55) is expressible in the form

$$
S_b(q,\omega) = \frac{q^2}{2} \int_{\substack{|l|\leq 1 \\ l+\alpha>1}} dl \frac{[\varepsilon_>(l+\alpha) - 3]}{[\omega - 2q(l-1)]^2} \int_0^{\ln\sqrt{2/(1-l)}} d\phi
$$
$$
\times \delta \left(\Delta(l,\alpha) + 8(1-l)\sinh^2\phi - \omega \right) f .
\tag{3.58}
$$

Performing the rapidity integration we find

$$
S_b(q,\omega) = \frac{q^2}{4} \int_{\substack{|l|\leq 1 \\ l+\alpha>1}} dl \frac{[\varepsilon_>(l+\alpha) - 3]}{[\omega - \Delta(l,\alpha) - (l+1)^2 + q^2]^2}
$$
$$
\times \frac{\theta\left(\omega - \Delta(l,\alpha)\right) \theta\left(\Delta(l,\alpha) + (l+1)^2 - \omega\right)}{\sqrt{\omega - \Delta(l,\alpha)} \sqrt{\omega - \Delta(l,\alpha) + 8(1-l)}} .
\tag{3.59}
$$

Bethe Quasi Particle-Hole Content: Symplectic Ensemble

The energy conserving delta function in Eq. (3.56) can be rewritten using an effective energy variable $\varepsilon_<^a(k|\theta) = \varepsilon_<(k) - 8(1+k)\sinh^2\theta$, which implies $\omega = \varepsilon_>(k+q) - \varepsilon_<^a(k|\theta)$. The energy $\varepsilon_<^a(k|\theta)$ varies between the limits $2k^2 + 1$ [i.e. $\varepsilon_<(k)$] and $k^2 + 2k$ [i.e. $\varepsilon_<(k) - (k-1)^2$]. It is thus evident that we may interpret $\varepsilon_<^a(k|\theta)$ as an effective hole, i.e a composite object. One possible way to decompose it is to write schematically for the bare annihilation operator a representation as a quasihole plus a quasi particle-hole pair:

$$
c(k) \sim \sum_{k\leq p\leq \frac{k+1}{2}} B^\dagger(p - k - 1)B^\dagger(-p)A^\dagger(1) .
\tag{3.60}
$$

The restriction on the range of p is such that we avoid double counting the pair and have a natural ordering of the two quasiholes. The energy of the effective hole is then $E_B(-p) + E_B(p - k - 1) + E_A(1)$, with the constraint $k \leq p \leq \frac{k+1}{2}$, which from Eqs. (3.39) and (3.41) reproduces the range required by the rapidity variation. Therefore, the operator ρ_q is seen to be formally a two quasi particle-hole object,

$$
c^\dagger(k+q)c(k) \sim \sum_{k\leq p\leq \frac{k+1}{2}} B^\dagger(p - k - 1)B^\dagger(-p)A^\dagger(1)A^\dagger(k+q) .
\tag{3.61}
$$

This scheme for the density fluctuation is illustrated in Fig. 3-11.

In the second piece of S^s [Eq. (3.58)], once again the energy conserving delta function can be rewritten introducing an effective energy variable for the hole $\varepsilon_<^b(l|\phi) = \varepsilon_<(l) - 8(1-l)\sinh^2\phi$, which implies $\omega = \varepsilon_>(l+\alpha) - \varepsilon_<^b(l|\phi)$. The effective hole energy $\varepsilon_<^b(l|\phi)$ varies between $\varepsilon_<(l)$ and $\varepsilon_<(l) - (1+l)^2$, corresponding to a predominantly left moving object, and may be decomposed again into a hole and a particle-hole pair. Schematically we have

$$
c(l) \sim \sum_{\frac{l-1}{2}\leq p\leq l} B^\dagger(-p)A^\dagger(-1)B^\dagger(1 + p - l) .
$$

39

Using the quasienergies Eqs. (3.39) and (3.41) this complex has energy $E_B(p) + E_B(1 + p - l) + E_A(-1)$, with the physical constraint $\frac{l-1}{2} \leq p \leq l$, which reproduces the range implied by the variation of the rapidity. Owing to momentum conservation, we must regard the creation operator $c^\dagger(l + q)$ as $A^\dagger(l + q - 2)$ times a particle-hole pair with energy zero and momentum 2, i.e. $A^\dagger(1)B^\dagger(1)$. We may eliminate a 'zero pair' $A^\dagger(-1)B^\dagger(1)$ and thus obtain the scheme for the density fluctuation operator ρ_q,

$$c^\dagger(l + q)c(l) \sim \sum_{\frac{l-1}{2} \leq p \leq l} A^\dagger(l + q - 2)A^\dagger(1)B^\dagger(-p)B^\dagger(1 + p - l) . \tag{3.62}$$

The term S_b then evidently may be regarded as a two quasi particle-hole object, and is illustrated in Fig. 3-11.

Summarizing, in process (a), we may regard the density fluctuation as being built up from a particular set of (non-interacting) pair states consisting of creating two particles at momenta 1 and $k + q$, and destroying a pair with total momentum $k + 1$, distributed over all possible relative momenta with appropriate form factors. Likewise, in process (b), we may regard the density fluctuation as being built up from a particular set of (non-interacting) pair states consisting of creating two particles at momenta 1 and $l+q-2$, and destroying a pair with total momentum $l-1$, distributed over all possible relative momenta with appropriate form factors.

3.5 Spin 1/2 Heisenberg systems

In this section we will study the moments I_n of the $1/r^2$ spin system. For comparison purposes, we will also briefly review some well-known results for another standard 1/2 Heisenberg antiferromagnetic system, namely the Bethe chain [62]. The Heisenberg spin chain model with a $1/r^2$ interaction was introduced by Haldane [38] and Shastry [39]. It is defined by the Hamiltonian

$$H = J\phi^2 \sum_{i<j} \frac{\vec{S}_i \cdot \vec{S}_j}{\sin^2[\phi(r_i - r_j)]} , \tag{3.63}$$

where $\phi = \frac{\pi}{L}$, $r_i = 0, 1, ..., L - 1$ (L integer), and the spins are 1/2. In this case the natural operators one can use to introduce a dynamical structure function $S^d(Q, \omega)$ are the $\hat{S}_i^z$: we define a "charge operator" $\hat{\rho}_i = (\hat{S}_i^z + 1/2)$ and use (3.5) to write

$$S^d(Q, \omega) \equiv \frac{1}{N} \sum_{\nu \neq 0} |\langle \nu | \hat{S}_Q | 0 \rangle|^2 \delta(\omega - E_\nu + E_0) , \tag{3.64}$$

with E_ν as the energy eigenvalues of the Hamiltonian and the lattice Fourier transform

$$\hat{S}_Q^z = \sum_{j=1}^{L} \hat{S}_j^z e^{-iQr_j} , \tag{3.65}$$

where Q is the lattice momentum $Q = (2\pi/L) \times$ integer. N is the number of spin deviations or the number of hard-core bosons. We set $N = \hat{d}L$, so that $\hat{d} = 1/2$ for half filling. The Fermi momentum is then $k_F = \pi\hat{d}$, and we will scale $Q = \pi\hat{d}\hat{Q}$ in order to compare with the continuum model results.

We cannot calculate $S^d(Q, \omega)$ directly, but we know some moments of this distribution, just as we did for the continuum model. As in the continuum, we restrict ourselves to $n = 0, 1$, and -1.

3.5.1 Static correlation functions and the zeroth moment

We begin with the zeroth moment, or the static structure factor

$$I_0^d(Q) = \int_0^\infty S^d(Q, \omega) \, d\omega. \tag{3.66}$$

There is a remarkable theorem by Mehta and Mehta [63] stating that the static correlation function is identical to that of the repulsive ($\beta = 4$) continuum model in real space. This object was also calculated independently for half filling in Ref.[64], and the result (in Q space) is for the half filled case:

$$I_0^d(Q) = -\frac{1}{2} \ln\left(1 - \frac{|Q|}{\pi}\right), \tag{3.67}$$

in the scheme where we restrict $|Q| \leq \pi$.

The correlation function I_0 is also available from Ref. [63], for *arbitrary* densities $\hat{d} \leq \frac{1}{2}$. The density-density correlator can be written as

$$\langle \hat{\rho}_0 \hat{\rho}_r \rangle = \hat{d}\delta_{r,0} + (1 - \delta_{r,0}) \, \hat{d}^2 \left[1 + D(r)\right], \tag{3.68}$$

in a manner similar to Eq.(3.18). The function D is given [63] explicitly in the thermodynamic limit as

$$D(r) = -\left[\frac{\sin(2\pi r\hat{d})}{2\pi r\hat{d}}\right]^2 + \left(\int_0^{2\pi r\hat{d}} dt \frac{\sin t}{t}\right) \frac{(2\pi r\hat{d})\cos(2\pi r\hat{d}) - \sin(2\pi r\hat{d})}{(2\pi r\hat{d})^2}. \tag{3.69}$$

Using the relation $\hat{S}_i^z = \hat{\rho}_i - \frac{1}{2}$, we find

$$\langle \hat{S}_0^z \hat{S}_r^z \rangle = \frac{1}{4} + \hat{d}(1 - \hat{d})(\delta_{r,0} - 1) + (1 - \delta_{r,0}) \, \hat{d}^2 \, D(r). \tag{3.70}$$

Inverting the Fourier series, we have

$$I_0^d(Q) = 1 + \hat{d} \sum_r \exp(iQr) \, D(r). \tag{3.71}$$

We may convert the sum over r to an integral, remembering that Q and $Q+2\pi \times$integer are equivalent. We will work in the reduced zone scheme $|Q| \leq \pi$, for which two cases

may be distinguished, case (A) $\hat{d} \leq \frac{1}{4}$ and case (B) $\frac{1}{4} < \hat{d} \leq \frac{1}{2}$. The correlations are given for $Q \geq 0$, and may be obtained for negative Q by using the evenness in Q of I_0. For case (A) $\hat{d} \leq \frac{1}{4}$ we find

$$I_0^d(Q) = 1 + \theta(4\pi\hat{d} - Q)A(Q) \tag{3.72}$$

$$A(Q) = \frac{Q}{4\pi\hat{d}} - 1 - \frac{Q}{8\pi\hat{d}} \ln\left|1 - \frac{Q}{2\pi\hat{d}}\right|, \tag{3.73}$$

and for case (B) $\frac{1}{4} < \hat{d} \leq \frac{1}{2}$ we find

$$I_0^d(Q) = 1 + A(Q) + \theta(Q - 2\pi + 4\pi\hat{d}) \, A(2\pi - Q). \tag{3.74}$$

It can be checked for $\hat{d} = 1/2$ that Eq. (3.74) is identical with Eq. (3.67). For $\hat{d} \leq 1/4$, the expression in Eq. (3.73) is identical to the symplectic case Eq. (3.13), apart from a scale factor of $\hat{d}$. Eq. (3.74) is in fact nothing but the Umklapp reduction of the continuation of Eq. (3.73), i.e. Q is allowed to extend up to $4\hat{d}\pi$, and the part beyond π is declared to belong to $Q - 2\pi$, after subtracting unity from the structure function.

The correlation function, in scaled variables, is given by [compare Eq. (3.20)]

$$D(\hat{r}/\hat{d}) = \int_{-1/\hat{d}}^{1/\hat{d}} \frac{d\hat{Q}}{2} \exp(i\hat{Q}\pi\hat{r}) \left[I_0^d(\hat{Q}\pi\hat{d}) - 1\right]. \tag{3.75}$$

The theorem of Mehta and Mehta asserts the equality of the scaled correlation functions for $\beta = 2, 4$ for all integer r, i.e. for $\hat{r} = \hat{d} \times$ integer

$$D(r \to \hat{r}/\hat{d}) = C(r \to \hat{r}/d). \tag{3.76}$$

3.5.2 Other moments

As opposed to the case when particles are in the continuum, the moment $I_1(Q)$ is not interaction independent for a system where the particles sit on a lattice: this is a well-known effect of the lattice systems with interaction [40]. However, we can work out an expression for the $1/r^2$ spin chain, using the usual definition as a double commutator. In the remaining part we will assume that $\hat{d} = 1/2$ and write

$$I_1(Q) = \left\langle \left[[\hat{S}_Q^z, H], \hat{S}_{-Q}^z\right]\right\rangle. \tag{3.77}$$

Calculating the commutator, we find

$$\begin{aligned}
I_1^d(Q) &= \frac{2}{L}\sum_{i,j}(-J_{i,j})\left[1 - \cos\left(Q(r_i - r_j)\right)\right]\langle \hat{S}_i^z \hat{S}_j^z\rangle \\
&= -2J\phi^2 \sum_{r\neq 0} \frac{1}{\sin^2(\phi r)}[1 - \cos(Qr)]\langle \hat{S}_0^z \hat{S}_r^z\rangle. \tag{3.78}
\end{aligned}$$

Using Eq. (3.67), we rewrite this as

$$I_1^d(Q) = \frac{\pi J}{2L} \sum_{|k| \leq \pi} \ln(1 - |k|/\pi) \sum_{r \neq 0} \left[\frac{\phi^2}{\sin^2(\phi r)} \right] [1 - \cos(kr)] \cos(kr). \qquad (3.79)$$

Using the fact that, for $|k| \leq \pi$ [38],

$$\sum_{r \neq 0} \left[\frac{\phi^2}{\sin^2(\phi r)} \right] \cos(kr) = \frac{\pi^2}{3}(1 - 1/L^2) - \pi|k| \left(1 - \frac{|k|}{2\pi} \right), \qquad (3.80)$$

we find with $[k] \equiv (k - 2\pi m)$ $[m$ integer$||[k]| \leq \pi]$

$$
\begin{aligned}
I_1^d(Q) &= \frac{\pi J}{4L} \sum_{|k| \leq \pi} \ln \left(1 - \frac{|k|}{\pi} \right) \bigg[|[Q+k]| + |[Q-k]| - 2|k| \\
&\quad - \frac{1}{2\pi} \{ [Q+k]^2 + [q-k]^2 - 2k^2 \} \bigg].
\end{aligned}
\qquad (3.81)
$$

After turning the sum to an integral, we can integrate the expression and find, for $|Q| < \pi$,

$$I_1^d(Q) = \frac{J\pi^2}{8} \left[1 - \left(1 - \frac{|Q|}{\pi} \right)^2 + 2 \left(1 - \frac{|Q|}{\pi} \right)^2 \ln \left(1 - \frac{|Q|}{\pi} \right) \right]. \qquad (3.82)$$

In the limit $Q \to 0$, we see that $I_1^d(Q) \to JQ^2/4$ but for larger Q there is substantial departure from the pure quadratic behavior of the continuum models Eq. (3.8).

In the hydrodynamic limit the moment $I_{-1}(Q)$ can be obtained from the spin susceptibility χ_{spin}, which is known explicitly [43]:

$$I_{-1}^d(Q) \xrightarrow{Q \to 0} \left[L \left(\frac{\partial^2 E_0}{\partial \mathcal{M}^2} \right)_{\mathcal{M}=0} \right]^{-1} = \frac{\chi_{spin}(Q \to 0)}{L} = \frac{1}{\pi^2 J}, \qquad (3.83)$$

where $\mathcal{M} = (\hat{N}_\uparrow - \hat{N}_\downarrow)/L$ is the magnetization and the operators $\hat{N}_{\uparrow\downarrow}$ count the number of up or down spins in the chain (notice that we have $\hat{N}_\uparrow + \hat{N}_\downarrow = L/2$).

With these moments at hand, we can define characteristic frequencies for the excitation spectrum, in the same way as we did before. The important point is that all those frequencies will have the same value as $Q \to 0$:

$$\frac{I_1^d(Q)}{I_0^d(Q)} \xrightarrow{Q \to 0} \frac{I_0^d(Q)}{I_{-1}^d(Q)} \xrightarrow{Q \to 0} \sqrt{\frac{I_1^d(Q)}{I_{-1}^d(Q)}} \xrightarrow{Q \to 0} J\pi \frac{|Q|}{2}. \qquad (3.84)$$

This means that in the hydrodynamic limit the spectrum is exhausted by the excitations with dispersion relation $\omega = J\pi|Q|/2$ [38, 39]. Although this might be taken as a common feature for continuum systems, this is not so in general, as we shall see below.

43

We notice that, by choosing appropriate energy scale ($J \to \frac{16}{\pi^2}$), the $1/r^2$ discrete spin model moments map exactly onto the continuum symplectic ones for $Q \to 0$. The dimensionless moments are identical in this limit,

$$I_n^d(Q = \pi\bar{q}/2) \xrightarrow{Q\to 0} \frac{1}{k_F^n} \, I_n^s(q = k_F\bar{q}), \qquad (3.85)$$

where the factor of $1/2$ arises from the different normalization in Eqs. (3.5) and (3.64). It would be very interesting to pursue the calculation of more moments at $q > 0$ for both models to check whether the discrete one shares the same unusual characteristics of the continuum ($\beta = 4$) model excitation spectrum.

We now turn to the Bethe chain, which is defined by the Hamiltonian $H = J_B \sum_i \vec{S}_i \cdot \vec{S}_{i+1}$. The literature about this model is very extensive; here, for the sake of briefness, we only refer to contributions related to our discussion. For instance, Hohenberg and Brinkman [58] have studied this model and found that it shows no saturation at $Q \to 0$. Let us describe a simple argument favoring this conclusion. The moments I_1 and I_{-1} for this model are known [58], but not I_0:

$$I_1^B(Q) = \frac{J_B}{4}(2\ln 2 - 1/2)(1 - \cos Q) \,, \qquad (3.86)$$

and

$$I_{-1}^B(Q) \xrightarrow{Q\to 0} \frac{1}{\pi^2 J_B} \,. \qquad (3.87)$$

On the other hand, the spinon spectrum of the Bethe chain is known from Faddeev and Takhtajan's work [65]:

$$\omega_{sp}(Q) = (\pi J_B/2)\sin|Q| \qquad (3.88)$$

(the same dispersion relation had been obtained long before by des Cloizeaux and Pearson [66], but they concluded that the excitation had a three-fold degeneracy, rather than four fold, as shown in Ref. [65]). Therefore, we could look for saturation by the spinon, and hence form the ratio

$$\lim_{Q\to 0}\left[\frac{1}{\omega_{sp}(Q)}\sqrt{\frac{I_1^B(Q)}{I_{-1}^B(Q)}}\right] \approx 1.08706 \,. \qquad (3.89)$$

Consequently, it is clear that the small Q behavior of $S(Q,\omega)$ *is not* exhausted by the spinons in the Bethe chain, unlike in the $1/r^2$ model, where *it is*.

3.6 Conclusions

We have seen that the results of the calculation of Simons *et al* [12, 14, 15, 16, 50] for the dynamical structure function have a representation in terms of the Bethe quasiparticle and quasihole energies. The representation obtained in this work has the character of two particle-hole pairs representing the bare density fluctuation. We

should note, however, that this representation is far from unique, for one thing one may add an arbitrary number of "zero pairs". Also, for example, we could decompose our two holes and a particle as three holes and two particles, by e.g. forcing the momenta of two holes to coincide, and by suitably restricting the momenta. However, it is not possible to decompose the results into those of a single particle-hole pair; our representation in terms of two pairs appears to be minimal in some sense. The striking feature which underlines the dynamical structure factors presented here is the truncation at very low orders of series like Eq. (3.42). Therefore, the excited states for systems with $\beta = 1, 2$, and 4 will always involve a small number of quasi particle-hole pairs.

We have also shown that the discrete model shares the property of saturation of the Feynman sum rule by the lowest mode as $q \to 0$. The static structure function obtained by a direct calculation [64] is shown to be consistent with the older calculation of Mehta's Ref. [63], provided that one interprets the weight outside the Brillouin zone appropriately by umklapping it. The first moment of the discrete model is obtained using the known result for the two-point static correlator, and shows interesting structure and departure from the first moment of the continuum model, and should provide a non trivial check on the structure function of the discrete model. We stress that the saturation of the structure function by the sound modes at small q is a general property characterizing this class of models.

As a final remark, we mention that by the time this work had been completed we learned that Haldane and Zirnbauer [67] have employed the supersymmetry technique to calculate exactly the dynamical structure factor of the $1/r^2$ spin 1/2 chain. They obtained results which are essentially equivalent to ours. Very recently, Haldane [68] has conjectured a generalization of the dynamical density correlations to include the $SU(n)$ spin chain and the Calogero-Sutherland model for integer values of the coupling constant. Since then, at least two groups [69, 70] have been able to prove that this conjecture is indeed correct.
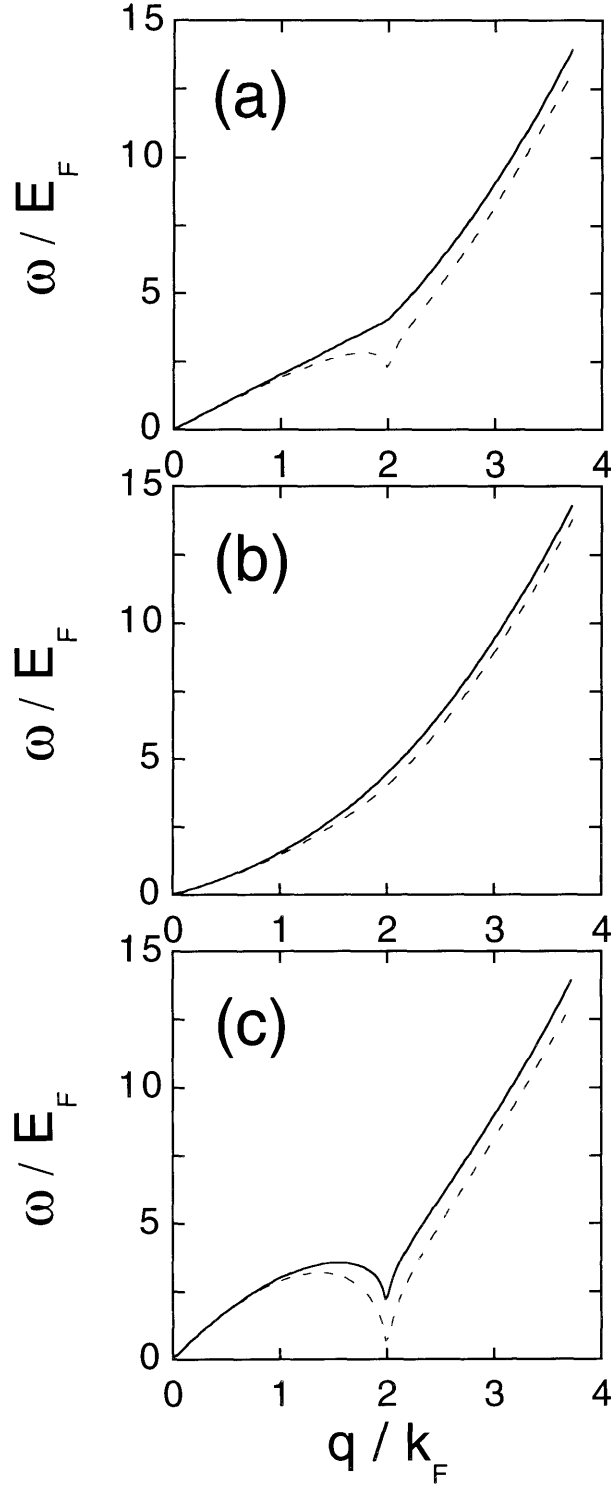
Figure 3-1: Characteristic frequencies of $S(q, \omega)$. The solid line corresponds to the Feynman spectrum $\omega_{\mathcal{F}}(q)$ and the dashed line corresponds to the hydrodynamical spectrum $\omega_{\mathcal{H}}(q)$: (a) $\beta = 2$; (b) $\beta = 1$; (c) $\beta = 4$.
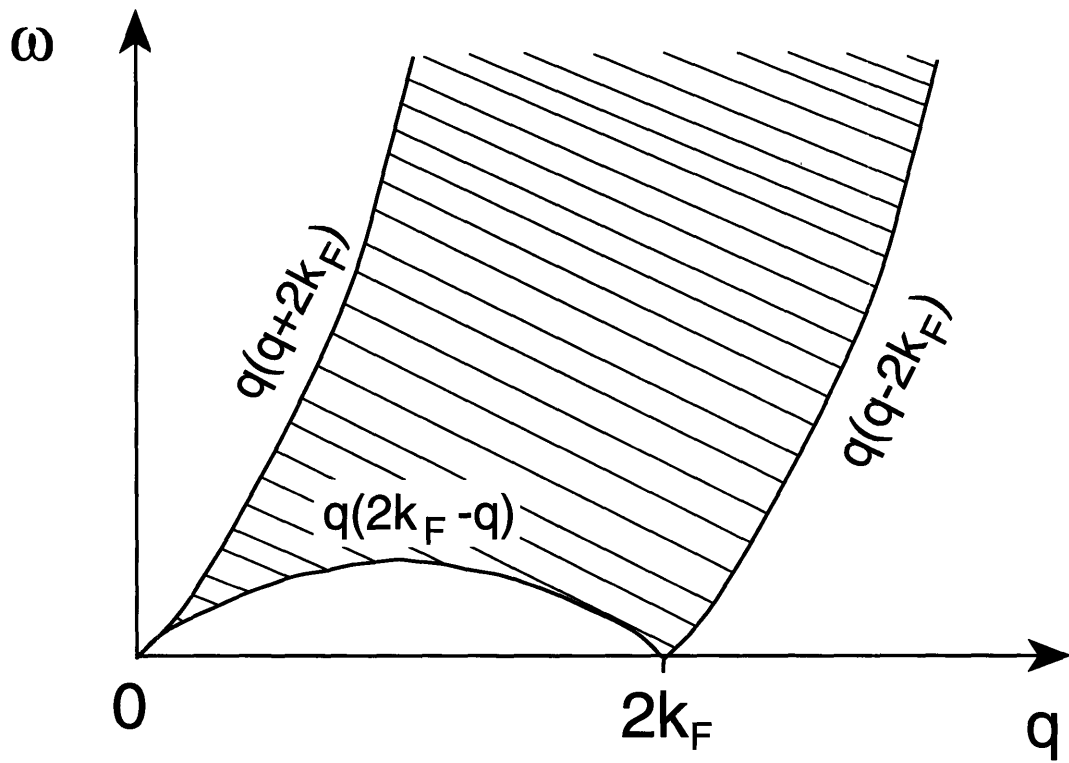
Figure 3-2: Region where $S^u(q, \omega) \neq 0$ ($\beta = 2$). The equations for the boundaries are indicated.
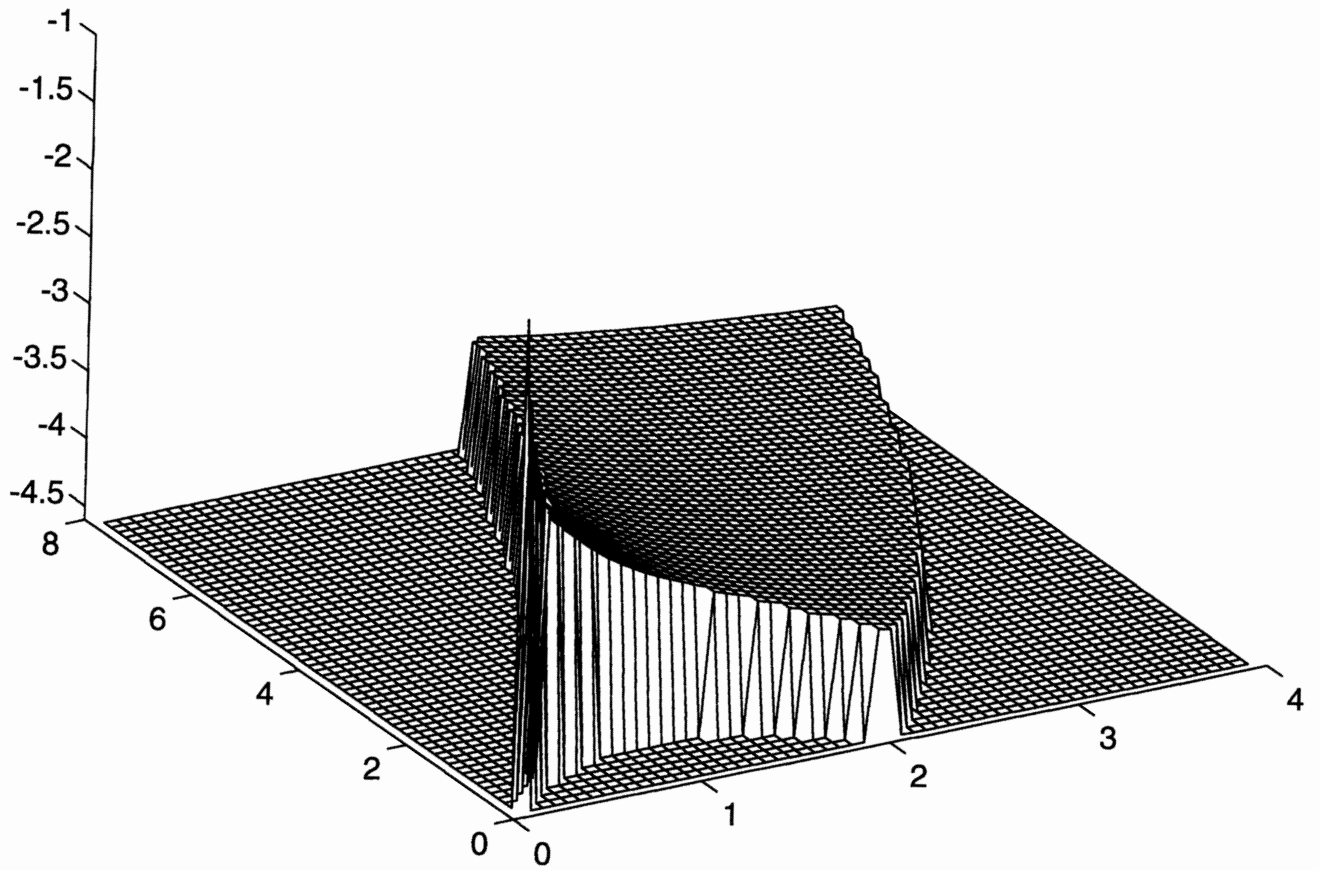
Figure 3-3: Tridimensional plot of $S(q, \omega)$ ($\beta = 2$) for the unitary case. The vertica'
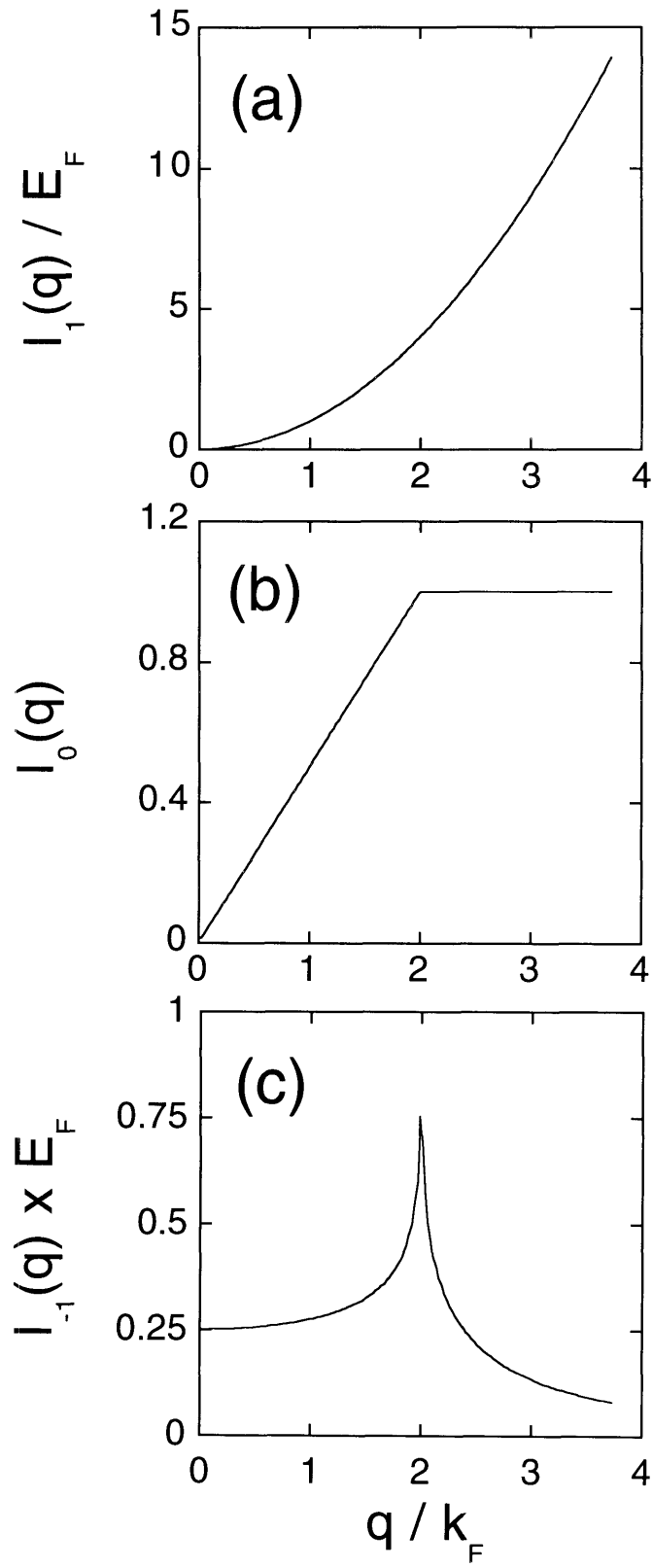axis has a logarithmic scale.

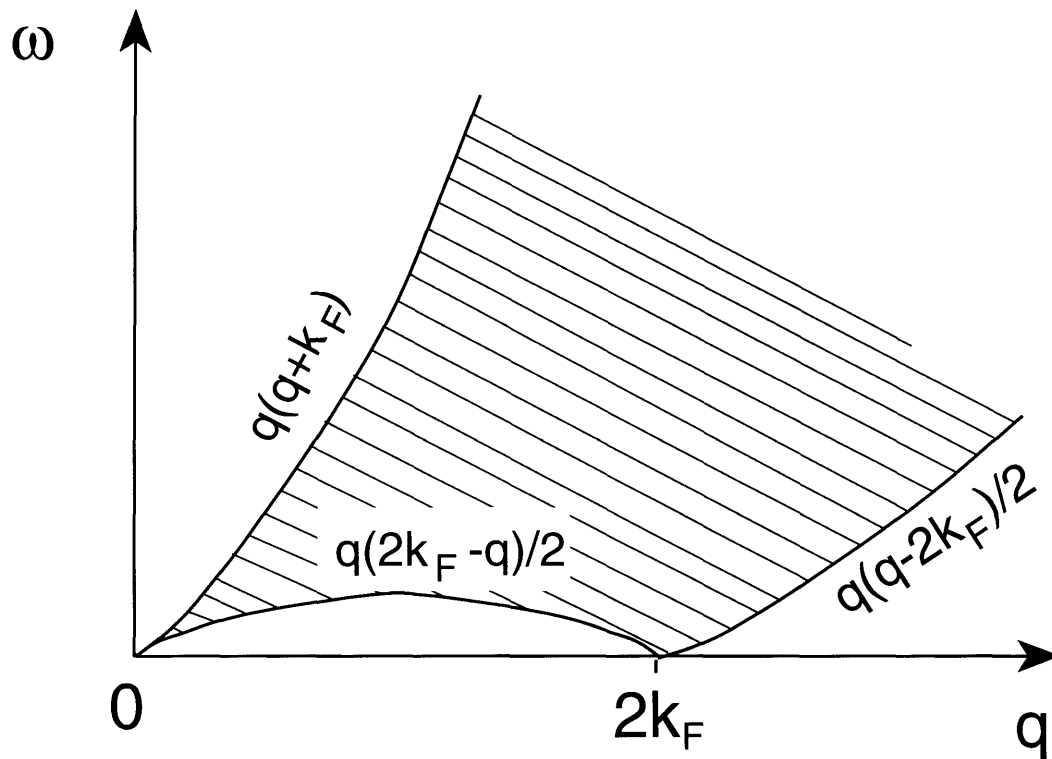Figure 3-4: Moments of $S(q, \omega)$ for $\beta = 2$: (a) $I_1(q)$; (b) $I_0(q)$; (c) $I_{-1}(q)$.

49

Figure 3-5: Region where $S^o(q, \omega) \neq 0$ ($\beta = 1$). The equations for the boundaries are indicated.
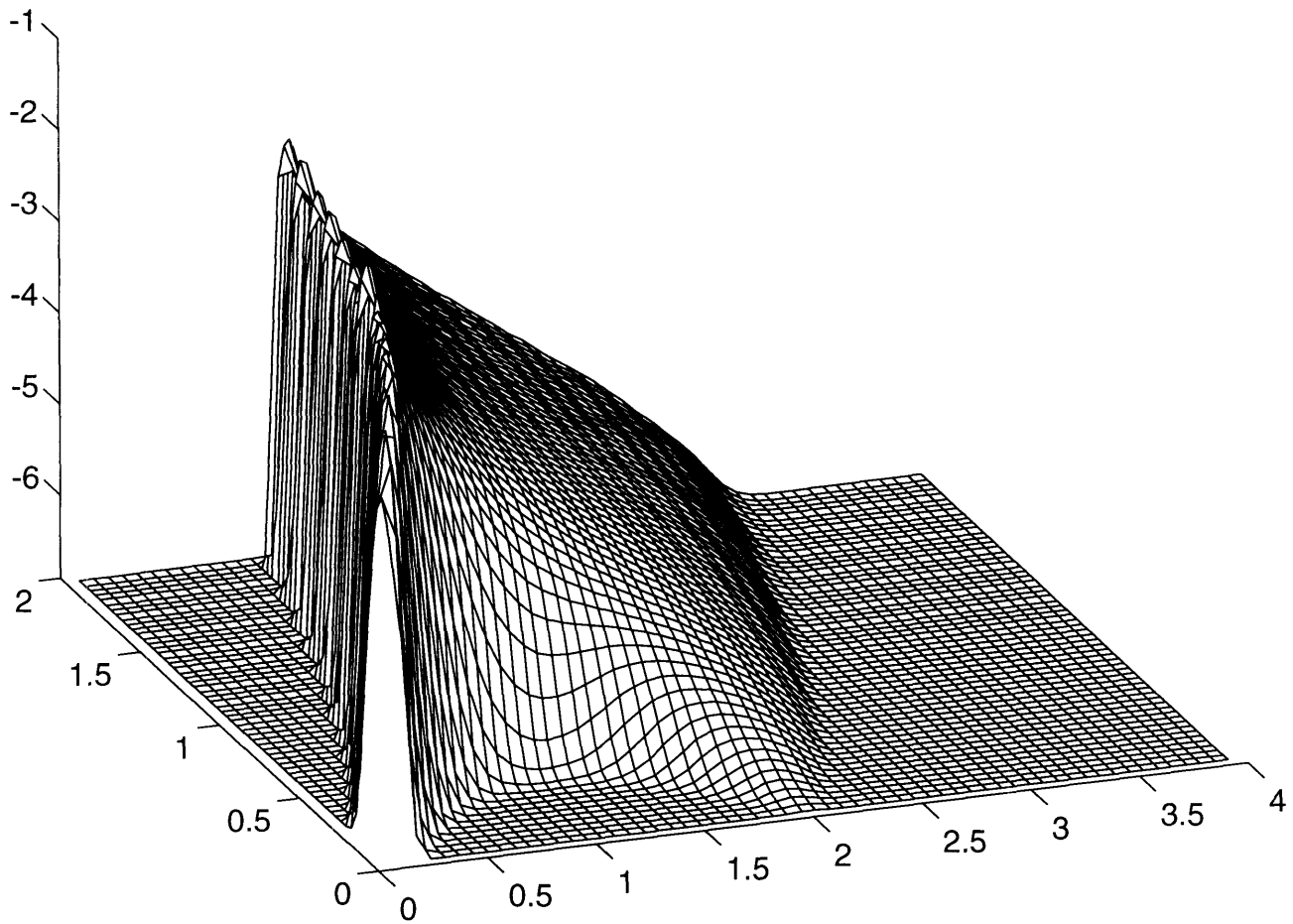
Figure 3-6: Tridimensional plot of $S(q, \omega)$ for the orthogonal case ($\beta = 1$). The delta function of Eq. (3.24) has been regularized by a Gaussian. The vertical axis has a logarithmic scale.
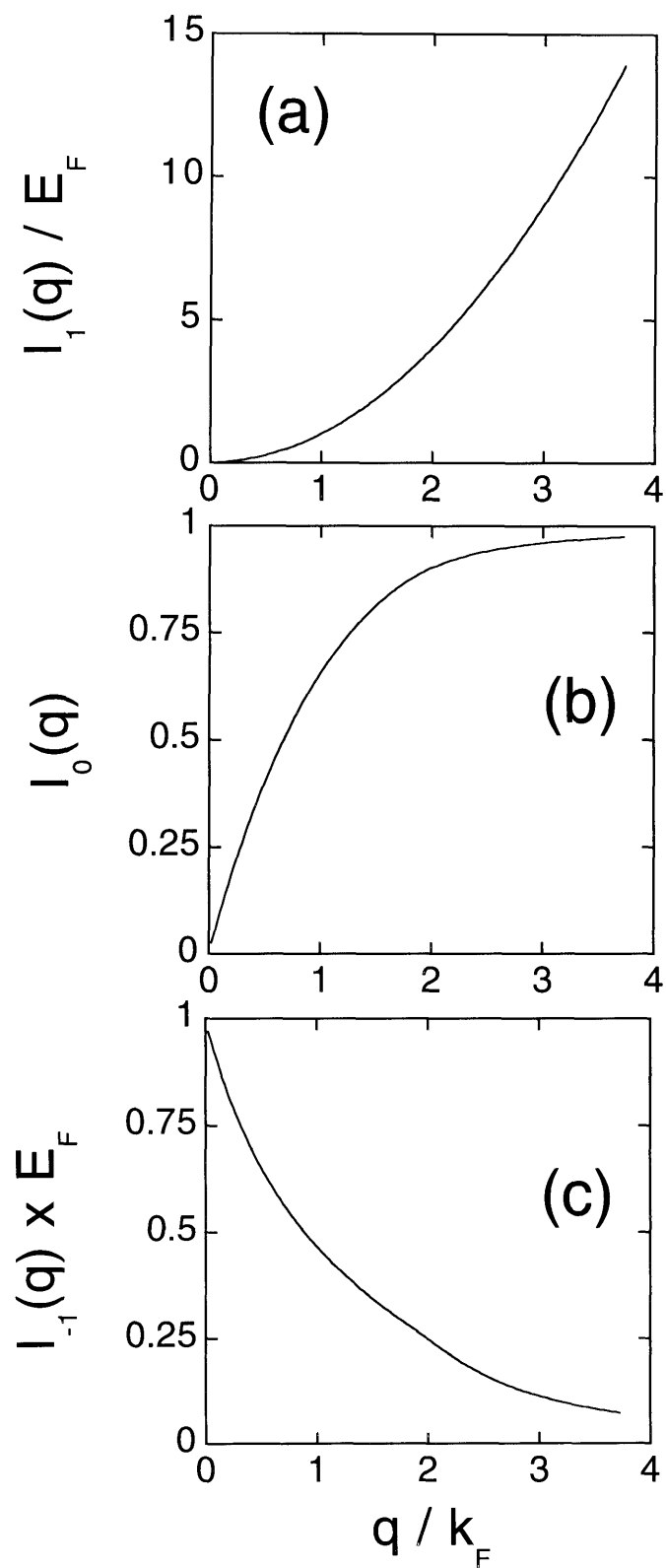
Figure 3-7: Moments of $S(q,\omega)$ for $\beta = 1$: (a) $I_1(q)$; (b) $I_0(q)$; (c) $I_{-1}(q)$.
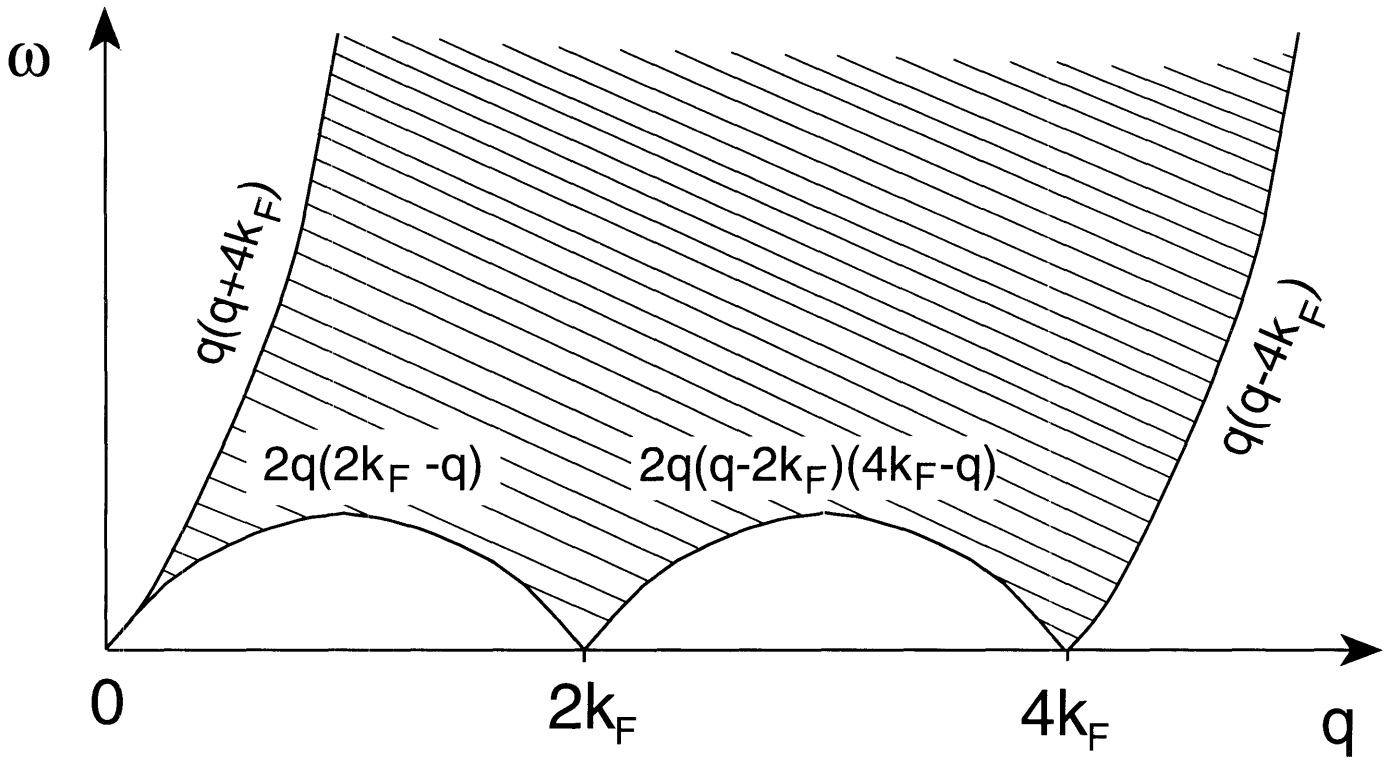
Figure 3-8: Region where $S^s(q, \omega) \neq 0$ ($\beta = 4$). The equations for the boundaries are indicated.
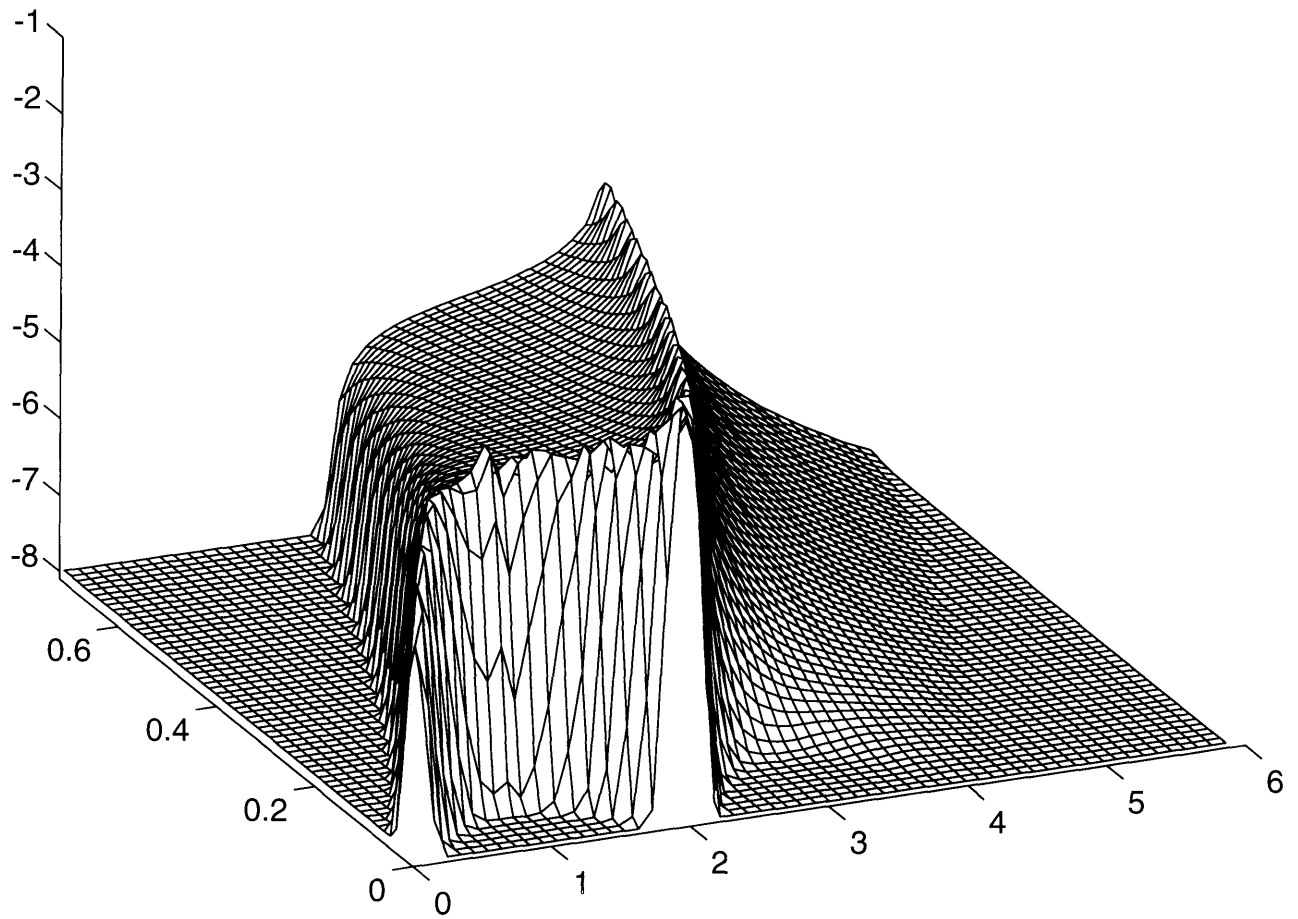
Figure 3-9: Tridimensional plot of $S(q, \omega)$ for the symplectic case ($\beta = 4$). The delta function of Eq. (3.26) has been regularized by a Gaussian. The vertical axis has a logarithmic scale.
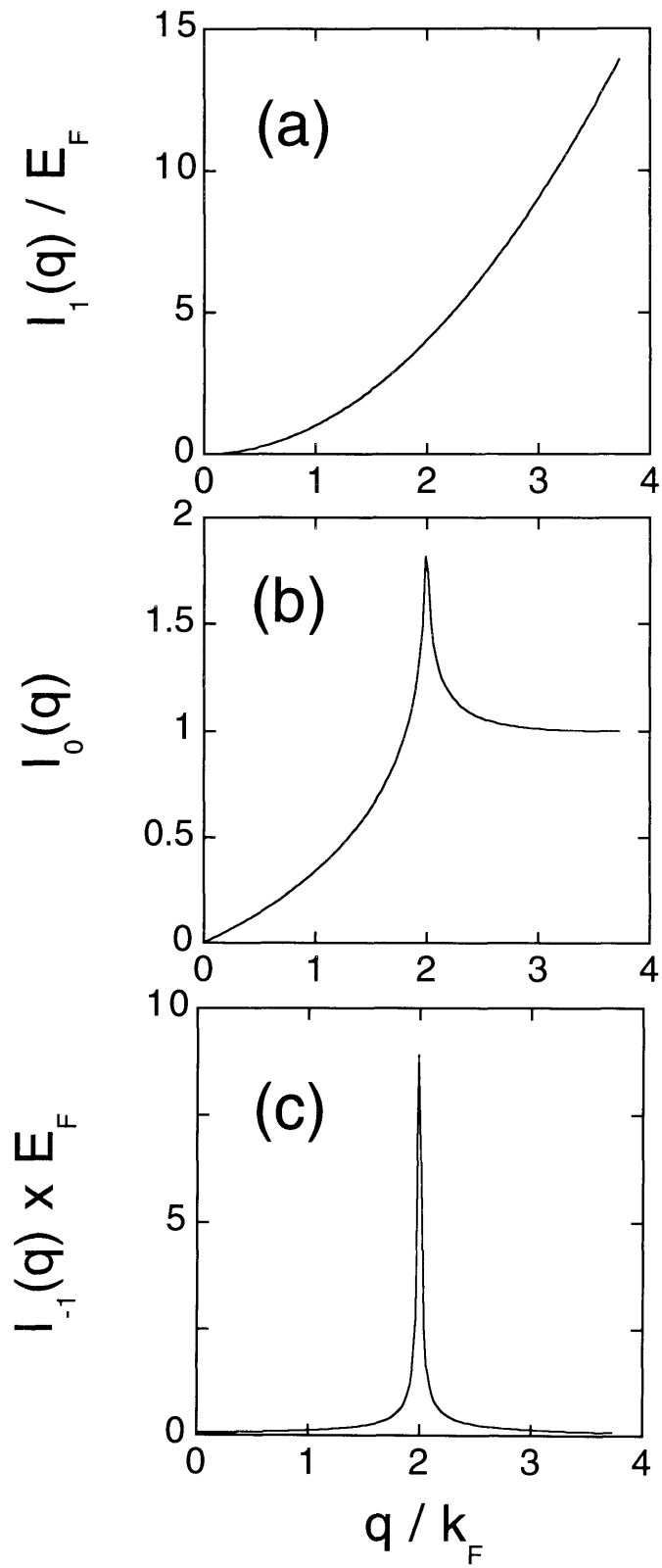
Figure 3-10: Moments of $S(q, \omega)$ for $\beta = 4$: (a) $I_1(q)$; (b) $I_0(q)$; (c) $I_{-1}(q)$.
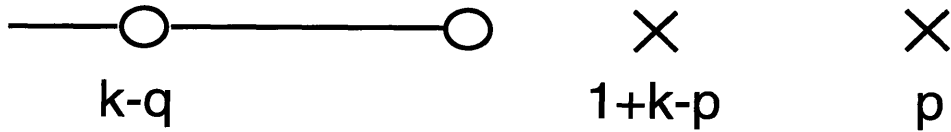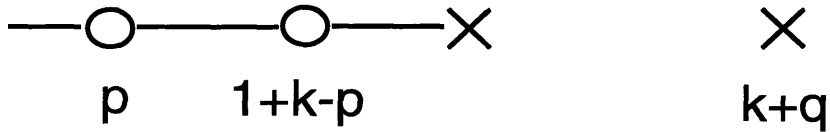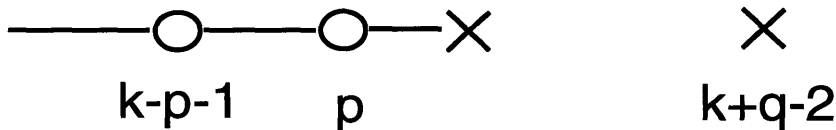
Figure 3-11: The two quasiparticle-quasihole pair scheme for the orthogonal and symplectic cases. $'\times'$ denotes particles and $'\bigcirc'$ denotes holes, and the solid line indicates the range $-1 \leq k \leq 1$, i.e. the Fermi sea ($k_F = 1$). The symplectic ensemble has two pieces: case (a) corresponding to S_a and case (b) corresponding to S_b.

Chapter 4

Manifestation of Quantum Chaos in Electronic Band Structures

4.1   Introduction

The great success of band-structure theory in providing a very accurate description of electronic properties of many materials is a well-established fact. Using few ingredients (such as crystal structure and atomic number), one can obtain a great variety of material-dependent results (optical and transport properties, phonon spectrum, etc.) in very good agreement with the available experimental data. However, the implementation of a realistic band-structure calculation is not a straightforward task and usually requires very complicated numerical algorithms. One is then led to ask whether there is some universal (material-independent) behavior which may lay hidden in the apparent regularity of the bands. The universality should express some common characteristic of the underlying physical systems, in this case crystals. For instance, in the *muffin-tin approximation*, the motion of a valence electron inside a crystal can be pictured as that of a particle in a periodic billiard structure of smooth walls, whose classical dynamics is very likely to be chaotic [20, 71]. If this simple analogy is valid, then one should be able to find in the electronic spectra of real crystals some of the universal signatures of quantum chaos [72, 73].

Quantum chaos occurs when a system exhibits chaotic dynamics in the classical limit. The best way to observe chaos is to break all continuous symmetries, so that the only constant of motion left is the total energy. In this case, we expect the energy spectrum to show some chaotic behavior, as well as some regularities (the so-called clean features). Chaos and discrete symmetries can coexist: one good example is the Sinai billiard [19]. However, discrete symmetries imply the partition of the eigenstates into classes and, consequently, the existence of degeneracies in the spectrum. As we shall see below, lifting these degeneracies usually means removing part of the clean features, resulting in an enhancement of the universalities.

In a crystalline material the translation invariance allows us to reduce the problem to the study of the electron motion in a single unit cell with quasiperiodic boundary conditions. Denoting the periodic part of the single-electron wave function as $u_{\vec{k}}(\vec{r})$,

the Schrödinger equation becomes

$$H_{\vec{k}}\, u_{\vec{k}}(\vec{r}\,) = E(\vec{k})\, u_{\vec{k}}(\vec{r}\,) \ , \qquad (4.1)$$

where $\vec{k}$ is the Bloch momentum and the reduced Hamiltonian is

$$H_{\vec{k}} = -\frac{\hbar^2}{2m}(\, \nabla + i\vec{k}\,)^2 + V(\vec{r}\,) \ . \qquad (4.2)$$

The effective potential $V(\vec{r}\,)$ has all the discrete symmetries (rotation, inversion, reflection, etc.) of the unit cell. The quasiperiodic boundary conditions provide a torus geometry to the unit cell and the Bloch momenta act as Aharonov-Bohm fluxes [74]. Notice that for $\vec{k} = 0$ (at the so-called Γ point) the Hamiltonian is real and time-reversal (T) symmetric. Any $\vec{k} \neq 0$ internal to the Brillouin zone (i.e., which is not equivalent to $-\vec{k}$ by umklapping) breaks T. The potential removes the translational symmetry within the torus, making the problem chaotic.

Normally, one solves Eq. (4.1) for $\vec{k}$ varying along some special symmetry lines of the Brillouin zone and most bands calculated in this way will be degenerate. When we vary $\vec{k}$ away from the planes and lines of symmetry, all discrete symmetries of $H_{\vec{k}}$ are broken and all degeneracies are lifted, resulting in a "spaghetti" of bands (in this work we do not consider spin-orbit coupling or strong magnetic fields and Kramers degeneracy is *always* present). As an illustration, suppose we select a set of bands that are degenerate at the Γ point and then follow them as we move in $\vec{k}$ space. We will notice that the bands split; eventually, some of them may come close together again, but if we do not cross any symmetry line, they will always "repel" (anticross) each other. Therefore, the Bloch momentum can be regarded as an external parameter that drives the system out of the partial integrability of the symmetry points and into a region where the spectrum is chaotic and bands are strongly correlated.

We expect the regions of the spectrum where chaos dominates to be short ranged, since chaos and the consequent universality appear at very long time scales, translating into short energy scales. The clean features, on the other hand, are connected to the classical periodic orbits (short time scale) [71], which do not probe large portions of phase space: They will prevail in regions of the Brillouin zone close to the symmetry points, but can also be visible elsewhere.

We should contrast this view of chaos in crystals whose unit cells are fairly simple (few atoms per unit cell) with the more commonly discussed case of chaos in small disordered metallic grains (quantum dots). When there is no order or symmetry, but the system is small enough for individual energy levels to be distinguishable, it is very natural to study the level repulsion characteristic of quantum chaos and consider its implications to the thermodynamical properties of the system [75, 76]. One can, for example, explore how much disorder is necessary to switch the system from nonchaotic to chaotic and how this crossover takes place [77]. Another idea which so far has only been developed theoretically is the study of chaos in arrays of identical disordered unit cells [20, 21]. The translational invariance in these systems leads to the Hamiltonian of Eq. (4.2) and the same considerations we have just

made for an elementary crystal should apply to the array of identical quantum dots. The only difference in this case is that the unit cell has no discrete symmetry and the spectrum is more likely to indicate strong chaotic dynamics. The clean features which persist in the band structure of the supercrystal will disappear after ensemble averaging.

The traditional diagnostic of quantum chaos derives from the original works of Wigner, Dyson, and Mehta on the theory of random matrices [55], which was initially designed for the study of statistical properties in nuclear physics. They have introduced most of the necessary mathematical tools: level spacing distributions, cluster functions, and several statistics, all focusing on level correlations. When a quantum system is subjected to an external perturbation, there are alternative ways to characterize chaoticity [13, 14, 15, 16, 72, 78, 79, 80, 81, 82]. The parametric correlation functions [13, 14, 15, 16, 81, 82] obtained by this approach are directly related to the transport properties of the system, hence bringing some important physical insight.

In this chapter, we show that an appropriate analysis of energy spectra obtained by band-structure calculations indicates the unambiguous manifestation of quantum chaos in crystalline materials. Here we consider Si as an example of a crystal that can be viewed as a quantum chaotic system with a particularly simple (diatomic) unit cell. Despite the fact that T is broken for an internal $\vec{k}$, the space-inversion symmetry of the Si crystal yields a *false* time-reversal violation [83] and the system is described by the Gaussian orthogonal ensemble (GOE) in the entire Brillouin zone. In contrast to Si, we also study the supercrystal formed by complex $Al_xGa_{1-x}As$ cells. In these systems, chaos can be enhanced by increasing the amount of disorder through changing the concentration x. The lack of inversion symmetry of the unit cell causes T to be quickly broken outside the Γ point and, therefore, the ensemble is unitary (GUE).

4.2 The Silicon band structure and quantum chaos

In order to look for quantum chaos, we have to avoid doing the analysis of the spectrum at the Γ point or at any symmetry point of the Brillouin zone. The effect of setting an internal $\vec{k} \neq 0$ is not just to lift the degeneracies caused by the point symmetries of the unit cell. The Bloch momentum also serves to help increase the statistics by acting as a three-component external parameter. Once we have reached a region in the Brillouin zone where chaos is well developed and regularities are weak, we can tune $\vec{k}$ to generate a large number of spectra and hence facilitate the analysis.

As we have argued in the Introduction, even crystals with fairly simple unit cells should show quantum chaos. In order to verify this prediction, we have performed *ab initio* electronic structure calculations of the Si energy bands. Our calculations were based on the local-density-functional and pseudopotential approximations. Details of the method are presented elsewhere [84]. A plane-wave cutoff of 15 Ry was used in order to ensure a faithful description of the higher bands, which are most likely to show chaotic behavior than the low-lying ones.

The typical band dispersion for Si is shown in Fig. 4-1. The momentum varies

from the Γ point to the boundary of the Brillouin zone, passing by the center of mass (CM) of the irreducible part. Notice the band splitting for $\vec{k} \neq 0$. If the bands are truly uncorrelated, the distribution of band spacings ϵ is Poisson-like [72, 73]: $P(\epsilon) \propto e^{-\epsilon}$ (hereafter we will always express energies in units of the mean band spacing). If any correlation is present, the bands will tend to repel each other and $P(\epsilon \to 0) \to 0$. In Fig. 4-1 we see that several sets of bands that are degenerate at the Γ point remain quite close together and do not seem to interact very much. This is caused by the presence of symmetry lines in the vicinity of the direction we have chosen to plot the bands. Indeed, this "memory effect" is very strong in the band structure of Si and led us to concentrate our analysis at a small region around the CM, which is reasonably far from the Γ point and other symmetry points.

It is clear from Eq. (4.2) that $H_{\vec{k}}$ is neither invariant under T, nor under space inversion (P), in spite of the fact that $V(\vec{r}) = V(-\vec{r})$ for Si. In this case, however, $H_{\vec{k}}$ is invariant under the antiunitary combination TP and this is sufficient to lead to GOE fluctuations, instead of GUE as one might naively expect [83].

The two most popular diagnostics of quantum chaos originally from random matrix theory (RMT) are the nearest-neighbor level spacing distribution $P(\varepsilon)$ and the rigidity of the spectrum, the so-called Δ_3 statistics. There is no expression for $P(\varepsilon)$ in closed form, but, as an excellent approximation, Wigner has proposed the surmise $P(\varepsilon) \propto \varepsilon^\beta e^{-c_\beta \varepsilon^2}$, where $\beta = 1$ and $c_1 = \pi/4$ for GOE, and $\beta = 2$ and $c_2 = 4/\pi$ for GUE. The Δ_3 statistics measures the variance of the number of levels found in an interval of length L [55]:

$$\Delta_3(L) = \frac{1}{L} \left\langle \min_{a,b} \int_{\bar{E}-L/2}^{\bar{E}+L/2} dE \, [N(E) - aE + b]^2 \right\rangle , \qquad (4.3)$$

where $N(E)$ is the number of energy levels below the energy E. The average indicated in Eq. (4.3) is performed over $\bar{E}$ (i.e., over nonoverlaping intervals between $\bar{E} - L/2$ and $\bar{E} + L/2$), but in our study it is also taken over points in $\vec{k}$ space. When the levels are completely uncorrelated (Poisson statistics), we have $\Delta_3(L) = \frac{L}{15}$. In the opposite limit of equally spaced levels, $\Delta_3(L) = \frac{1}{12}$. Sitting in between these two limits are the curves drawn from RMT, which have the $L \gg 1$ asymptotics [55]

$$\Delta_3(L) \approx \frac{1}{\pi^2} \ln(L) - 0.00696 \qquad \text{(GOE)} , \qquad (4.4)$$

and

$$\Delta_3(L) \approx \frac{1}{2\pi^2} \ln(L) + 0.0590 \qquad \text{(GUE)} . \qquad (4.5)$$

In addition to these two quantities, RMT has also a prediction about the density-density (two-point) correlation function [55], here defined as

$$R(\omega) = \langle \rho(\Omega + \omega)\rho(\Omega) \rangle - \langle \rho \rangle^2 , \qquad (4.6)$$

where $\rho(\Omega) = \sum_n \delta(\Omega - \varepsilon_n)$, and $\varepsilon_n = E_n$. The function $R(\omega)$ behaves differently depending on the particular ensemble: For GOE, it is linear close to $\omega = 0$, and then

monotonically saturates to 1 at around $\omega \approx 1$, whereas for GUE it starts as quadratic and then oscillates until it reaches saturation around the same values.

In Fig. 4-2 we compare the statistical properties of the Si spectrum with the RMT predictions. The data was extracted from a set of 80 high-energy eigenvalues corresponding to 343 $\vec{k}$-points (a $7 \times 7 \times 7$ cube) around the CM. Notice the good agreement with the GOE result, in contrast to GUE. The deviation between the data points and the GOE curve for the Δ_3 statistics at large L (Fig. 4-2c) is expected because of the presence of clean features when we consider large portions of the spectrum.

The Bloch momentum can be used as an external, continuous, parameter, allowing us to evaluate "dynamical" universal correlation functions of the spectrum. For this purpose, one needs a scaling parameter, $\sqrt{C_{\mu\nu}(0)}$, which is related to the spectrum response to $\vec{k}$:

$$C_{\mu\nu}(0) = \left\langle \frac{\partial E_n(\vec{k})}{\partial k_\mu} \frac{\partial E_n(\vec{k})}{\partial k_\nu} \right\rangle , \qquad (4.7)$$

where the average is performed over many energy bands (the index n), as well as over $\vec{k}$ points. Because in our study we dealt with correlation over small regions in $\vec{k}$ space, it was a good approximation to assume isotropy, i.e., $C_{\mu\nu}(0) = C(0)$ for all μ, ν. After performing the rescaling $x = \sqrt{C(0)}\, k_\mu$, where μ denotes some direction in $\vec{k}$ space, we evaluated one of the simplest correlation function one can study [13, 14, 15, 16], which is the autocorrelator of crystal velocities,

$$c(x) = \left\langle \frac{\partial \epsilon_n(\bar{x} + x)}{\partial \bar{x}} \frac{\partial \epsilon_n(\bar{x})}{\partial \bar{x}} \right\rangle , \qquad (4.8)$$

It is important to notice that in both Eq. (4.7) and (4.8) the bands $E_n(\vec{k})$ have to be corrected for any possible drift. The way we have proceeded was to estimate the local average drift $\bar{v}_n = \langle \partial E_n(\vec{k})/\partial \vec{k} \rangle$ and then subtract it from the crystal velocities. We have found that $c(x)$ agrees reasonably with the universal form introduced in Ref. [14, 15, 16] for the pure GOE case (see Fig. 4-2d). The small, but visible, discrepancy is understandable: We have used only seven points along each $\vec{k}$ direction and it is difficult to perform a good estimate of $C(0)$ and $\bar{v}_n$ for such a short interval.

4.3   Quantum chaos in the $Al_xGa_{1-x}As$ alloy

In contrast to crystalline materials with simple unit cells, where the existence of symmetries causes partial integrability and the regularities in the spectrum tend to hide the underlying chaotic dynamics, disordered system are the ideal case to study. Classically, the motion of an electrons inside a disordered grain is that of a particle being repeatedly scattered by an irregular potential: The complete lack of symmetries will give rise to a strong chaotic motion. As a result, electronic disordered systems show very clear signatures of quantum chaos and the concept of universality is generally valid. The universal conductance fluctuations in mesoscopics systems [1] are a

good example of a phenomenon related to the chaotic dynamics of the electron in the sample.

If there is one disadvantage of disordered systems over pure crystalline materials, it is the lack of Bloch momenta. From the theoretical view point, the natural way to solve this problem is to impose quasiperiodic boundary conditions to the disordered grain [21] and thus form a superlattice of identical complex unit cells. The band structure of this supercrystal can then be explored much in the same way as we did for Si.

In the analysis that follows we have chosen the widely studied $Al_xGa_{1-x}As$ to demonstrate that it is indeed a good example of a quantum chaotic system and to illustrate the applicability of the parametric correlation functions to characterize quantum chaos. Alloys are a good example of weakly disordered systems when their components do not differ remarkably. If the sample is small enough (mesoscopic), the average level spacing can be resolved experimentally [9] and it makes sense to address the statistical properties of the spectrum. The absence of discrete symmetries in the unit cell guarantees that there are no degeneracies in the spectrum, although some regularities may occurs and they are usually connected to the nonuniversal features carried by the isolated components of the alloy.

Our study of the $Al_xGa_{1-x}As$ supercrystals is based on a semiempirical tight-binding method, with matrix elements taken from the sp^3s^* parametrization suggested by Vogl et al. [85]. Several ensemble realizations of a 216-atom basic cluster were independently generated and solved (the electron wave function was subjected to quasiperiodic boundary conditions). For each realization, Al and Ga atoms were randomly distributed in the group-III sublattice according to the aimed alloy composition. Alloy properties are calculated as ensemble averages for each composition. This method has been successfully used in the study of gap properties of the random $Al_xGa_{1-x}As$ alloy [86].

We begin by calculating the level spacing distribution of $Al_xGa_{1-x}As$ at the Γ point (hence the boundary conditions are periodic) for three different compositions, namely $x \approx 0.1$, 0.3, and 0.5 (note that for $0 < x < 1$ the spectrum is completely nondegenerate). The results for the level spacing distribution are shown in Fig. 4-3. For a given composition x, the averaging is done over high-energy levels and over 20 realizations. Notice that as the disorder increases, we move from a Poisson-like law to a GOE-like, Wigner-Dyson, distribution (remember that at the Γ point there is no T breaking). Another indication of the crossover between weakly to strongly correlated energy levels can be seen in Fig. 4-4, where we have plotted the Δ_3 statistics for the three alloy compositions.

Next we introduce phases to the boundary conditions to obtain the dispersion of the bands with the Bloch momenta. In Fig. 4-5 we show a typical set of bands at the high-energy part of the spectrum for a composition $x \approx 0.5$. As for the case of Si, we restrict our analysis to the region surrounding the CM. The clean features now are fewer and usually related to regularities found in the band structure of $AlAs$ and $GaAs$ [87]; one can be seen in the upper part of Fig. 4-5.

Focusing on the high-energy bands and averaging over nine realizations, we obtain the results shown in Fig. 4-6. Notice the excellent agreement with the GUE predic-

tions. For any Bloch momentum outside the Γ point, T is fully broken and since the unit cell is not invariant under space inversion, we naively expect the statistics to be GUE. In fact, this issue is more subtle. There is a continuous change from GOE to GUE as we move away from the Γ point [73] and the typical range of this crossover will depend on the specific system under study. After the proper rescaling, the crossover should be universal and at least two theoretical investigations based on the supersymmetry technique have demonstrated this point [88, 34]. We have, as yet, not performed an analysis of this crossover for the band structure of the $Al_xGa_{1-x}As$ supercrystal. Nevertheless, we stress that our results show that at the CM the system has already attained the GUE limit.

It is worth to remark on the good agreement between the data for $c(x)$ and the curve obtained in Ref. [14, 15, 16] through numerical simulations (see Fig. 4-6d). The deviation at $x \sim 1$ happens because nonuniversal features dominate the correlation at large distances. We mention that, in principle, we should be able to see the universal behavior of the response function predicted in Ref. [21] by calculating suitable matrix elements of chaotic eigenstates. We leave this subject for future investigation.

4.4 Conclusions

In summary, we have demonstrated that quantum chaos is present in the band structures of Si and of the $Al_xGa_{1-x}As$ supercrystal. We have argued that this should hold true for any crystal because valence electrons exhibit classical chaotic dynamics at the level of the unit cell. The Bloch momentum can be viewed as an external parameter which can be tuned to break the discrete symmetries of the unit cell and revel the quantum chaos hidden in the regularity of the band structure. Any crystal whose unit cell is invariant under space inversion should be described by the GOE statistics. Violation of the inversion symmetry combined with a deviation from the Γ point drives the system to GUE statistics. The parametric correlation functions were shown to be a good diagnostic of quantum chaos, not only for system with complex unit cells, like the supercrystal of $Al_xGa_{1-x}As$, but also for the diatomic unit cell case of Si. The important result of our work is that there exists universality in band structures. The implications of this property to experiments may, however, be limited. For instance, the optical properties of crystals are usually defined by few, low-lying, bands close to the Fermi level, which do not show very strong quantum chaos. One way to increase the complexity of low energy levels is to consider real crystals with polyatomic unit cells.

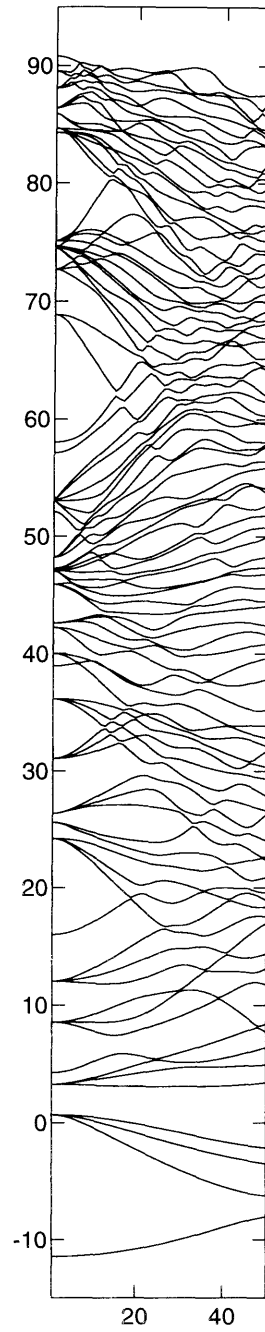Figure 4-1: The band structure for Si. The Bloch momentum runs from the Γ point ($\vec{k} = 0$) to the boundary of the Brillouin zone, passing through the center of mass of the irreducible part (CM). The scale is such that $k = 1$ at the CM.
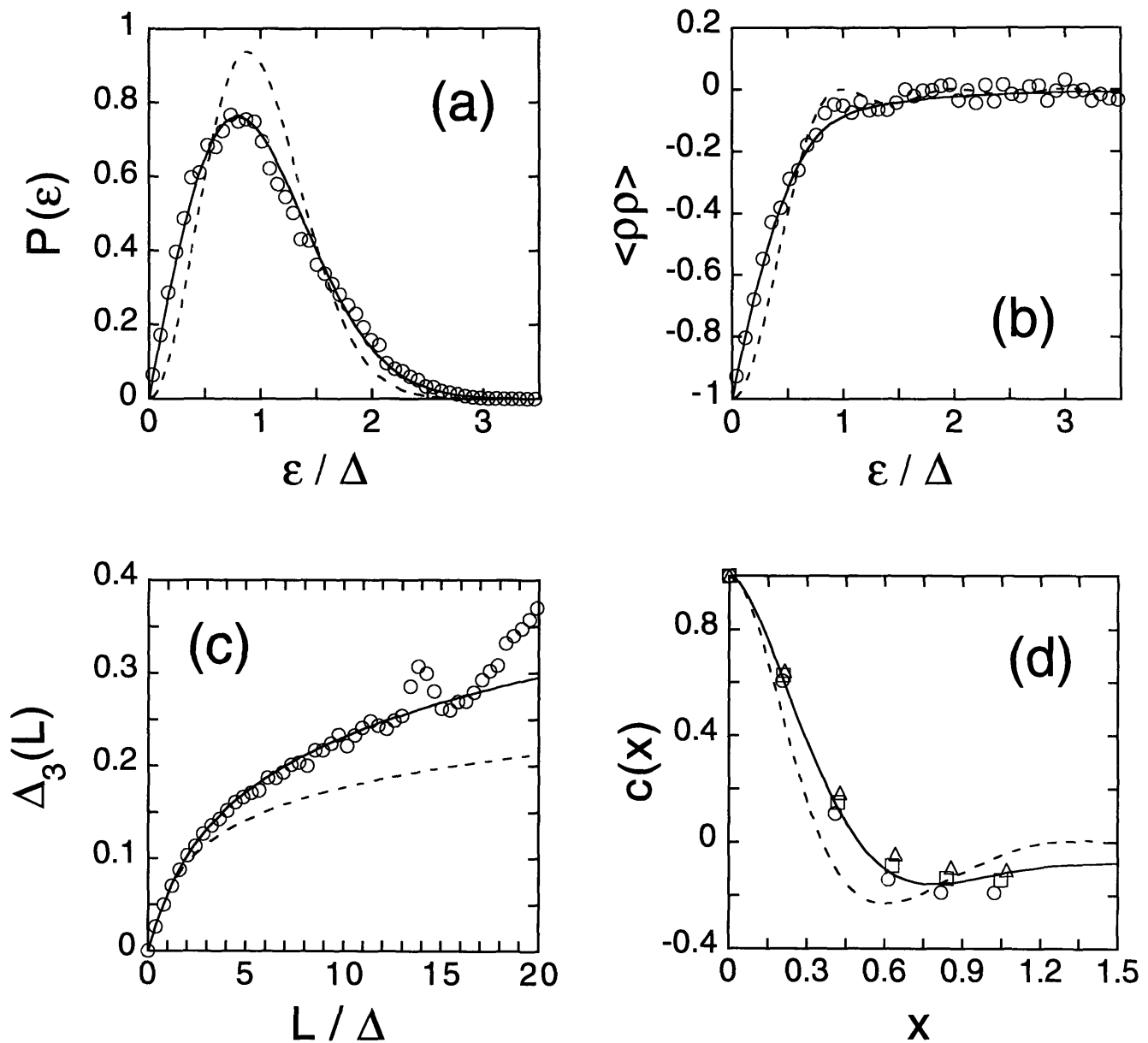
Figure 4-2: Statistical properties of 90 high-energy bands of Si around the CM point. The solid and dashed lines are the GOE and GUE predictions, respectively. Figure (a) is the band spacing distribution; (b) is the autocorrelator of density of states (rescaled to $\langle \rho \rangle = 1$); (c) is the Δ_3 statistics; (d) is the crystal velocity correlation function $c(x)$. Error bars are of the order of the data point symbol size or smaller, whenever not indicated. For all curves the average was taken over the bands and $\vec{k}$-points. The sets of points in (d) differ by the number of bands used in the estimate of the local average drift, $\langle \partial E_n(\vec{k})/\partial \vec{k} \rangle$. They correspond to: 7 (circles), 9 (triangles), and 11 bands (diamonds).
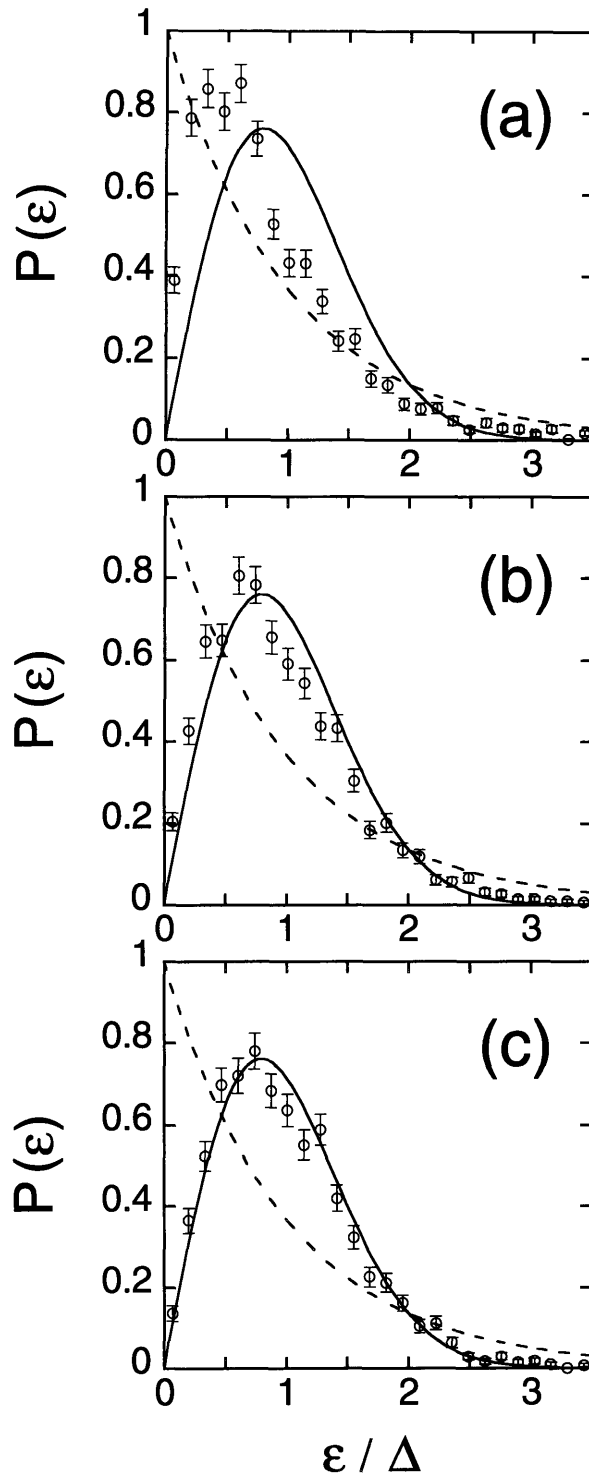
Figure 4-3: The level spacing distribution involving about 150 high-energy eigenstates at Γ in the $Al_xGa_{1-x}As$ supercrystal for concentrations: (a) $x \approx 0.1$; (b) $x \approx 0.3$; (c) $x \approx 0.5$. The average was taken over 20 realizations of a given concentration. The circles indicate the data and the solid and dashed lines the GOE and Poisson statistics, respectively.
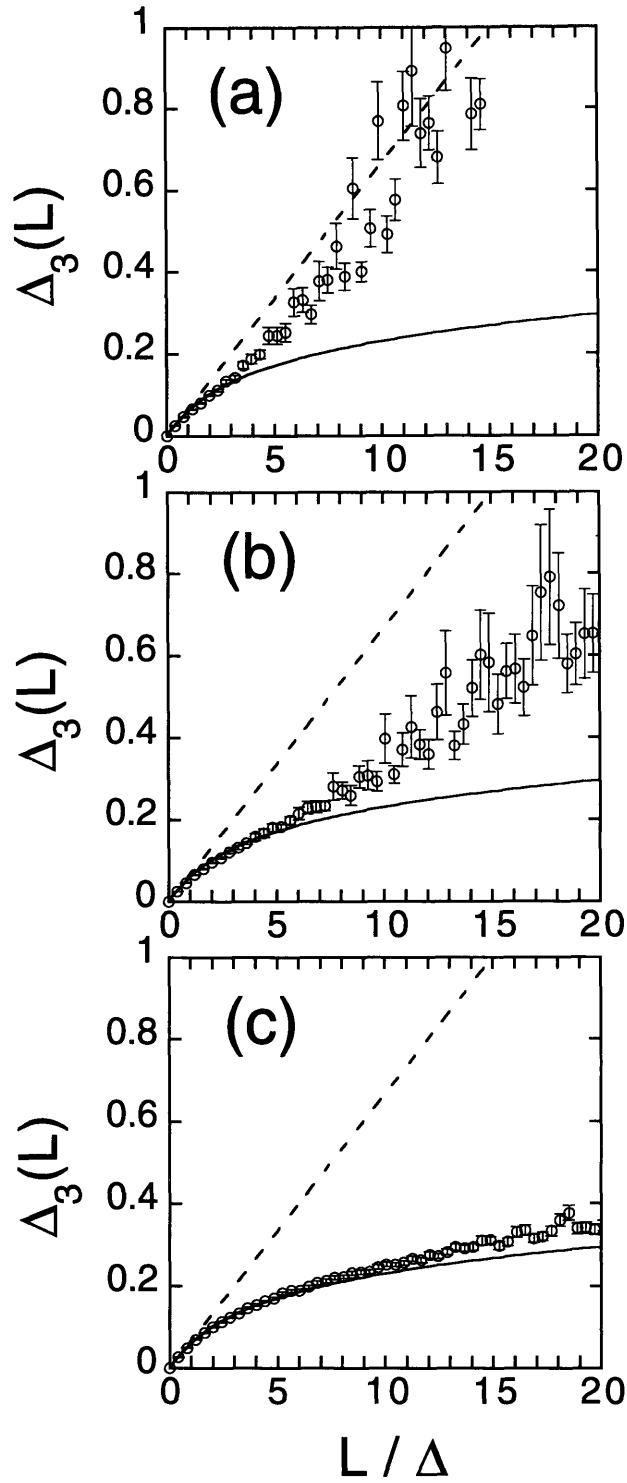
Figure 4-4: The Δ_3 statistics for the same set of levels and realizations of Fig. 3, following the same conventions.

Figure 4-5: Typical band dispersion around the CM point for the supercrystal of $Al_xGa_{1-x}As$ cells ($x = 0.5$). The r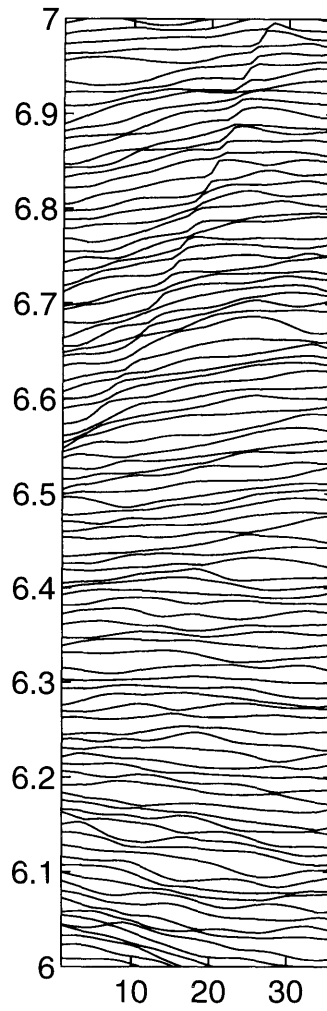egion presented here is particularly free of strong clean features, although a weak one can be seen at the top of the spectrum. The scale of the momentum axis has arbitrary units and is centered at the CM.
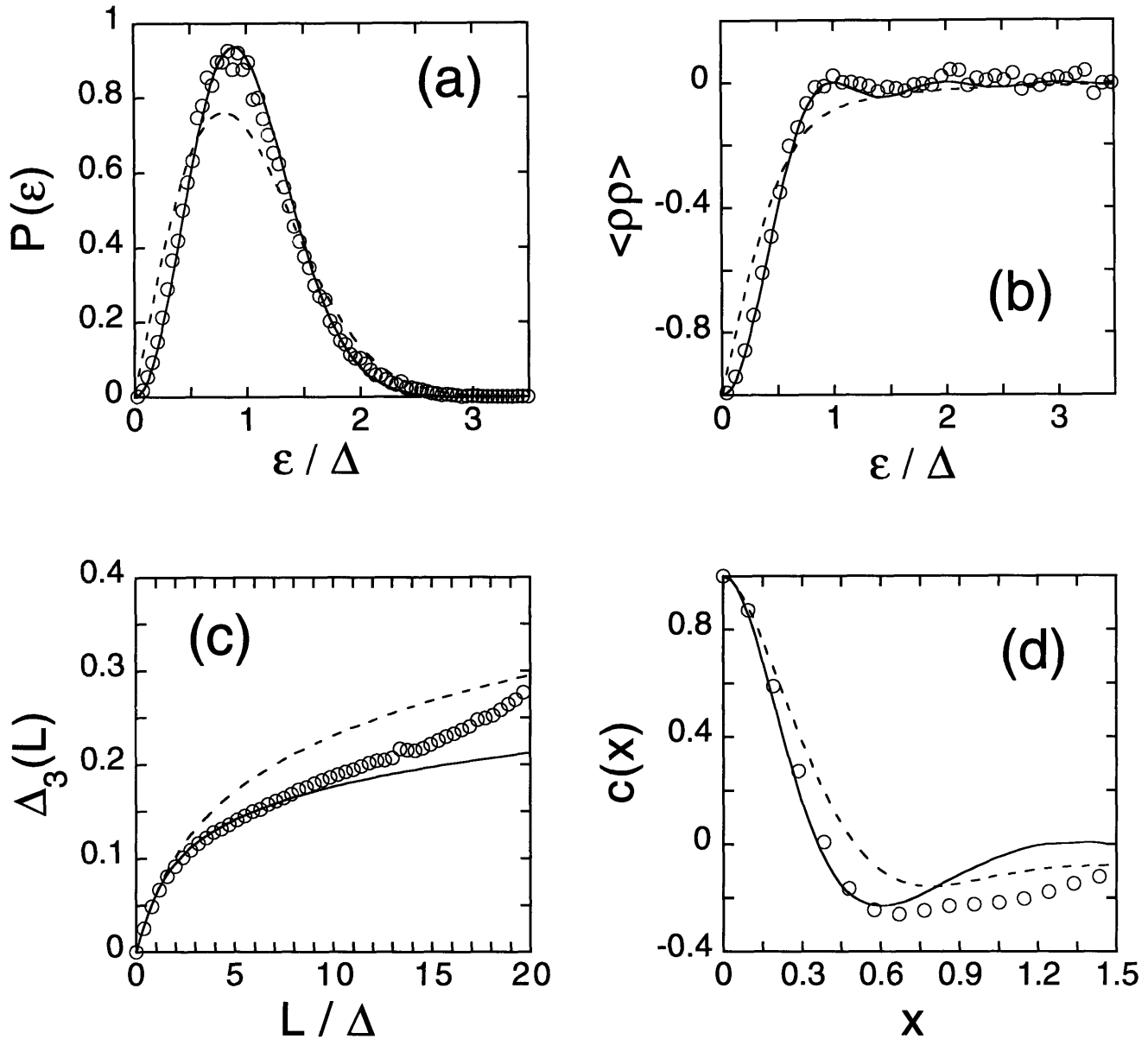
Figure 4-6: Statistical properties for the high-energy bands of the $Al_xGa_{1-x}As$ supercrystal around the CM point at $x = 0.5$. The circles indicate the data and the solid and dashed lines the GUE and GOE predictions, respectively (error bars are typically smaller than the circles). Figure (a) is the band spacing distribution; (b) is the autocorrelator of density of states; (c) is the Δ_3 statistics; (d) is the crystal velocity correlation function $c(x)$. For (a), (b) and (c) the average was taken over bands and ensemble (9 realizations); for (d) the average was only over ensembles. The data for $c(x)$ was found to be insensitive to the way the average drift was estimated.

Appendix A

Brief Introduction to the Supersymmetry Method

In this appendix we will present the basic elements of the supersymmetry technique employed in the derivation of Eqs. (2.20), (3.21), (3.23), and (3.25). For simplicity, we will take as an example the calculation of the average density of states of a random matrix of the Gaussian unitary ensemble (GUE). Most results will be quoted without proof; for a detailed explanation of the method the reader is recommended to the review articles by Efetov [11] and the Heidelberg group [30]. Many subtle points, as well as the nonlinear σ model formulation and its recent applications [12, 14, 15, 16, 21, 25, 33, 35, 50, 88, 93, 94, 95] will not be discussed.

A.1   Basic supermathematics

We begin by defining a supervector ψ as an array of commuting and anticommuting variables,

$$\psi \;\equiv\; \begin{pmatrix} S \\ \chi \end{pmatrix} , \qquad\qquad (A.1)$$

where S and χ are N-component vectors obeying the relations

$$S_i S_j - S_j S_i \;=\; 0 \qquad\qquad (A.2)$$

$$\chi_i \chi_j + \chi_j \chi_i \;=\; 0 \,, \qquad\qquad (A.3)$$

with $i, j = 1, \ldots, N$. Complex conjugation for commuting variables is defined in the usual way, namely, $(S_i)^* = S_i^*$ and $(S_i^*)^* = S_i$. For anticommuting variables the definition is slightly different: $(\chi_i)^* = \chi_i^*$ and $(\chi_i^*)^* = -\chi_i$. We remark that conjugate variables, say S_i and S_i^*, or χ_i and χ_i^*, should be taken as independent from each other.

Integration over commuting variables is also carried out in the conventional way.

In particular, we mention the well-known Gaussian integrals

$$\int d[S] \exp(-S^\dagger A S) = \frac{1}{\det(A)} \tag{A.4}$$

and

$$\int d[S] S_i S_j^* \exp(-S^\dagger A S) = \frac{[A^{-1}]_{ij}}{\det(A)} , \tag{A.5}$$

where $d[S] \equiv \Pi_{i=1}^N (2\pi)^{-1} dS_i^* dS_i$, $S^\dagger = (S^*)^T$, with T standing for transpose, and A is a $N \times N$ positively defined matrix. Similar relations can be derived for anticommuting variables. If we define

$$\int d\chi_i \equiv 0 \quad \text{and} \quad \int \chi_i d\chi_i \equiv \frac{1}{\sqrt{2\pi}} , \tag{A.6}$$

we obtain

$$\int d[\chi] \exp(-\chi^\dagger A \chi) = \det(A) \tag{A.7}$$

and

$$\int d[\chi] \chi_i \chi_j^* \exp(-\chi^\dagger A \chi) = \det(A)[A^{-1}]_{ij} , \tag{A.8}$$

where $d[\chi] \equiv \Pi_{i=1}^N (2\pi) d\chi_i^* d\chi_i$ and $\chi^\dagger = (\chi^*)^T$. We can now combine Eqs. (A.4), (A.5), (A.7), and (A.8) to cancel the determinant and get

$$\int d[\psi] \exp(-\psi^\dagger M \psi) = 1 \tag{A.9}$$

and

$$\int d[\psi] \psi_{\mu i} \psi_{\mu j}^* \exp(-\psi^\dagger M \psi) = [A^{-1}]_{ij} , \tag{A.10}$$

where $\mu = 1$ (commuting) or 2 (anticommuting), $d[\psi] \equiv d[S]d[\chi]$, and

$$M = \begin{pmatrix} A & \emptyset \\ \emptyset & A \end{pmatrix} . \tag{A.11}$$

Equations (A.9) and (A.10) are the essence of the supersymmetry method. They indicate that one can immediately ensemble average $[A^{-1}]_{ij}$ without having to worry about weighting denominators.

What happens when M has a more generic form? In order to answer this question we define a supermatrix $\mathcal{F}$ as a $2N \times 2N$ matrix which takes any supervector into another supervector, i.e.,

$$\psi' = \mathcal{F}\psi . \tag{A.12}$$

It is then simple to show that $\mathcal{F}$ must be of the form

$$\mathcal{F} = \begin{pmatrix} \mathcal{F}_{bb} & \mathcal{F}_{bf} \\ \mathcal{F}_{fb} & \mathcal{F}_{ff} \end{pmatrix} , \tag{A.13}$$

where the $N \times N$ block matrices involve commuting ($\mathcal{F}_{bb}$ and $\mathcal{F}_{ff}$) and anticommuting

variables ($\mathcal{F}_{bf}$ and $\mathcal{F}_{fb}$). The supertrace and superdeterminants of a supermatrix are defined, respectively, as

$$\text{Str}(\mathcal{F}) \equiv \text{tr}(\mathcal{F}_{ff}) - \text{tr}(\mathcal{F}_{bb}) \tag{A.14}$$

and

$$\begin{aligned}
\text{Sdet}(\mathcal{F}) &\equiv \exp[\text{Str}(\ln \mathcal{F})] \\
&= \frac{\det(\mathcal{F}_{ff} - \mathcal{F}_{fb}\mathcal{F}_{bb}^{-1}\mathcal{F}_{bf})}{\det(\mathcal{F}_{bb})} \ .
\end{aligned} \tag{A.15}$$

Following these definitions, it is not very difficult to write the equivalent of Eqs. (A.9) and (A.10) for supermatrices, namely,

$$\int d[\psi] \exp(-\psi^\dagger \mathcal{F} \psi) = \text{Sdet}(\mathcal{F}) \ , \tag{A.16}$$

and

$$\int d[\psi] \psi_{\mu i} \psi_{\nu j}^* \exp(-\psi^\dagger \mathcal{F} \psi) = \text{Sdet}(\mathcal{F})[\mathcal{F}^{-1}]_{\mu i, \nu j} \ . \tag{A.17}$$

We point out that $\mathcal{F}_{bb}$ has to be a positive matrix for these integrals to be well-defined.

A.2 Green's functions

We can use Eqs. (A.9) and (A.10) to express retarded (R) and advanced (A) one-point Green's functions of a Schrödinger operator in terms of an integration over supervectors. Let us choose $A_\pm = \mp i(\varepsilon - H \pm i\gamma)$, where H is a $N \times N$ random Hamiltonian and ε and γ are real numbers ($\gamma > 0$). We then have

$$\begin{aligned}
G_{ij}^{R,A}(\varepsilon) &\equiv \left[\frac{1}{\varepsilon - H \pm i\gamma} \right]_{ij} \\
&= \mp i \int d[\psi] S_i S_j^* \exp(-\psi^\dagger A_\pm \psi) \ ,
\end{aligned} \tag{A.18}$$

where we have dropped the notation of Eq. (A.11) and used $A_\pm$ explicitly.

In practice, it turns out to be very convenient to rewrite Eq. (A.18) in terms of a generating function $Z(J, J^*)$, where J and J^* are N-component complex vectors which couple only to the commuting variables in ψ. In other words,

$$G_{ij}^{R,A}(\varepsilon) = \mp i \left[\frac{\partial^2 Z(J, J^*)}{\partial J_i^* \partial J_j} \right]_{J, J^* = 0} , \tag{A.19}$$

with the definition

$$Z(J, J^*) \equiv \int d[\psi] \exp(-\psi^\dagger A_\pm \psi + J^\dagger P_b^T \psi + \psi^\dagger P_b J) \ , \tag{A.20}$$

where P_b is a two-component vector that projects the supervector ψ onto the subspace

of commuting (bosonic) variables, i.e., in our notation,

$$P_b = \begin{pmatrix} 1 \\ 0 \end{pmatrix} .$$
(A.21)

In order to generate the n-th power of the one-point Green's function $G_{ij}^{R,A}(\varepsilon)$ all we need to do to is to differentiate the generating function n times with respect to the variables J_i^* and J_j. The situation becomes more complicated if we want to calculate products of Green's functions with different arguments. In this case one has to introduce more components into the supervector ψ and therefore increase the size of the matrix M and of the vectors J and J^*.

A.3 Ensemble average and the Hubbard-Stratonovich transformation

Let us concentrate on the calculation of the ensemble average of single retarded Green's function. GUE statistics means that we assume that time-reversal symmetry is fully broken and that different elements of the hermitian matrix H fluctuate independently according to a common Gaussian distribution. Hence,

$$\langle H_{ij} \rangle = 0 \quad \text{and} \quad \langle H_{ij} H_{kl} \rangle = \frac{\lambda^2}{N} \delta_{il} \delta_{jk} .$$
(A.22)

These two moments completely define the probability distribution of H.

We can evaluate $\left\langle G_{ij}^R(\varepsilon) \right\rangle$ by first averaging the generating function and then taking derivatives with respect to the source terms J and J^*. Proceeding in this way, we have

$$
\begin{aligned}
\langle Z(J, J^*) \rangle &= \int d[\psi] \exp[-L_0(\psi, \psi^*, J, J^*)] \left\langle \exp(-i\psi^\dagger H \psi) \right\rangle \\
&= \int d[\psi] \exp\left[-L_0(\psi, \psi^*, J, J^*) - L_1(\psi, \psi^*)\right] ,
\end{aligned}
$$
(A.23)

where

$$L_0(\psi, \psi^*, J, J^*) = -i\psi^\dagger(\varepsilon + i\gamma)\psi - J^\dagger P_b^T \psi - \psi^\dagger P_b J$$
(A.24)

and

$$L_1(\psi, \psi^*) = -\frac{\lambda^2}{2N} \operatorname{Str}\left(\mathcal{A}^2\right) ,$$
(A.25)

with $\mathcal{A} = \sum_{i=1}^N \psi_i \psi_i^\dagger$. As a short remark, we mention that for any calculation with real orthogonal matrices the form of the supervector chosen in Eq. (A.1) is not suitable. To ensemble average $Z(J, J^*)$ over GOE matrices one has to include not just the vectors S and χ in ψ, but also their complex conjugated counterparts S^* and χ^*.

We have been able to perform the ensemble average of $Z(J, J^*)$ quite easily, but

now we have gained an interacting quartic term (L_1), making the evaluation of the integration over the supervector impossible to be carried out. The same problem occurs in the replica method [89] and the usual solution adopted is the introduction of a $2n \times 2n$ Q matrix which decouples the interaction term L_1 through a Hubbard-Stratonovich transformation. The supersymmetry method follows the same approach, with the basic difference that its Q matrix displays the same symmetry properties of the 2×2 supermatrix $\mathcal{A}$ and therefore involves only two real commuting variables (a, b) and two anticommuting variables (η, η^*). We can then write

$$Q = \begin{pmatrix} ia & \eta^* \\ \eta & b \end{pmatrix} . \tag{A.26}$$

(The factor i in front of a is introduced to guarantee convergence.) Explicitly, the Hubbard-Stratonovich transformation reads

$$\int d[Q] \exp\left[-\frac{N}{2}\text{Str}\left(Q^2\right) + \lambda\text{Str}(\mathcal{A}Q) \right] = \exp\left[\frac{\lambda^2}{2N}\text{Str}\left(\mathcal{A}^2\right) \right] , \tag{A.27}$$

with the differential defined as $d[Q] \equiv da\, db\, d\eta\, d\eta^*$. After a minor manipulation, we can rewrite Eq. (A.23) in the following way,

$$\begin{aligned} \langle Z(J, J^*) \rangle &= \int d[Q] \exp\left[-\frac{N}{2}\,\text{Str}\left(Q^2\right) \right] \int d[\psi] \exp[i\psi^\dagger \mathcal{G}^{-1}(Q)\psi \\ &\quad + J^\dagger P_b^T \psi + \psi^\dagger P_b J] , \end{aligned} \tag{A.28}$$

where

$$\mathcal{G}^{-1}(Q) = \varepsilon + i\gamma + i\lambda Q . \tag{A.29}$$

The integration over the supervector ψ is carried out using Eq. (A.16) and the transformations $\psi \to \psi + i\mathcal{G}P_b J$ and $\psi^\dagger \to \psi^\dagger + iJ^\dagger P_b^T \mathcal{G}$. As a result, we get

$$\langle Z(J, J^*) \rangle = \int d[Q] \exp[-F(Q, J, J^*)] , \tag{A.30}$$

with

$$F(Q, J, J^*) = \left\{ \frac{N}{2}\text{Str}\left(Q^2\right) - N\text{Str}\left[\ln(-i\mathcal{G}^{-1}) \right] + iJ^\dagger P_b^T \mathcal{G}P_b J \right\} . \tag{A.31}$$

(Since $\mathcal{G}^{-1}$ is diagonal with respect to the N-components, in the above expression we have already taken the normal trace.) Notice the substantial simplification achieved: The original $2N$ variables $\{\psi_i\}$ have been replaced by only two commuting and two anticommuting variables. Nevertheless, the evaluation of $\langle Z(J, J^*) \rangle$ is still a nontrivial problem, since the integration over Q in Eq. (A.30) cannot be done exactly.

A.4 The saddle-point approximation

The usual procedure to evaluate the integral over Q is to take the limit $N \gg 1$ and use the saddle-point approximation. Setting $J = 0$ and $J^* = 0$ in Eq. (A.31), we obtain the following equation for the stationary condition

$$\frac{\delta}{\delta Q} \left\{ \frac{1}{2} \mathrm{Str} \left(Q^2 \right) - \mathrm{Str} \left[\ln \mathcal{G}^{-1}(Q) \right] \right\}_{Q=Q_0} = 0 \,, \qquad (A.32)$$

which yields

$$Q_0 \mathcal{G}^{-1}(Q_0) + i\lambda = 0 \,. \qquad (A.33)$$

Taking $\gamma = 0$, one finds that the only nontrivial solution of this equation is

$$Q_0 = \begin{pmatrix} q(\varepsilon/\lambda) & 0 \\ 0 & q(\varepsilon/\lambda) \end{pmatrix} \,, \qquad (A.34)$$

where $q(x) = -ix/2 \pm \sqrt{1 - x^2/4}$. The choice of sign has to be such that $\mathrm{Sdet}(\varepsilon + i\gamma - i\lambda Q) \neq 0$, which in this case means '+'. The elements a_0 and b_0 of Q_0 are not real, but one can check that this fact does not influence the convergence of the integral in Eq. (A.30). The saddle-point Q_0 always has a very simple structure for a supersymmetry theory of a one-point Green's function. However, it turns out that for two-point functions the stationary condition leads to a manifold of solutions which has to be carefully parametrized in order to keep the original symmetries of the matrix $\mathcal{A}$.

Expanding the Q matrix around Q_0, namely, $Q = Q_0 + \delta Q$, where

$$\delta Q = \begin{pmatrix} i\delta a & \eta^* \\ \eta & \delta b \end{pmatrix} \,, \qquad (A.35)$$

we arrive at

$$F(Q, J, J^*) \approx \frac{N}{2} \left[1 + q(\varepsilon/\lambda)^2 \right] \mathrm{Str} \left(\delta Q^2 \right) - \frac{1}{\lambda} J^\dagger P_b^T Q_0 P_b J \,. \qquad (A.36)$$

[We are allowed to neglect any contribution of the source terms of order higher than $O(1)$ in δQ.] After performing the remaining Gaussian integration over δQ, we get

$$\langle Z(J, J^*) \rangle \approx \exp \left[-\frac{q(\varepsilon/\lambda)}{\lambda} J^\dagger J \right] \,. \qquad (A.37)$$

The final formula for the ensemble averaged one-point Green's function in the saddle-point approximation is

$$\left\langle G_{ij}^R(\varepsilon) \right\rangle = \frac{\delta_{ij}}{2\lambda^2} \left(\varepsilon - i\sqrt{4\lambda^2 - \varepsilon^2} \right) \,. \qquad (A.38)$$

From this expression we can immediately find that the average level density of the

Hamiltonian H is equal to

$$\langle \rho(\varepsilon) \rangle \equiv -\frac{1}{N\pi} \sum_{i=1}^{N} \left\langle G_{ii}^{R}(\varepsilon) \right\rangle = \frac{1}{2\pi\lambda^2}\sqrt{4\lambda^2 - \varepsilon^2} \ , \qquad (A.39)$$

which is the celebrated Wigner's semi-circle law. The interpretation of the parameter λ is now transparent: $\Delta = 4\lambda/N$ is the average level spacing.

Appendix B

The Calculation of $Q_2(v_1, v_2; r)$

B.1 Preliminary remarks

The joint distribution of level widths Q_2 [Eq. (2.19)] for the unitary ensemble was first obtained by Prigodin [35], although in his work he does not present the calculation. The purpose of this appendix is to provide a schematic explanation of the steps involved in the derivation without working out all the mathematical details. For a complete justification of the supersymmetry method and the nonlinear σ model the reader is advised to consult Ref. [11].

Any distribution can be determined once we know all its moments. Specifically for the case of Q_2, the idea is the following [91] (we will simplify the notation by dropping the index 2 and not writing explicitly the parameter r): Let us call $\mathcal{Q}(s_1, s_2)$ the two-dimensional Laplace transform of $Q(v_1, v_2)$, namely,

$$\mathcal{Q}(s_1, s_2) = \int_0^\infty dv_1 \int_0^\infty dv_2 \ e^{-s_1 v_1 - s_2 v_2} \ Q(v_1, v_2) \ . \tag{B.1}$$

Expanding the exponential in a Taylor series we obtain

$$\begin{aligned}
\mathcal{Q}(s_1, s_2) &= \sum_{n,m=0}^\infty (-1)^{n+m} \frac{s_1^n s_2^m}{n! m!} \int_0^\infty dv_1 \int_0^\infty dv_2 \ v_1^n v_2^m \ Q(v_1, v_2) \\
&= \sum_{n,m=0}^\infty (-1)^{n+m} \frac{s_1^n s_2^m}{n! m!} \ \langle v_1^n v_2^m \rangle \ .
\end{aligned} \tag{B.2}$$

Once we know an expression for $\langle v_1^n v_2^m \rangle$, we can obtain $\mathcal{Q}(s_1, s_2)$ and then calculate $\mathcal{Q}(s_1, s_2)$ through the inverse transform formula

$$Q(v_1, v_2) = \frac{1}{(2\pi i)^2} \int_{c_1 - i\infty}^{c_1 + i\infty} ds_1 \int_{c_2 - i\infty}^{c_2 + i\infty} ds_2 \ e^{v_1 s_1 + v_2 s_2} \ \mathcal{Q}(s_1, s_2) \ , \tag{B.3}$$

where the real numbers c_1 and c_2 are larger than the real parts of all poles in $\mathcal{Q}(s_1, s_2)$.

The problem therefore is reduced to the evaluation of $\langle v_1^n v_2^m \rangle$. This calculation can be done with the nonperturbative supersymmetry method introduced by Efetov [92] to study electronic states in disordered metals.

B.2 Green's functions

The first step towards the evaluation of $\langle v_1^n v_2^m \rangle$ is to express the amplitudes $v_{1,2}$ in terms of retarded and advanced one-point Green's functions,

$$G_E^{R,A}(r,r) = \sum_{k=1}^{N} \frac{|\varphi_k(r)|^2}{E - \varepsilon_k \pm i\Gamma_k} ,$$ (B.4)

where ε_k and $\varphi_k(r)$ are eigenvalues and eigenfunctions of the $N \times N$ single-particle Hamiltonian H, namely, $H\varphi_k(r) = \varepsilon_k \varphi_k(r)$. For a closed system ($\gamma \approx \Gamma_k \ll \Delta$, where Δ is the mean level spacing), it has been shown [90, 91] that

$$\langle v_1^n v_2^m \rangle = \frac{(i)^{n-m}(n-1)!(m-1)!}{2\mathcal{N}(n+m-2)!} \lim_{\gamma \to 0} \left[\left(\frac{\gamma V}{\pi} \right)^{n+m-1} \left\langle \left[G_{\varepsilon_l}^R(r_1, r_1) \right]^n \left[G_{\varepsilon_l}^A(r_2, r_2) \right]^m \right\rangle \right] ,$$ (B.5)

where $\mathcal{N} = 1/\Delta V$ is the density of states, V is the system volume, and $v_{1,2} \equiv V|\varphi_l(r_{1,2})|^2$, with ε_l the closest eigenvalue to E.

B.3 The supersymmetry formulation

The next step is to express the product of powers of Green's functions in terms of integrals over supervectors. We can basically follow the procedure described in Appendix A, making only two modifications: The first one is to use twice as many components in the supervectors, since now we are dealing with the product of two distinct Green's functions. The second one is that now we need to work in the space representation. Therefore, let us call S_μ and χ_μ N-component vectors of commuting and anticommuting variables, respectively. The index μ will be associated with the retarded (1) and advanced (2) parts. The space dependence of the Green's functions can be made explicit by using the complete eigenbasis $\{\varphi_k(r)\}$ to switch from vectors to fields, namely,

$$S_\mu(r) \equiv \sum_{k=1}^{N} S_{\mu k} \varphi_k(r)$$ (B.6)

and

$$\chi_\mu(r) \equiv \sum_{k=1}^{N} \chi_{\mu k} \varphi_k(r) .$$ (B.7)

The superfields are then defined as

$$\psi_\mu(r) \equiv \begin{pmatrix} S_\mu(r) \\ \chi_\mu(r) \end{pmatrix} .$$ (B.8)

The generating function of products of Green's functions is written as the func-

tional integral

$$Z(J_1, J_1^*, J_2, J_2^*, \omega) = \int \mathcal{D}\psi_1 \mathcal{D}\psi_2 \exp\left\{-L_1[\psi_1, J_1, J_1^*, \omega] - L_2[\psi_2, J_2, J_2^*, \omega]\right\} , \quad (B.9)$$

where

$$\begin{aligned}
L_1[\psi_1, J_1, J_1^*, \omega] &= -i\int dr\left\{\psi_1^\dagger(r)[E + \omega/2 - H(r) + i\gamma]\psi_1(r)\right. \\
&\quad \left. -iJ_1^\dagger(r)P_b^T\psi_1(r) - i\psi_1^*(r)P_bJ_1(r)\right\}
\end{aligned} \quad (B.10)$$

and

$$\begin{aligned}
L_2[\psi_2, J_2, J_2^*, \omega] &= i\int dr\left\{\psi_2^\dagger(r)[E - \omega/2 - H(r) - i\gamma]\psi_2(r)\right. \\
&\quad \left. +iJ_2^\dagger(r)P_b^T\psi_2(r) + i\psi_2^*(r)P_bJ_2(r)\right\} .
\end{aligned} \quad (B.11)$$

[The operator P_b projects $\psi_\mu(r)$ onto the subspace of commuting variables.] We then have

$$\left[G_{E+\omega/2}^R(r_1, r_1)\right]^n \left[G_{E-\omega/2}^A(r_2, r_2)\right]^m =$$

$$= \frac{(i)^{m-n}}{n!m!}\left\{[D_1]^n [D_2]^m Z(J_1, J_1^*, J_2, J_2^*)\right\}_{J_1, J_1^*, J_2, J_2^* = 0} , \quad (B.12)$$

where the differential operators have the form

$$D_\mu \equiv \frac{\delta}{\delta J_\mu^*(r_\mu)}\frac{\delta}{\delta J_\mu(r_\mu)} . \quad (B.13)$$

The notation becomes much simpler if we combine both advanced and retarded fields into a single field:

$$\Psi(r) \equiv \begin{pmatrix} \psi_1(r) \\ \psi_2(r) \end{pmatrix} \quad \text{and} \quad J(r) \equiv \begin{pmatrix} J_1(r) \\ J_2(r) \end{pmatrix} . \quad (B.14)$$

The result is

$$Z(J, J^*, \omega) = \int \mathcal{D}\Psi \exp\left\{-L[\Psi, J, J^*, \omega]\right\} , \quad (B.15)$$

where

$$\begin{aligned}
L[\Psi, J, J^*, \omega] &= -i\int dr\left\{\Psi^\dagger(r)\Lambda^{1/2}\left[E - H(r) + \Lambda(i\gamma + \omega/2)\right]\Lambda^{1/2}\Psi(r)\right. \\
&\quad \left. -iJ^\dagger(r)P_b^T\Psi(r) - i\Psi^\dagger(r)P_bJ(r)\right\} ,
\end{aligned} \quad (B.16)$$

and

$$\Lambda = \begin{pmatrix} 1 & 0 \\ 0 & -1 \end{pmatrix} . \quad (B.17)$$

We proceed further by evaluating the ensemble average of the generating function. The Hamiltonian is divided into two contributions: $H(r) = H_0(r) + U(r)$, where $H_0(r)$

79

is fixed (typically, it contains the kinetic term) and $U(r)$ is Gaussian correlated with the first two moments

$$\langle U(r) \rangle = 0 \quad \text{and} \quad \langle U(r)U(r') \rangle = \frac{\delta(r - r')}{2\pi \mathcal{N} \tau} \ . \tag{B.18}$$

The term $U(r)$ represents the disordered part of the background potential and τ can be interpreted as the average time between collisions. Separating the factor in $Z(J, J^*)$ which depends on $U(r)$ we obtain

$$\left\langle \exp \left\{ -i \int dr \left[\Psi^\dagger(r)U(r)\Lambda\Psi(r) \right] \right\} \right\rangle = \exp \left\{ \frac{-1}{4\pi \mathcal{N} \tau} \int dr \left[\Psi^\dagger(r)\Lambda\Psi(r) \right]^2 \right\} . \tag{B.19}$$

The quartic term can be decoupled into a quadratic one through a Hubbard-Stratonovich transformation. Let us we introduce a 4×4 $Q(r)$ supermatrix with the same symmetries of $\Psi(r)\Lambda\Psi^\dagger(r)$, i.e.,

$$Q = \begin{pmatrix} Q^{11} & Q^{12} \\ Q^{21} & Q^{22} \end{pmatrix} , \tag{B.20}$$

where the submatrices (also supermatrices) are of the form

$$Q^{11} = \begin{pmatrix} ia_1 & \eta_1^* \\ \eta_1 & b_1 \end{pmatrix} \ , \quad Q^{12} = \begin{pmatrix} ic & \xi^* \\ \zeta & d \end{pmatrix} \ ,$$

$$Q^{21} = \begin{pmatrix} ic^* & \zeta^* \\ \xi & d^* \end{pmatrix} \ , \quad Q^{22} = \begin{pmatrix} ia_2 & \eta_2^* \\ \eta_2 & b_2 \end{pmatrix} \ . \tag{B.21}$$

(Hereafter we will drop the explicit dependence on the position in order to make the notation more compact.) The Greek letters indicate anticommuting variables; a_1, a_2, b_1, and b_2 are real numbers, whereas c and d are complex. The factors of i present in Eq. (B.21) were included for convergence purposes. The supertrace of a generic supermatrix M of the form shown in Eq. (B.20) is conventionally broken into two parts: $\mathrm{Str}(M) = \mathrm{Str}(M^{11}) + \mathrm{Str}(M^{22})$. Therefore, we can write the following identity,

$$\int \mathcal{D}Q \exp \left\{ -\int dr \left[\frac{\pi \mathcal{N}}{4\tau} \mathrm{Str}(Q^2) - \frac{1}{2\tau} \Psi^\dagger Q \Lambda \Psi \right] \right\} =$$
$$= \exp \left\{ -\frac{1}{4\pi \mathcal{N} \tau} \int dr \left(\Psi^\dagger \Lambda \Psi \right)^2 \right\} \ , \tag{B.22}$$

which yields

$$\langle Z(J, J^*, \omega) \rangle = \int \mathcal{D}Q \exp \left\{ -\int dr \left[\frac{\pi \mathcal{N}}{4\tau} \mathrm{Str}(Q^2) \right] \right\}$$
$$\times \int \mathcal{D}\Psi \exp \left\{ -L_Q[\Psi, J, J^*, \omega] \right\} \ , \tag{B.23}$$

with

$$L_Q[\Psi, J, J^*, \omega] = -i \int dr \left[\Psi^\dagger \Lambda^{1/2} \left(E - H_0 + \Lambda(i\gamma + \omega/2) + iQ/2\tau \right) \Lambda^{1/2} \Psi \right.$$
$$\left. -iJ^\dagger P_b^T \Psi - i\Psi^\dagger P_b J \right] . \tag{B.24}$$

{We have used the fact that $\mathrm{Str}(Q\Psi\Lambda\Psi^\dagger) = -\Psi^\dagger Q\Lambda\Psi$ and $\mathrm{Str}[(\Psi\Psi^\dagger)^2] = -(\Psi^\dagger\Lambda\Psi)^2$}. Performing the integration over the superfields we obtain

$$\langle Z(J, J^*, \omega) \rangle = \int \mathcal{D}Q \exp\left\{ -F[Q] \right\} , \tag{B.25}$$

where the "free energy" is given by

$$F[Q] = \int dr \left\{ \frac{\pi\mathcal{N}}{4\tau} \mathrm{Str}(Q^2) - \mathrm{Str}\left[\ln\left(-i\mathcal{G}^{-1} \right) \right] - iJ^\dagger P_b^T \Lambda^{-1/2} \mathcal{G} \Lambda^{-1/2} P_b J \right\} \tag{B.26}$$

and

$$\mathcal{G} = \frac{1}{E - H_0 + \Lambda(i\gamma + \omega/2) + iQ/2\tau} . \tag{B.27}$$

The integral in Eq. (B.25) cannot be evaluated exactly. For $E_F\tau \gg 1$ (E_F is the Fermi energy), we can apply the saddle-point approximation and find that the stationary condition

$$\left. \frac{\delta F[Q]}{\delta Q} \right|_{Q=Q_0} = 0 \tag{B.28}$$

yields the equation

$$\frac{\pi\mathcal{N}}{2\tau} Q_0 - \frac{1}{2\tau} \mathrm{tr} \left[\frac{1}{iE - iH_0 + \Lambda(-\gamma + i\omega/2) + Q_0/2\tau} \right] = 0 , \tag{B.29}$$

where the trace is to be taken over an eigenbasis of H_0. One finds that in the limit $\omega, \gamma \to 0$ the stationary condition can be written as

$$Q_0^2 = 1 . \tag{B.30}$$

This equation has a manifold of solutions. The manifold can be parametrized in several different ways. For a generic form, one can write

$$Q_0 = T^{-1}\Lambda T , \tag{B.31}$$

where T is a superunitary matrix. Expanding Eq. (B.26) to second order around Q_0 one finds that the effective "free energy" becomes

$$F[Q_0] = \int dr \left\{ \frac{\pi\mathcal{N}}{4} \mathrm{Str}\left[D\left(\nabla Q_0\right)^2 + (-\gamma + i\omega/2)\Lambda Q_0 \right] - iJ^\dagger P_b^T \Lambda^{-1/2} \mathcal{G}_0 \Lambda^{-1/2} P_b J \right\} , \tag{B.32}$$

81

where $D = v_F^2/\tau$ is the diffusion constant. One notices that we have obtained a nonlinear σ model in terms of the supermatrix Q_0. This is still a difficult problem to solve, therefore we are led to yet another approximation: Assuming that the system is small, i.e., $D/L^2 \gg \omega, \Delta$, where L is a typical linear dimension of the system, we can neglect any space dependence in Q_0. This is the so-called zero-mode approximation, where "free energy" is reduced to

$$F[Q_0] \approx -\frac{\pi(\gamma - i\omega/2)}{4\Delta} \text{Str}(\Lambda Q_0) - i \int dr \left[J^\dagger P_b^T \Lambda^{-1/2} \mathcal{G}_0 \Lambda^{-1/2} P_b J \right] . \qquad (B.33)$$

We will not discuss how the integration over the manifold of Q_0 can be implemented, since this is a rather long (but standard) subject [11]. Instead, we will move to the next step, which is the calculation of the functional derivatives of the average generating function. After Eqs. (B.23) and (B.33) we have

$$\langle Z(J, J^*, \omega) \rangle = \left\langle \exp \left[i \int dr \left(J_1^* \mathcal{G}_{bb}^{11} J_1 + J_1^* \mathcal{G}_{bb}^{12} J_2 - J_2^* \mathcal{G}_{bb}^{21} J_1 - J_2^* \mathcal{G}_{bb}^{22} J_2 \right) \right] \right\rangle_{Q_0} , \qquad (B.34)$$

where $\langle \cdots \rangle_{Q_0} \equiv \int d(Q_0) \exp\{-F[Q_0]\}$. It is simple to check that each pair of derivatives $(\delta^2/\delta J_k^* \delta J_l)$ will bring down a factor proportional to $\mathcal{G}_{bb}^{kl}$. Indeed, using Eqs. (B.12) and (B.34) one finds that

$$\left[G_{E+\omega/2}^R(r_1, r_1) \right]^n \left[G_{E-\omega/2}^A(r_2, r_2) \right]^m = \frac{1}{n!m!} \sum_{p=p_0}^n C_p^{n,m} \left\langle [\langle r_1 | \mathcal{G}_{bb}^{11} | r_1 \rangle]^p \right.$$

$$\times [\langle r_1 | \mathcal{G}_{bb}^{12} | r_2 \rangle]^{n-p} [\langle r_2 | \mathcal{G}_{bb}^{21} | r_1 \rangle]^{n-p} [\langle r_2 | \mathcal{G}_{bb}^{22} | r_2 \rangle]^{m-n+p} \Big\rangle_{Q_0} , \qquad (B.35)$$

where the combinatorial coefficient is equal to

$$C_p^{n,m} = \frac{n!m!}{p!(m-n+p)![(n-p)!]^2} \qquad (B.36)$$

and $p_0 = \max\{0, n-m\}$. Using Eq. (B.31) the supermatrix elements of Eq. (B.35) can be broken into two parts, namely,

$$\langle r_\mu | \mathcal{G} | r_\nu \rangle = \left\langle r_\mu \left| \frac{1}{E - H_0 + iQ/2\tau} \right| r_\nu \right\rangle$$
$$= \alpha(r_\mu, r_\nu) + i\beta(r_\mu, r_\nu) Q_0 , \qquad (B.37)$$

where $\alpha(r_\mu, r_\nu)$ and $\beta(r_\mu, r_\nu)$ are, respectively, the real and imaginary parts of $k(r_\mu, r_\nu) = \langle r_\mu | [E - H_0 + i/2\tau]^{-1} | r_\nu \rangle$. These functions can be evaluated with the assumption that the background potential is flat, i.e., $H_0 = p^2/2m - E_F$, where p is the linear momentum operator. Thus, for a two-dimensional system we have

$$k(r_\mu, r_\nu) = V \int \frac{d^2p}{(2\pi)^2} \frac{\exp[-ip \cdot (r_\mu - r_\nu)]}{(E - p^2/2m + E_F + i/2\tau)}$$

$$\approx -\frac{i}{\Delta} J_0(k_F r) , \tag{B.38}$$

with $J_0(z)$ as the zeroth order Bessel function. In derivating this last equation we have assumed that the distance $r = |r_\mu - r_\nu|$ is much smaller than the mean free path $l = \tau/v_F$, resulting that $\alpha(r_\mu, r_\nu) = 0$ and $\beta(r_\mu, r_\nu) = -(1/\Delta)f(r)$. For a three-dimensional system, these relations would still hold, but $f(r)$ would be a function different from $J_0(k_F r)$. Going back to Eq. (B.35) we can now write

$$\left[G^R_{E+\omega/2}(r_1, r_1)\right]^n \left[G^A_{E-\omega/2}(r_2, r_2)\right]^m = \frac{1}{n!m!} \left(\frac{-i}{\Delta}\right)^{n+m} \sum_{p=p_0}^n C_p^{n,m} \left\langle [Q_{bb}^{11}]^p \right.$$
$$\left. \times [f(r)^2 Q_{11}^{12} Q_{bb}^{21}]^{n-p}[Q_{bb}^{22}]^{m-n+p} \right\rangle_{Q_0} , \tag{B.39}$$

At this point one has to evaluate the integration over the saddle-point manifold. The result, expressed in terms of the moments of the distribution, turns out to be

$$\begin{aligned}
\langle v_1^n v_2^m \rangle &= n!m! \sum_{p=p_0}^n C_p^{n,m} \left[f(r)^2\right]^{n-p} \\
&= \frac{n!m!}{2\pi i} \oint_{|z|<1} \frac{dz}{z} \left\{[1 + zf(r)]^n [1 + (1/z)f(r)]^m\right\} . \tag{B.40}
\end{aligned}$$

One can now go back to Eq. (B.2) and compute the Laplace transform $\mathcal{Q}(s_1, s_2)$:

$$\begin{aligned}
\mathcal{Q}(s_1, s_2) &= \frac{1}{2\pi i} \oint_{|z|<1} \frac{dz}{z} \sum_{n,m=0}^\infty (-1)^{n+m} s_1^n s_2^m [1 + f(r)z]^n [1 + f(r)/z]^m \\
&= \frac{1}{2\pi i} \oint_{|z|<1} \frac{dz}{\{1 + s_1[1 + f(r)z]\}\{z + s_2[z + f(r)]\}} \\
&= \frac{1}{[(1 + s_1)(1 + s_2) - s_1 s_2 f(r)^2]} . \tag{B.41}
\end{aligned}$$

Finally, we calculate the inverse transform [see Eq. (B.3)],

$$\begin{aligned}
Q(v_1, v_2) &= \frac{1}{(2\pi i)^2} \int_{c_1-i\infty}^{c_1+i\infty} ds_1\, e^{v_1 s_1} \int_{c_2-i\infty}^{c_2+i\infty} \frac{ds_2\, e^{v_2 s_2}}{[(1 + s_1)(1 + s_2) - s_1 s_2 f(r)^2]} \\
&= \frac{1}{[1 - f(r)^2]} \exp\left(-\frac{v_1 + v_2}{[1 - f(r)^2]}\right) I_0\left(\frac{2f(r)\sqrt{v_1 v_2}}{[1 - f(r)^2]}\right) , \tag{B.42}
\end{aligned}$$

where $I_0(z)$ is the modified Bessel function of zeroth order.

Bibliography

[1] There is an extensive literature on this topic. For a recent review, see *Mesoscopic Phenomena in Solids*, edited by B. L. Altshuler, P. A. Lee, and R. A. Webb (North-Holland, Amsterdam, 1991).

[2] B. L. Altshuler and A. G. Aronov in *Electron-Electron Interactions in Disordered Systems*, edited by A. L. Efros and M. Pollack (North-Holland, Amsterdam, 1985).

[3] *Nanostructures and Mesoscopic Systems*, edited by W. P. Kirk and M. A. Reed (Academic Press, San Diego, 1992).

[4] C. M. Marcus, R. M. Westervelt, P. F. Hopkins, and A. C. Gossard, Phys. Rev. B **48**, 2460 (1993); Chaos **3**, 643 (1993).

[5] D. Weiss, K. Richter, A. Menschig, R. Bergmann, H. Schweizer, K. von Klitzing, and G. Weimann, Phys. Rev. Lett. **70**, 4118 (1993).

[6] M. J. Berry, J. A. Katine, C. M. Marcus, R. M. Westervelt, and A. C. Gossard, Surf. Sci. **305**, 480 (1994).

[7] M. W. Keller, O. Millo, A. Mittal, D. E. Prober, and R. N. Sacks, Surf. Sci. **305**, 501 (1994).

[8] T. M. Fromhold, M. L. Leadbeater, L. Eaves, T. J. Foster, P. C. Main, and F. W. Sheard, Surf. Sci. **305**, 511 (1994).

[9] M. A. Kastner, Rev. Mod. Phys. **64**, 849 (1992).

[10] *Single Charge Tunneling*, edited by H. Grabert and M. Devoret (Plenum Press, New York, 1992).

[11] K. B. Efetov, Adv. in Phys. **32**, 53 (1983).

[12] B. D. Simons, P. A. Lee, and B. L. Altshuler, Phys. Rev. Lett. **70**, 4122 (1993).

[13] A. Szafer and B. L. Altshuler, Phys. Rev. Lett. **70**, 587 (1993).

[14] B.D. Simons, A. Szafer, and B. L. Altshuler, Pis'ma Zh. Eksp. Teor. Fiz. **57**, 268 (1993) [JETP Lett. **57**, 276 (1993)].

[15] B. D. Simons and B. L. Altshuler, Phys. Rev. Lett. **70**, 4063 (1993).

[16] B. D. Simons and B. L. Altshuler, Phys. Rev. B **48**, 5422 (1993).

[17] B. Sutherland, J. Math. Phys. **12**, 246 (1971); *ibid.* **12**, 251 (1971).

[18] B. Sutherland, Phys. Rev. A **4**, 2019 (1971); *ibid.* **5**, 1372 (1972).

[19] Ya. G. Sinai, Ups. Mat. Nauk. **25**, 137 (1970) [Russ. Math. Surv. **25**, 137 (1970)].

[20] R. B. Laughlin, Nucl. Phys. B (Proc. Suppl.) **2**, 213 (1987).

[21] N. Taniguchi and B. L. Altshuler, Phys. Rev. Lett. **71**, 4031 (1993).

[22] M. V. Berry, in *Chaos and Quantum Physics*, edited by M.-J. Giannoni, A. Voros, and J. Zinn-Justin (North-Holland, Amsterdam, 1991); Philos. Trans. R. Soc. London **A237**, 237 (1977).

[23] R. Landauer, IBM J. Res. Dev. **1**, 223 (1957); Philos. Mag. **21**, 863 (1970).

[24] M. Büttiker, Phys. Rev. Lett. **57**, 1761 (1986); IBM J. Res. Dev. **32**, 317 (1988).

[25] V. N. Prigodin, K. B. Efetov, and S. Iida, Phys. Rev. Lett. **71**, 1230 (1993).

[26] H. U. Baranger and P. A. Mello, Phys. Rev. Lett. **73**, 142 (1994).

[27] R. A. Jalabert, J.-L. Pichard, and C. W. J. Beenakker, Europhys. Lett. (to be published).

[28] R. A. Jalabert, A. D. Stone, Y. Alhassid, Phys. Rev. Lett. **68**, 3468 (1992).

[29] A. D. Stone and H. Bruus, Physica B **189**, 43 (1993); Surf. Sci. **305**, 490 (1994).

[30] J. J. M. Verbaarschot, H. A. Weidenmüller, and M. R. Zirnbauer, Phys. Rep. **129**, 367 (1985).

[31] H. U. Baranger, R. A. Jalabert, and A. D. Stone, Chaos **3**, 665 (1993).

[32] S. Tomsovic and E. J. Heller, Phys. Rev. Lett. **70**, 1405 (1993).

[33] M. R. Zirnbauer, Phys. Rev. Lett. **69**, 1584 (1992).

[34] N. Taniguchi, A. Hashimoto, B. D. Simons, and B. L. Altshuler, Europhys. Lett. (to be published).

[35] V. N. Prigodin (unpublished).

[36] F. Calogero, J. Math. Phys. **10**, 2191, 2197 (1969).

[37] F. J. Dyson, J. Math. Phys. **3**, 140, 157,166, 1191 (1963).

[38] F. D. M. Haldane, Phys. Rev. Lett. **60**, 635 (1988).

[39] B. S. Shastry, Phys. Rev. Lett. **60**, 639 (1988).

[40] B. S. Shastry and B. Sutherland, Phys. Rev. Lett. **65**, 243 (1990).

[41] F. D. M. Haldane, Phys. Rev. Lett. **66**, 1529 (1991).

[42] B. Sutherland, Phys. Rev. B **45**, 907 (1992).

[43] B. S. Shastry, Phys. Rev. Lett. **69**, 164 (1992).

[44] A. P. Polychronakos, Phys. Rev. Lett. **69**, 703 (1992).

[45] B. S. Shastry and B. Sutherland, Phys. Rev. Lett. **70**, 4029 (1993).

[46] B. Sutherland and B. S. Shastry, Phys. Rev. Lett. **71**, 5 (1993).

[47] Y. Kuramoto and H. Yokoyama, Phys. Rev. Lett. **67**, 1338 (1991).

[48] N. Kawakami and S.-K. Yang, Phys. Rev. Lett. **67**, 2493 (1991).

[49] N. Kawakami, Phys. Rev. B **46**, 1005 (1992).

[50] B. D. Simons, P. A. Lee, and B. L. Altshuler, Phys. Rev. B. **48**, 11450 (1993).

[51] O. Narayan and B. S. Shastry, Phys. Rev. Lett. **71**, 2106 (1993).

[52] B. D. Simons, P. A. Lee, and B. L. Altshuler, Nucl. Phys. B **409**, 487 (1993).

[53] B. Sutherland, in *Exactly Solvable Problems in Condensed Matter and Relativistic Field Theory*, edited by B. S. Shastry *et al.*, Lecture Notes in Physics (Springer-Verlag, Berlin, 1985), Vol. 242.

[54] D. Pines and P. Nozières, *The Theory of Quantum Liquids* (Addison-Wesley, Redwood City, 1989), Vol. I, Chap. II.

[55] M. L. Mehta, *Random Matrices*, 2nd ed. (Academic Press, San Diego, 1991).

[56] P. J. Forrester, Nucl. Phys. B **338**, 671 (1992).

[57] P. J. Forrester, Phys. Lett. A **179**, 127 (1993).

[58] P. C. Hohenberg and W. F. Brinkman, Phys. Rev. B **10**, 128 (1974).

[59] R. P. Feynman, in *Progress in Low Temperature Physics*, edited by C. J. Gorter (North-Holland, Amsterdam, 1957), Vol. I, Chap. II.

[60] M. L. Mehta in [55], Eqs. (5.2.20), (6.4.14), and (7.2.6) for $\beta = 2$, 1, and 4, respectively.

[61] L. D. Landau, Zh. Eksp. Teor. Fiz. **30**, 1058 (1956) [Sov. Phys. JETP **3**, 920 (1956)].

[62] H. Bethe, Z. Phys. **71**, 205 (1931).

[63] M. L. Mehta and G. C. Mehta, J. Math. Phys. **16**, 1256 (1975).

[64] F. Gebhard and D. Vollhardt, Phys. Rev. Lett. **59**, 1472 (1987).

[65] L. Faddeev and L. Takhtajan, Phys. Lett. A **85**, 375 (1981).

[66] J. des Cloizeaux and J. J. Pearson, Phys. Rev. **128**, 2131 (1962).

[67] F. D. M. Haldane and M. R. Zirnbauer, Phys. Rev. Lett. **71**, 4055 (1993).

[68] F. D. M. Haldane in *Proceedings of the 16th Taniguchi Symposium on Condensed Matter Physics, Kashikojima, Japan, 1993*, edited by A. Okiji and N. Kawakami (Springer, 1994).

[69] V. Pasquier *et al.* (preprint).

[70] Z. N. C. Ha (preprint).

[71] M. C. Gutzwiller, *Chaos in Classical and Quantum Mechanics* (Springer-Verlag, New York, 1990).

[72] F. Haake, *Quantum Signatures of Chaos* (Springer-Verlag, Berlin, 1991).

[73] O. Bohigas in *Chaos and Quantum Physics*, edited by M.-J. Giannoni, A. Voros, and J. Zinn-Justin (North-Holland, Amsterdam, 1991).

[74] M. V. Berry and M. Robnik, J. Phys. A **19**, 649 (1986).

[75] L. P. Gor'kov and G. M. Eliashberg, Zh. Eksp. Teor. Fiz. **48**, 1407 (1965) [Sov. Phys. JETP **21**, 940 (1965)].

[76] B. Mühlschlegel, in Ref. [73].

[77] O. Bohigas, M.-J. Giannoni, and C. Schmidt, *Quantum Chaos and Statistical Nuclear Physics*, edited by T. H. Seligman and N. Nishioka (Springer-Verlag, Berlin, 1986).

[78] M. Wilkinson, J. Phys. A **21**, 4021 (1988); Phys. Rev. A **41**, 4645 (1990).

[79] P. Gaspard, S. A. Rice, H. J. Mikeska, and K. Nakamura, Phys. Rev. B **42**, 4015 (1990).

[80] J. Zakrzewski and D. Delande, Phys. Rev. E **47**, 1650 (1993).

[81] J. Goldberg, U. Smilansky, M. V. Berry, W. Schweizer, G. Wunner, and G. Zeller, Nonlinearity **4**, 1 (1991).

[82] C. W. J. Beenakker, Phys. Rev. Lett. **70**, 4126 (1993); C. W. J. Beenakker and B. Rejaei, Phys. Rev. B **49**, 7499 (1994).

[83] M. Robnik and M. V. Berry, J. Phys. A **19**, 669 (1986).

[84] M. C. Payne, M. P. Teter, D. C. Allan, T. A. Arias, and J. D. Joannopoulos, Rev. Mod. Phys. **64**, 1045 (1992).

[85] P. Vogl, H. P. Hjalmarson, and J. D. Dow, J. Phys. Chem. Solids **44**, 365 (1983).

[86] R. B. Capaz, G. C. de Araújo, B. Koiller, and J. P. von der Weid, J. Appl. Phys. **74**, 5531 (1993); R. B. Capaz, J. P. von der Weid, and B. Koiller, Appl. Phys. Lett. **60**, 704 (1992).

[87] The band folding caused by the contraction of the Brillouin zone makes it hard to associate a specific clean feature found in the band structure of the $Al_xGa_{1-x}As$ supercrystal to its counterpart in the band structures of *AlAs* or *GaAs*.

[88] A. Altland, S. Iida, and K. B. Efetov, J. Phys. A **26**, 3545 (1993).

[89] F. Wegner, Z. Phys. B **35**, 207 (1979).

[90] F. Wegner, Z. Phys. B **36**, 207 (1980).

[91] B. L. Altshuler and V. N. Prigodin, Zh. Eksp. Teor. Fiz. **95**, 348 (1989) [Sov. Phys. JETP **68**, 198 (1989)].

[92] K. B. Efetov, Zh. Eksp. Teor. Fiz. **82**, 872 (1982) [Sov. Phys. JETP **55**, 514 (1982)].

[93] K. B. Efetov and V. N. Prigodin, Phys. Rev. Lett. **70**, 1315 (1993).

[94] V. N. Prigodin, B. L. Altshuler, K. B. Efetov, and S. Iida, Phys. Rev. Lett. **72**, 546 (1994).

[95] A. D. Mirlin and Y. V. Fyodorov, Phys. Rev. Lett. **72**, 526 (1994).